NASA CONTRACTOR REPORT

ANALYSIS OF AN OPTIMAL CELESTIAL-INERTIAL NAVIGATION CONCEPT FOR LOW-THRUST INTERPLANETARY VEHICLES

by Alan L. Friedlander

Prepared under Contract No. NAS 2-2401 *by*
IIT RESEARCH INSTITUTE
Chicago, Ill.
for Ames Research Center

NATIONAL AERONAUTICS AND SPACE ADMINISTRATION - WASHINGTON, D. C. - MAY 1966

NASA CR-457

ANALYSIS OF AN OPTIMAL CELESTIAL-INERTIAL NAVIGATION CONCEPT FOR LOW-THRUST INTERPLANETARY VEHICLES

By Alan L. Friedlander

Prepared under Contract No. NAS 2-2401
IIT RESEARCH INSTITUTE
Chicago, Ill.

for Ames Research Center

NATIONAL AERONAUTICS AND SPACE ADMINISTRATION

For sale by the Clearinghouse for Federal Scientific and Technical Information
Springfield, Virginia 22151 – Price $4.00

FOREWORD

This report documents the work performed by the IIT Research Institute, Chicago, Illinois in fulfillment of the requirements of the National Aeronautics and Space Administration Contract NAS2-2401. This contract was administered under the technical cognizance of Mr. John S. White of the Ames Research Center, Moffett Field, California.

Studies presented in this report began in October, 1964 and were concluded in August, 1965. The work was performed by the Guidance and Control Section under the direction of Alan L. Friedlander as Project Engineer. Principal contributors to the project were Messrs. H. Feingold, A. Friedlander, and J. Waters.

SUMMARY

This report describes the results of a navigation study applied to thrusted interplanetary vehicles powered by an electric propulsion system. A navigation concept is formulated wherein both celestial and inertial source information are utilized for in-flight determination of vehicle motion. The celestial observations provide the means for significantly reducing the long term effects of inertial gyro and accelerometer errors. Summary Figure 1(a) illustrates the navigation system concept in functional block diagram form. A pair of gimballed star trackers (stellar monitor) integral with the inertial measurement unit serve to align and stabilize the space-fixed coordinate frame. Additional celestial sensors such as planet trackers or sextants measure appropriate space angles from which vehicle position may be found. Of principal interest to this study is the navigation computer whose main function is to process the available information so as to obtain the best estimate of the vehicle state in the presence of random instrumentation errors.

Summary Figure 1(b) shows the computational structure of the state estimation procedure. This procedure is based on concepts of optimal linear filter theory (Kalman filter). The vehicle state includes, in addition to position and velocity, instrumentation errors having time-correlated statistical properties. Hence, the estimation procedure allows in-flight calibration and correction of instrumentation errors. Of particular importance here is the estimation of the low-level accelerometer errors

which may be significantly improved over Earth-based calibration methods. As indicated in the figure, celestial angle measurements are assumed to be made at discrete times whereas acceleration measurements are assumed continuous (or, effectively continuous compared with the celestial sampling rate). The filtering process is also discrete. At the celestial measurement time, the weighted difference between the measured and estimated space angle is the incremental correction applied to the previous estimate of the state. The new and improved estimate, then, is the updated initial condition used in the solution ofthe dynamical state equations over the next cycle.

A digital computer simulation was developed to evaluate the performance of the celestial-inertial navigation concept for several different missions and error parameter assumptions. This simulation obtains the ensemble second-order statistics, or covariance, of the error in estimating the state at each successive observation point. Summary Figure 2 shows a representative performance comparison between an inertial-only and an optimal celestial-inertial estimation of vehicle position. Plotted is the RMS position uncertainty as a function of time for a 205.4 day Mars rendezvous mission. The reference trajectory has a 97 day coast period beginning at about 52 days from heliocentric injection, and has an average thrust acceleration level of about 10^{-4}g. The RMS error parameters assumed are (1) initial velocity uncertainty-5 m/sec, (2) accelerometer bias and random error-10^{-7}g, and (3) random celestial sensor error - 10 sec arc. The lines-of sight to both Earth and Mars are measures at 2 day intervals.

It is seen that the unbounded effect of inertial system errors result in a position uncertainty of about 300,000 km at the nominal rendezvous time. In contrast, this position uncertainty is only 500 km for the celestial-inertial system. Furthermore, the improved performance over the entire flight is quite significant. Similar results are found for velocity estimation where the terminal uncertainty is only 0.25 m/sec as compared with 40 m/sec for inertial-only measurements. Also, the accelerometer bias estimate is improved by a factor of 35 as a result of the celestial observations.

It is perhaps unrealistic to expect the low-frequency accelerometer error to remain constant throughout the entire mission, i.e., to be a pure bias. More practically, this error may result from a slowly changing calibration, such as due to aging. To account for this situation, the low-frequency error was modeled more generally by an exponentially-correlated random process having a rather long time constant. Summary Figure 2 includes the position uncertainty characteristic for a correlation time of 200 days. It is seen that, beyond mid-flight, the position uncertainty becomes significantly larger than that associated with the pure bias. At the terminal time, the position uncertainty is about 1500 km. The cause of the poorer performance is due to the difficulty in estimating a non-constant accelerometer error even when the correlation time is of the same order as the total flight time. This was a somewhat surprising and discouraging result. Perhaps more frequent planet sightings would improve this situation.

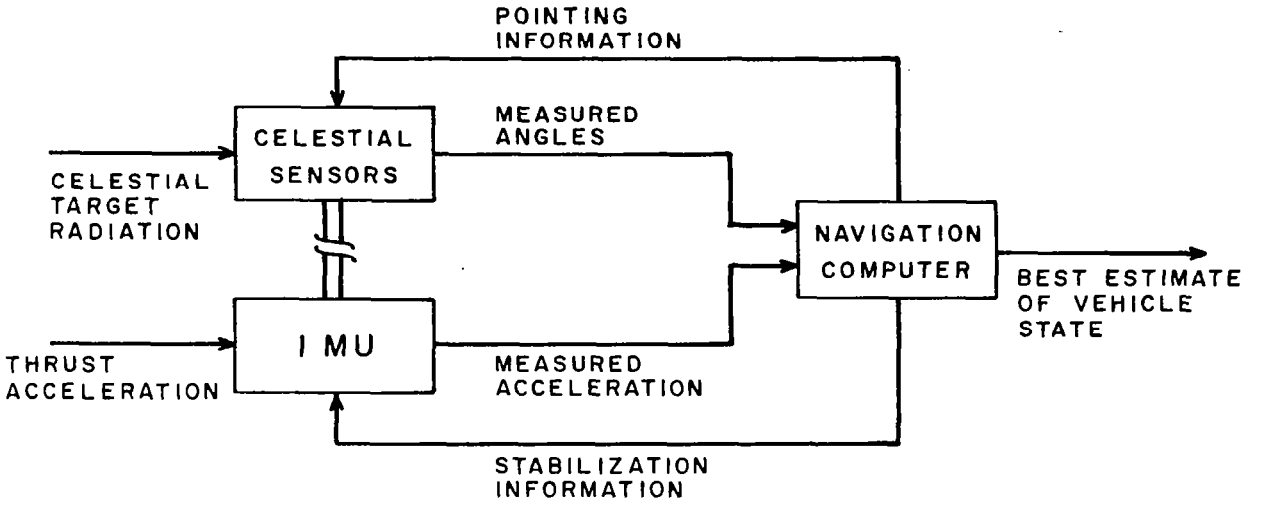

(a) CELESTIAL-INERTIAL NAVIGATION SYSTEM

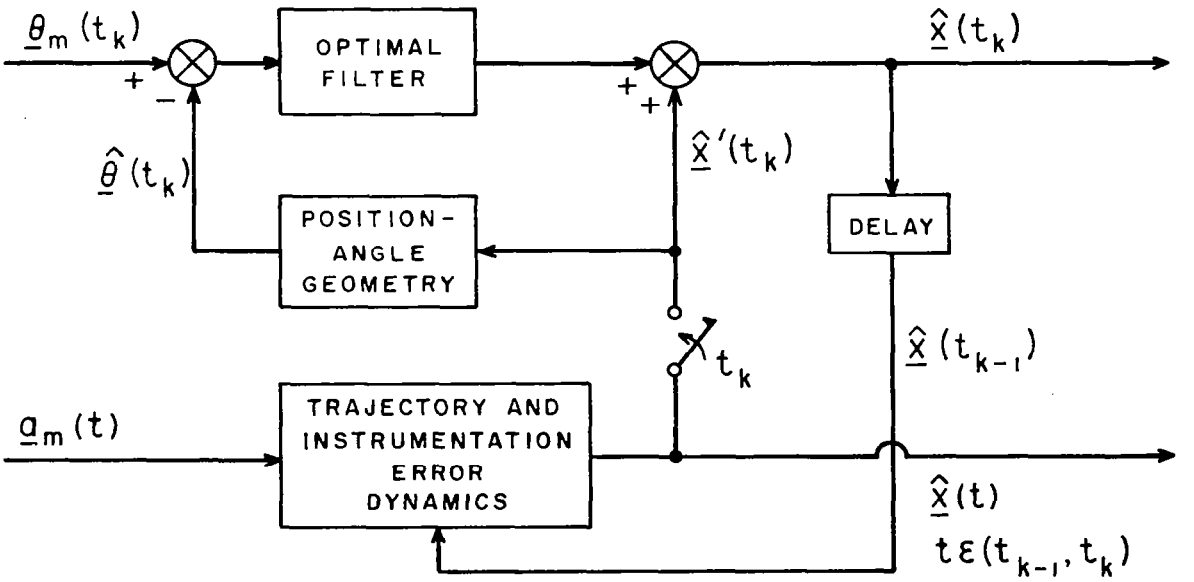

(b) NAVIGATION COMPUTER

SUMMARY FIGURE 1

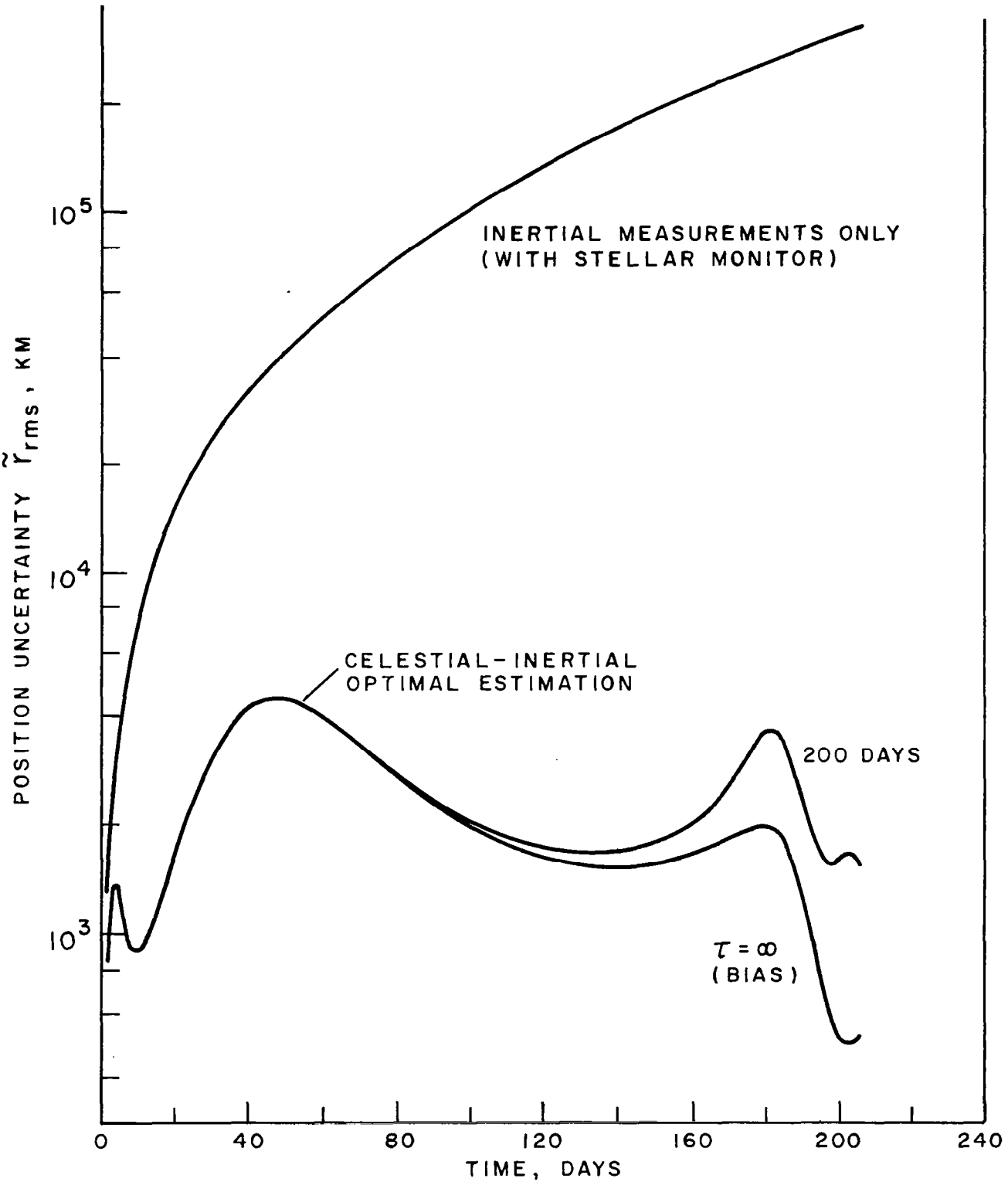

SUMMARY FIGURE 2 NAVIGATION PERFORMANCE COMPARISON FOR 205.4 DAY MARS RENDEZVOUS MISSION, τ = CORRELATION TIME OF LOW-FREQUENCY ACCELEROMETER ERROR

TABLE OF CONTENTS

TABLE OF CONTENTS (cont'd)

ANALYSIS OF AN OPTIMAL CELESTIAL-INERTIAL NAVIGATION CONCEPT FOR LOW-THRUST INTERPLANETARY VEHICLES

1. INTRODUCTION

The application of electric propulsion systems (low thrust, high specific impulse) to upper stage space vehicles is looked upon as offering a high performance potential for carrying out a long-range, comprehensive plan of solar system exploration. Considerable effort is now underway toward the development of lightweight and reliable advanced propulsion systems which are necessary if this potential is to be realized. Delineation and solution of the guidance problems associated with such vehicle systems is considered to be an important complementary step in this development effort.

To be definitive, the term guidance is meant to encompass both the navigation and trajectory control functions. Navigation is the process of determining, through appropriate measurements, the vehicle's present state as given, for example, by position and velocity in some known frame of reference. The trajectory control function is to utilize the navigational information in some computational (prediction) procedure as to provide thrust acceleration commands that will direct the vehicle to its desired target.

The study described herein is concerned only with the navigation or trajectory estimation problem. In particular, the overall objective of this study is the theoretical formulation and performance evaluation of a low-thrust navigation procedure which utilizes inertial and celestial source information obtained from instrumentation contained on board the vehicle. The instrumentation system is invariably imperfect; that is, the measurements are subject to unpredictable or random errors. As a result of these errors and the uncertainty of initial conditions, the present vehicle state can never be known precisely. The function of the navigation procedure, then, is to process the available information in such a manner as to obtain the best estimate of the vehicle state. It is towards this purpose of obtaining the best estimate that both inertial and celestial measurements are considered. The motivating factor here lies in the tacit assumption that the undesirable effects of the error characteristics inherent to each type of navigation system acting alone can be minimized by properly combining or mixing the information of both systems acting together. Thus, for example, stellar sightings may be used to compensate for gyro drift while planetary sightings yield position data which act to damp the unbounded effects of accelerometer errors. On the other hand, direct measurement of acceleration provides a better source of velocity information than could normally be obtained from celestial angle measurements.

The problem of estimating vehicle position and velocity from information subject to random errors is basically a data filtering problem. Accordingly, the problem is treated by means of optimal statistical filter theory, prinicpally due to Kalman (Ref. 1). The optimizing criterion is, effectively, the minimization of the estimation error variance. This theory has been applied in several studies of lunar and interplanetary trajectory estimation for vehicles under "free-fall" or ballistic conditions where information is assumed to be available from celestial observations (Refs. 2,3,4,5). It has also been applied to the low-thrust navigation problem where only celestial observations were assumed available (Ref. 6). The present study is an extension of this previous work, and differs mainly in that information regarding both the input and output determinants of vehicle motion are considered.

The content and organization of this report is as follows: Section 2 presents a brief background discussion of low-thrust propulsion, trajectory and mission characteristics, and of the navigation problem. The mathematical formulation and analysis of the celestial-inertial navigation concept is presented in Section 3. Included in this section are a description of both the inertial and celestial measurement processes and the assumed statistical characteristics of the instrumentation errors, a brief analysis of gyro drift compensation provided by star fixes and appropriate correction of inertial

platform misalignment, the linearized trajectory model, and finally the state estimation equations. Section 4 describes the digital computer simulation program which was developed during the course of this study in order to evaluate the performance of the navigation procedure. Numerical results obtained from the computer program are discussed in Section 5.

2. BACKGROUND DISCUSSION

2.1 Summary of Propulsion/Trajectory Characteristics

Space navigation having been defined as the process of estimating the state of a vehicle's trajectory, it is clear that the navigation process will be influenced by the nature of the trajectory. The trajectory, in turn, is influenced by the mode of propulsion system operation. This influence may appear in the structure of the navigation concept and system and certainly in the magnitude of the system parameters. Since this study specifically treats the low-thrust navigation problem, a brief discussion of low-thrust propulsion and trajectory characteristics would appear to be in order at this point. The intent is to summarize these characteristics mainly as they relate to the navigation analysis and results to follow. A comprehensive discussion of electric propulsion systems and trajectories may be found in the numerous publications on this subject (e.g., references 7, 8 and 9).

Propulsion

Basically, an electric rocket engine is a device in which charged particles or ions are accelerated to high velocities by either electrostatic or electromagnetic fields, and then expelled rearward to produce useful thrust. Depending upon the particular vehicle system design and mission application, the thrust produced per unit vehicle weight will lie

within the range 10^{-5} to 10^{-3}. Due to this low acceleration level, the electric rocket must be operated continuously during a significant portion of a mission which may extend over many months or years. In addition, the nature of the mission trajectory differs from the familiar ballistic or "free-fall" trajectory. These factors make the low-thrust guidance problem somewhat unique.

Whereas chemical and nuclear propulsion systems are basically energy-limited, electric propulsion systems are power-limited, i.e., limited in performance by the characteristics (power level and weight) of the separate powerplant. It is generally assumed that the powerplant will be operated at its maximum power rating during periods of thrustor operation. This constant power constraint reflects upon the necessary regulation of propellant flow rate ($\dot{M}$) and jet velocity (V_j); or, alternatively, thrust (F) and specific impulse (I_{sp}). The quantitative relations are (in MKS units)

$$\begin{aligned} 2P_j &= \dot{M}V_j^2 \\ &= FV_j = FI_{sp}\, g_o \end{aligned} \tag{1}$$

where P_j is the kinetic power in the exhaust jet. In terms of thrust acceleration,

$$a = \frac{F}{M} = \frac{2P_j}{MI_{sp}\, g_o} \tag{2}$$

The limitation imposed on the acceleration level of electric propulsion systems is readily found from the above expression. Based on the projected state-of-the-art of nuclear-turboelectric powerplants, a realistic upper limit on P_j/M_o is of the order 45 watts/kg. Similarly, a realistic lower limit on I_{sp} for ion engine systems is about 3000 sec. Substitution of these numbers into (2) gives the result

$$a_o \leq 3 \times 10^{-3} \text{ m/sec}^2 \quad (3 \times 10^{-4} g)$$

Of course, for many missions the required I_{sp} will be much higher than 3000 sec. An initial acceleration of 10^{-4}g or less is more typical for interplanetary missions.

Combining equations (1) and (2) and integrating yields the characteristic mass equation for power-limited propulsion

$$\frac{1}{M(t_f)} = \frac{1}{M(0)} + \frac{1}{2P_j} \int_0^{t_f} a^2(t)\, dt \qquad (3)$$

For a given initial mass and jet power, it is seen that minimizing $\int a^2 dt$ is equivalent to maximizing the final mass of the vehicle. This criterion is commonly used in the formulation and solution of the trajectory optimization problem. Note that this result marks a basic difference between energy-limited and power-limited propulsion. For a constant thrust chemical system, the propellant-optimal trajectory requires that the characteristic velocity, $\int a\,dt$, be a minimum. Of course, in

the case where the electric propulsion system is operated at a constant thrust level (and, therefore, constant specific impulse), the two criteria are equivalent. This brings us to the final point to be made concerning propulsion; i.e., the mode of thrustor operation.

Two different modes of thrustor operation are considered in most trajectory and mission studies - one theoretical and the other practical. These are

1. Variable thrust
2. Constant thrust

In the variable thrust mode it is assumed that any thrust level and specific impulse can be obtained consistent with the constant power constraint. Hence, these parameters are allowed to vary with time (in conjunction with an optimum steering program) in an optimum fashion such that the trajectory boundary conditions of the mission are achieved with minimum $\int a^2 dt$. In this case, $\int a^2 dt$ is not a function of the propulsion system parameters but rather depends only upon the specified boundary conditions. Variable thrust, then, is the least restrictive mode of operation and, hence, yields the best possible performance (minimum propellant requirements).

In the constant thrust mode of operation, the constraint imposed upon thrust and specific impulse must result in a performance loss. Also, $\int a^2 dt$ depends upon the system parameters in addition to the trajectory boundary conditions. It is

possible to choose these parameters (e.g., a_o and I_{sp}) so that the performance loss is made small. Even so, the performance loss could be as high as 15 percent depending upon the mission application.

Although the constant thrust mode of operation is considered more realistic in terms of the electric thrustors currently under development, future advances in the state-of-the-art may allow the variable thrust mode. Even if a single thrustor could not be made to operate within a wide range of thrust and specific impulse, it may be possible to achieve the desired characteristic by employing several banks of thrustors each operating under different design conditions. To account for this possibility, both constant and variable thrust trajectories will be considered when illustrating the performance of the navigation concept.

Mission Applications

Of the various missions proposed for electrically propelled space vehicles, the following are representative classes

1. Earth orbital operations
2. Lunar transport ferry
3. Out-of-the ecliptic probes
4. Planetary fly-by and rendezvous

Earth orbital operations might include altitude and orbital plane maneuvers for the purpose of detailed mapping of scientific phenomena. It has been suggested that the transport ferry could efficiently deliver large payloads from Earth to lunar

orbit if the time factor is not critical. The high energy requirement of the out-of-the-ecliptic scientific mission makes electric propulsion particularly advantageous. This is true also of fly-by or orbiter (rendezvous and capture) missions to the outer planets, or round-trip missions to the inner planets. The interplanetary mission being of more general applicability, we shall restrict our attention to it.

A typical interplanetary mission may be conveniently divided into several distinct phases, namely, the escape spiral phase, the heliocentric or midcourse phase, and the capture spiral phase. The first phase begins in a low-altitude satellite orbit about Earth and terminates at or slightly beyond the escape energy condition which may occur at a distance of several hundred thousand miles. During this phase thrust is directed in such a manner as to efficiently increase the orbital energy. This causes the spacecraft to slowly spiral about Earth with increasing orbital altitude. The midcourse phase of the mission refers to the region of heliocentric space between the orbits of Earth and the destination planet. Duration of powered flight in this phase depends upon the particular vehicle and mission design. For example, a short trip time may necessitate continuous operation of the electric thrustors. For longer flights, coast periods may be inserted in order to conserve propellant. The capture spiral phase begins at a distance of several hundred thousand miles from the destination planet,

with thrust directed to cause the spacecraft to achieve the desired satellite orbit. In the case of the planetary fly-by mission, this final phase may either be entirely eliminated or terminated at some energy level prior to capture.

2.2 The Navigation Problem

Closed-loop guidance of electrically propelled spacecraft is made necessary by the fact that in-flight errors in establishing the proper initial conditions, thrust acceleration magnitude, and steering direction cause the spacecraft to deviate from its design trajectory. Correction of this deviation requires knowledge of the vehicle state, either continuously or at discrete time intervals. Assuming the desirability of a self-contained (on-board) navigation system, such information can be made available from either celestial measurements or inertial acceleration measurements, or both.

Celestial navigation techniques applicable to ballistic flight are well known. Basically, celestial angle measurements yield vehicle position information. Velocity information must be determined indirectly either through differentiation of position or, more commonly, via the laws of orbital mechanics. In the case of thrusted flight, position and velocity may still be determined by celestial means provided the acceleration time-history between observations is known. Therein lies the crux of the problem since velocity information so obtained is apt to be

relatively unreliable unless acceleration is accurately predictable or measured in-flight.

It is probably not realistic to expect an a priori prediction of acceleration magnitude and direction to be accurate enough for navigation requirements. Off-nominal thrust conditions of several percent can probably be expected from electric thrustors. Also, the vehicle mass may not be known exactly. Thrust direction errors resulting from imprecise attitude control or ion beam deflection may typically be on the order of one degree. Even if these errors were of smaller magnitude, their time variation would likely be unpredictable. As a means of alleviating this problem, celestial measurements could be utilized to obtain certain gross features of thrust acceleration, however, the accuracy of the celestial sensors would limit this approach. It would appear that no adequate substitute exists for high quality inertial measurements of acceleration.

A pure inertial system could, of course, perform the navigation function. However, the propagation of initial condition uncertainties and the errors of even high quality inertial components could prove significant over the long flight duration of low thrust missions. For example, an advanced state-of-the-art gyro having a constant drift as little as 0.001 deg/hr would cause the reference axes to be misaligned by 5 deg at the end of a 200 day flight. Or, an accelerometer

error of 10^{-} g would result in a position uncertainty of about 100,000 km at the end of this flight. Some means for damping or reducing these errors is necessary. A combined celestial-inertial navigation system would appear to be most suitable for this application. Of course, it may be possible and desirable to incorporate earth-based tracking information from time to time in order to further improve navigational accuracy. This question will not, however, be considered in the present study.

The actual configuration of a celestial-inertial system would depend on such factors as basic sensor accuracy, tolerable guidance accuracy, mechanization and reliability considerations, and whether the mission is manned or unmanned. The hybrid system concept might lie somewhere between the "simple" extremes (1) an inertially-aided celestial system wherein a body mounted accelerometer is used primarily to monitor thrust acceleration, and (2) a celestially-aided inertial system wherein stellar references are used to erect the inertial measurement unit and compensate for gyro drift. More realistically, the potential of both celestial and inertial navigation techniques would be used to full advantage. This latter approach is followed in the present study, where both types of information are combined to yield a statistically optimal navigation procedure.

3. FORMULATION OF THE NAVIGATION CONCEPT

The previous discussion has given a qualitative argument for considering a celestial-inertial navigation concept for low-thrust space flight and has described the basic information processes involved. In this section we consider the mathematical formulation and analysis of this concept, first in terms of the individual processes and error models, and then in terms of how the different types of information are combined to yield a statistically optimal estimate of the trajectory state.

3.1 Trajectory Kinematics

Motion of a space vehicle is determined by its initial position and velocity vectors, $\underline{R}_o$ and $\underline{V}_o$, the acceleration $\underline{g}(\underline{R},t)$ due to the gravitational potential field present, and the thrust acceleration $\underline{a}(t)$ imparted by the propulsion system. The differential equations of motion may be expressed quite generally as

$$\begin{aligned} \dot{\underline{R}} &= \underline{V} \\ \dot{\underline{V}} &= \underline{g}(\underline{R},t) + \underline{a}(t) \end{aligned} \tag{4}$$

The position and velocity components expressed in a fixed cartesian coordinate frame centered at some appropriate point are defined

$$\begin{aligned} \underline{R} &= (X,Y,Z) \\ \underline{V} &= (\dot{X},\dot{Y},\dot{Z}) \end{aligned} \tag{5}$$

To be somewhat more specific, if the gravitational potential field is primarily due to the Sun, the gravitational acceleration is

$$g_X = -\frac{\mu_S X}{|\underline{R}|^3} \quad , \qquad X \rightarrow Y, Z \tag{6}$$

Here, the coordinate system is centered at the sun having a gravitational constant μ_S.

As expressed by the set of six first-order differential equations, (4), the state variables of motion are identified with the six quantities $(X, Y, Z, \dot{X}, \dot{Y}, \dot{Z})$. In some cases the thrust acceleration may be expressed as an explicit function of the state variables, but more likely will be given as a function of time. Actually, this is a question of the trajectory computation and guidance procedure which is of no immediate concern here. Since the possibilities in this area are virtually unlimited, we would like to divorce the navigation problem from the trajectory control problem, at least in principle. For our purposes, then, we will consider $\underline{a}(t)$ to be the control variable, subject to measurement, but otherwise unspecified in functional form.

The trajectory kinematics, being nonlinear, will require modification in order to be easily incorporated in the linear navigation theory to be described. Following standard

practice, the equations of motion will be linearized about a nominal or reference trajectory. This does not imply, however, that the reference trajectory need be fixed a priori. Rather, the reference trajectory could be recomputed at repetitive intervals taking into account the conditions of actual flight. In this way, it is possible to extend the range of validity of the linearization procedure.

3.2 Inertial Measurements and Errors

Figure 1 shows a block diagram representation of a space stabilized, pure inertial system in standard form. The system is said to be dynamically exact in that the navigational outputs are error free for all dynamic conditions, i.e., there are no instrumentation or initial condition errors. Gyroscopic references establish the attitude of the three mutually orthogonal accelerometers in a known inertial coordinate frame. Inertial velocity is obtained by integrating the summation of thrust and gravitational acceleration, and a second integration yields position. The feedback loop, assumed instantaneous and exact, illustrates the functional dependence of gravitational acceleration on position.

The standard form of the system is adopted here so as to avoid any detailed consideration of how the inertially fixed frame is actually implemented in practice. In this regard, the two possibilities are the gimballed platform system and the strapdown system. In the well-known gimballed system, a

space-stabilized reference frame is physically achieved by a configuration of gimbals. The strapdown system creates an inertially fixed frame artificially by means of a computer. Here, the inertial measurement components are fixed to the vehicle frame. On the basis of rate measurements performed by the body-fixed gyros, the relationship between the vehicle frame and a desired inertial frame can be found. The computer then transforms the measured accelerations into the inertial frame. A discussion of the relative advantages and disadvantages of each system is beyond the scope of the present study. We simply note that, in the absence of significant computation errors, each system can be represented in principal by the standard form of Figure 1. Furthermore, the discussion of inertial measurement errors given below is broadly applicable to either system.

Aside from initial condition and computational errors, inaccuracy of pure inertial navigation is due to imprecise knowledge of the thrust acceleration vector. Errors in the measurement of this vector arise from (1) accelerometer errors $\underline{\varepsilon}_a$, and (2) inertial platform misalignment γ. For convenience, we use the term "platform misalignment" to denote any angular displacements or uncertainties of the instrumented (measurement) inertial axes relative to the reference (computational) inertial axes. Even if the accelerometers were perfect, this misalignment would cause erroneous cross-coupling of the acceleration components.

Assuming that the platform misalignment can be represented by small angle rotations $(\Upsilon_X, \Upsilon_Y, \Upsilon_Z)$, the total error in the acceleration measurement is expressed as

$$\begin{aligned} \underline{a}_m - \underline{a} &= \Delta\underline{a} \\ &= \underline{\varepsilon}_a + \underline{a} \times \underline{\Upsilon} \\ &= \underline{\varepsilon}_a + \Lambda\underline{\Upsilon} \end{aligned} \tag{7}$$

where the coefficient matrix Λ has the elements

$$\Lambda = \begin{bmatrix} 0 & -a_Z & a_Y \\ a_Z & 0 & -a_X \\ -a_Y & a_X & 0 \end{bmatrix} \tag{8}$$

The subscript m will be used to denote measured quantities.

When the above errors are included, the information available from the inertial system may be written

$$\ddot{\underline{R}}_m = \underline{g}(\underline{R}_m, t) + \underline{a} + \underline{\varepsilon}_a + \Lambda\underline{\Upsilon} \tag{9}$$

where

$$\underline{R}_m = \underline{R} + \Delta\underline{R}$$

$$\underline{g}(\underline{R}_m, t) = \underline{g}(\underline{R}, t) + \Delta\underline{g}$$

Assuming that it is possible to make the linear approximation

$$\Delta\underline{g} = \left[\frac{\partial \underline{g}}{\partial \underline{R}}\right]\Delta\underline{R} \equiv G\Delta\underline{R} \quad , \tag{10}$$

the propagation of inertial system errors may be obtained from the differential equations

$$\Delta\dot{\underline{R}} = \Delta\underline{V} \tag{11}$$

$$\Delta\dot{\underline{V}} = G\Delta\underline{R} + \underline{\varepsilon}_a + \Lambda\underline{\Upsilon} \tag{12}$$

The (3 x 3) coefficient matrices G and Λ are implicit functions of time and are to be evaluated about some nominal conditions. In the case of a pre-flight error analysis, these quantities may be evaluated along the pre-specified reference trajectory, $\underline{R}^*(t)$ and $\underline{a}^*(t)$. Here, it is assumed that the differences $(\underline{R}_m - \underline{R}^*)$ and $(\underline{R} - \underline{R}^*)$ are sufficiently small so as to validate the linear approximation. In the case of an in-flight error analysis, G and Λ should properly be evaluated about the estimated trajectory, $\underline{R}_m(t)$ and $\underline{a}_m(t)$.

Figure (2) illustrates the inertial system error analysis in block diagram form. The left-hand portion of the figure accounts for the dynamics of platform misalignment. The simplifying assumption is made that the rate of change of platform misalignment is due to gyro drift $\underline{\varepsilon}_g$, i.e.,

$$\dot{\underline{\Upsilon}} = \underline{\varepsilon}_g \tag{13}$$

Apart from initial condition errors, the accelerometer error and gyro drift appear as forcing functions for the position and velocity error responses. For error analysis purposes, $\underline{\varepsilon}_a$ and $\underline{\varepsilon}_g$ are best characterized in terms of their statistical

properties. That is, these errors are considered to be random variables either from an ensemble average or time-varying point of view. For instance, it has become standard practice in error analyses of inertial systems to model these errors as deterministic functions of acceleration with random coefficients, e.g.,

$$\varepsilon_a = k_0 + k_1 a + \text{higher order terms}$$

Here, k_0 and k_1 are the bias and linear scale factor uncertanties of an accelerometer which remain after calibration procedures. Normally, k_0 and k_1 are considered zero-mean random constants with variances (standard deviations) determined by averaging test results over an ensemble of similar components. For high acceleration launch vehicle applications, it is known that the linear scale factor uncertainty has a significant contribution to the overall error response. This is not expected, however, for low acceleration applications. To illustrate this point, suppose an accelerometer designed for low-thrust application has a bias uncertainty of 10^{-7}g and a 0.01 percent linearity. Taking 10^{-4}g as a typical acceleration level, the acceleration-dependent error is seen to be 1/10th that of the bias error and, thus, could be neglected. A similar argument could be made for neglecting "g-sensitive" gyro drift. It is realized, of course, that this extrapolation or analogy between high and low acceleration applications may not be quite valid. In particular, low-threshold accelerometers

are only in the laboratory development stage and little is known of their error characteristics. It is likely that such devices will have little resemblance to present day accelerometers in terms of principle of operation and design. Nevertheless, it seems quite reasonable to assume that the accelerometer error and gyro drift will not be g-sensitive.

We are still left with the task of modeling the statistical characteristics of the instrumentation errors. This task is made difficult by the fact that virtually no statistical test data is available for advanced inertial components. In the face of little concrete information to go on, the following approach is taken with respect to both accelerometer and gyro errors.

First, it is assumed that the instrumentation error may consist of several additive components, each statistically independent. Each of these components could be identified with a different time-varying noise characteristic, e.g., high and low-frequency random noise. Second, it is assumed that each error component may be described by a zero-mean, stationary random process having an exponential correlation function, i.e.,

$$\underline{E}\left[\varepsilon_i(t)\,\varepsilon_i(t+\tau)\right] = \phi_i(\tau) = \sigma_i^2\, e^{-\omega_i|\tau|} \tag{14}$$

Here, $\phi_i(0) = \sigma_i^2$ is the mean-squared value or variance of the i th error component and ω_i is the reciprocal of the correlation time, i.e., $\omega_i = 1/\tau_i$. This type of random process is commonly termed "band-limited" noise since it may be generated by passing "white" noise of power spectral density $\frac{1}{\pi}\sigma_i^2\omega_i$ through a simple lag filter, $G(s) = \frac{1}{s + \omega_i}$. The power spectral density of the "band-limited" noise is

$$P_i(\omega) = \frac{\frac{1}{\pi}\sigma_i^2\omega_i}{\omega^2 + \omega_i^2} \tag{15}$$

The form of (15) suggests a simplifying approximation when the noise frequency is significantly higher than the characteristic frequency of the system response (or, higher than the sampling rate of the system response). The high-frequency "band-limited" noise could be approximated by a "white" noise process with spectral density $\frac{\sigma^2 h}{\pi\omega_h}$. For analysis purposes, then, the high-frequency noise could be represented by the correlation function

$$\begin{aligned} \phi_h(\tau) &= \frac{2\sigma_h^2}{\omega_h}\,\delta(\tau) \\ &= 2\sigma_h^2\tau_h\delta(\tau) \end{aligned} \tag{16}$$

where $\delta(\tau)$ is the Dirac delta (unit impulse) function. This approximation, while introducing negligible error in the results, greatly simplifies the numerical computation procedure.

3.3 Celestial Measurements and Errors

The basic geometric observables of celestial navigation are space angles measured from the vehicle to selected celestial targets whose positions at the time of measurement are assumed to be known. These targets include the distant stars and the "near" bodies of the solar system (sun, planets, moons). The stars, being essentially infinitely far away and fixed in space, provide the directional references for determining vehicle position and attitude. The near bodies provide the finite distance references which are needed to complete the position fix.

In regard to position fixes, the information contained in a single space angle measurement may be expressed in the general form

$$\theta_m = \theta(\underline{R}) \tag{17}$$

Here, $\theta(\underline{R})$ is the geometric function which relates the position coordinates to the observable. Three independent space angle measurements suffice to determine $\underline{R}$. Consider, for the moment, the effect of measurement errors on position determination without regard to the specific observation policy. Assuming small errors, $\Delta\theta = \theta_m - \theta$, we have from (17)

$$\begin{aligned} \Delta\theta &= \underline{h} \cdot \Delta\underline{R} \\ &= \underline{h}^T \Delta\underline{R} \end{aligned} \tag{18}$$

where $\underline{h}^T$ is the row vector of partials

$$\underline{h}^T = \left[\frac{\partial\theta}{\partial\underline{R}}\right] = \left[\frac{\partial\theta}{\partial X} \quad \frac{\partial\theta}{\partial Y} \quad \frac{\partial\theta}{\partial Z}\right] \tag{19}$$

For three simultaneous observations, the error in determining position is found by inversion

$$\Delta\underline{R} = H^{-1}\Delta\underline{\theta} \tag{20}$$

where H is the (3 x 3) matrix associated with the observation policy

$$H = \begin{bmatrix} h_1^T \\ h_2^T \\ h_3^T \end{bmatrix} = \begin{bmatrix} \frac{\partial\theta_1}{\partial X} & \frac{\partial\theta_1}{\partial Y} & \frac{\partial\theta_1}{\partial Z} \\ \frac{\partial\theta_2}{\partial X} & \frac{\partial\theta_2}{\partial Y} & \frac{\partial\theta_2}{\partial Z} \\ \frac{\partial\theta_3}{\partial X} & \frac{\partial\theta_3}{\partial Y} & \frac{\partial\theta_3}{\partial Z} \end{bmatrix} \tag{21}$$

The necessity for independent observations is reflected in equation (20). If the observations were not independent, the determinant of H would be zero and, hence, H^{-1} would "blow up". In fact, the smaller the value of $|H|$, the greater is the sensitivity to measurement errors. Since $|H|$ may be expressed as the triple scalar product, $\underline{h}_1 \cdot (\underline{h}_2 \times h_3)$, the desire to minimize the error sensitivity requires that this product be as large as possible. Hence, the following important conclusion may be drawn. If the observation policy could be chosen arbitrarily, it should be chosen such that the geometry vectors $\underline{h}_1, \underline{h}_2$, and $\underline{h}_3$ are as large and mutually perpendicular as possible.

Inasmuch as the number of celestial bodies potentially available for observation is quite large, the various possibilities and combinations of angular measurements are virtually unlimited. Of course, not all celestial bodies are observable from a practical standpoint nor are they all equally useful in providing accurate navigational information. The choice of which set of observations to use in a given situation would depend upon such factors as (1) the effect of sensor errors on the accuracy of position determination, (2) the type of optical sensor employed, e.g., sextant or theodolite, and (3) the viewing constraints imposed by the vehicle structure and orientation requirements. The implication of these factors is largely a question of mission application and hardware design, and, as such, is beyond the scope of this research study. For the purpose of this study, we shall restrict our attention to planetary and stellar observations and consider two different types of space angle measurements:

1. Theodolite-type measurements - the observable here is the planet line-of-sight as measured by the latitude (α) and longitude (β) of the planet as seen from the vehicle. Possible implementation would consist of a gimballed theodolite or planet-tracker mounted integrally with the inertial measurement unit. When the planet is centered in the field of view, the two gimbal angles are a measure of α and β.

2. Sextant-type measurements - the observable here is the included angle (θ) between a star and the planet.

The geometry of these two measurement types is shown in Figure 3 .

For the theodolite-type measurement, the equations relating vehicle position and the observables are

$$\sin \alpha = \frac{Z_{vp}}{R_{vp}} \tag{22}$$

$$\sin \beta = \frac{Y_{vp}}{(X_{vp}^2 + Y_{vp}^2)^{1/2}} \qquad \cos \beta = \frac{X_{vp}}{(X_{vp}^2 + Y_{vp}^2)^{1/2}} \tag{23}$$

where $\underline{R}_{vp}$ is the vector from the vehicle to the observed planet, i.e.,

$$X_{vp} = X_p - X \quad , \quad X \rightarrow Y,Z \tag{24}$$

The planet position $\underline{R}_p$ is assumed known. The elements of the geometry vectors $\underline{h}_\alpha$ and $\underline{h}_\beta$ are found to be

$$\underline{h}_{\alpha} = \begin{bmatrix} \frac{\partial \alpha}{\partial X} \\ \frac{\partial \alpha}{\partial Y} \\ \frac{\partial \alpha}{\partial Z} \end{bmatrix} = \begin{bmatrix} \frac{\sin\alpha \cos\beta}{R_{vp}} \\ \frac{\sin\alpha \sin\beta}{R_{vp}} \\ \frac{-\cos\alpha}{R_{vp}} \end{bmatrix} \tag{25}$$

$$\underline{h}_{\beta} = \begin{bmatrix} \frac{\partial \beta}{\partial X} \\ \frac{\partial \beta}{\partial Y} \\ \frac{\partial \beta}{\partial Z} \end{bmatrix} = \begin{bmatrix} \frac{\sin\beta}{R_{vp} \cos\alpha} \\ \frac{-\cos\beta}{R_{vp} \cos\alpha} \\ 0 \end{bmatrix} \tag{26}$$

We can now be more specific regarding the question of error sensitivity. Suppose we measure the line-of-sight to two different planets, P_1 and P_2, obtaining the set of data (α_1, β_1) and (α_2, β_2). Since we have one extra piece of information, suppose, for the moment, that we neglect the second latitude measurement α_2. From equations (25) and (26), we note that $\underline{h}_{\alpha}^{(1)}$ and $\underline{h}_{\beta}^{(1)}$ are always orthogonal vectors, and that their cross product is

$$\underline{h}_{\alpha}^{(1)} \times \underline{h}_{\beta}^{(1)} = \left(\frac{-\cos\beta_1}{R_{vp_1}^2}\right) \underline{i}_X + \left(\frac{-\sin\beta_1}{R_{vp_1}^2}\right) \underline{i}_Y + \left(\frac{-\tan\alpha_1}{R_{vp_1}^2}\right) \underline{i}_Z$$

The triple scalar product is then found to be

$$\underline{h}_{\beta}^{(2)} \cdot \left[\underline{h}_{\alpha}^{(1)} \times \underline{h}_{\beta}^{(1)}\right] = \frac{\sin(\beta_1 - \beta_2)}{R_{vp_1}^{2} R_{vp_2} \cos\alpha_2}$$

For vehicles traveling in or near the ecliptic plane, α_1 and α_2 will be close to zero. Hence, the triple scalar product would be largest (minimum error sensitivity) if the two observed planets have a 90° separation as seen from the vehicle, and are as close to the vehicle as possible. Since this condition would rarely be satisfied in an actual mission, a trade-off between angular and distance separation would be necessary in choosing the best planets to observe.

In the case of sextant-type measurements, the equation relating vehicle position and the observable is

$$\cos\theta = \frac{\underline{R}_{vp} \cdot \underline{i}_s}{R_{vp}} \tag{27}$$

where $\underline{i}_s$ is a unit vector in the direction of the star having known direction components. The geometry vector in this case is

$$\underline{h}_{\theta} = \frac{1}{R_{vp} \sin\theta} \left(\underline{i}_s - \frac{\underline{R}_{vp} \cos\theta}{R_{vp}}\right) \tag{28}$$

Suppose the observation policy consists of measuring the included angles between a planet and two stars and the included angle between a second planet and a star. It is observed from (28) that

each $\underline{h}_\theta$ lies in the plane of the measurement, is perpendicular to the vehicle-planet line, and has a magnitude equal to $1/R_{pv}$. Again, for vehicles traveling in or near the ecliptic plane, the sufficient criteria for minimum error sensitivity are (1) close-by planets 90° apart as seen from the vehicle, and (2) two of the three stars should lie near the ecliptic plane and the third should lie near the ecliptic pole.

For either theodolite or sextant-type measurements, it is assumed that the sensor error (noise) consists of two additive components, one random and the other a bias, that is,

$$n(t_k) = n_r(t_k) + n_b \tag{29}$$

The random component is assumed to have zero mean, variance $\sigma_r^2(t_k)$, and be uncorrelated from one observation to the next, i.e.,

$$\begin{aligned} E\left[n_r(t_k) \right] &= 0 \\ E\left[n_r^2(t_k) \right] &= \sigma_r^2(t_k) \\ E\left[n_r(t_k) n_r(t_{k+i}) \right] &= 0 \end{aligned} \tag{30}$$

The assumption of uncorrelated random errors would appear to be justified for distrete-time observations sufficiently far apart, say 1 or 2 days. The bias component is considered a constant for a given sensor, but whose exact value after

calibration is uncertain. Statistics of this uncertainty on an ensemble basis are taken as

$$E\left[n_b\right] = 0$$
$$E\left[n_b^2\right] = \sigma_b^2 \tag{31}$$

The relationship between the angular measurement error, $\Delta\theta$, and the sensor noise, n, should be clarified at this point. For sextant measurements, the relationship is quite simple as shown in the sketch below

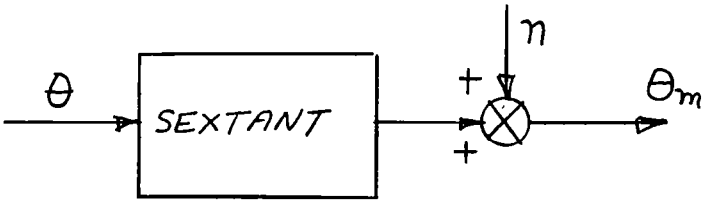

here,

$$\Delta\theta = \theta_m - \theta = n \tag{32}$$

For theodolite measurements, the physical connection between the theodolite and the inertial measurement unit needs to be taken into account as shown below

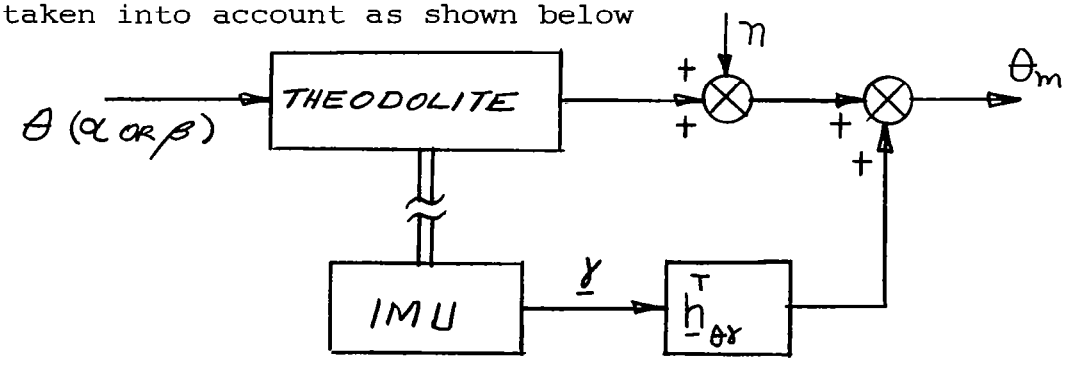

In this case, the platform misalignment $\underline{\gamma}$ contributes to the total measurement error.

$$\begin{aligned} \Delta\theta &= n + \left[\frac{\partial\theta}{\partial\gamma}\right]\underline{\gamma} \\ &= n + \underline{h}_{\theta\gamma}^{T}\,\underline{\gamma} \end{aligned} \tag{33}$$

The elements of $\underline{h}_{\theta\gamma}$ are readily found to be

$$\underline{h}_{\alpha\gamma}^{T} = (-\sin\beta \quad , \cos\beta \quad , 0) \tag{34}$$

$$\underline{h}_{\beta\gamma}^{T} = (\cos\beta\tan\alpha, \sin\beta\tan\alpha, -1) \tag{35}$$

3.4 Stellar-Monitored Inertial System

As previously mentioned, the effect of uncompensated gyro drift on the accuracy of a totally inertial navigation system could prove serious over the long operational times of low-thrust vehicles. In this section, we will examine the question of using external references, namely the stars, to measure and correct platform misalignment resulting from gyro drift. Again, we use the term "platform misalignment" in its general sense to mean either the physical displacement or computational uncertainty of the instrumented inertial axes relative to the reference inertial axes.

Platform Attitude Measurement

Since a star can be considered fixed in inertial space, the line-of-sight to the star as measured by a gimballed star

tracker integral with the inertial measurement unit provides information concerning platform attitude. In operation, of course, it is desired that the stellar monitor measure the angular deviation of the actual line-of-sight from the nominal computed direction; this quantity being a function of the platform misalignment. A single star tracker can only measure error components in a plane normal to the line-of-sight. Therefore, in order to determine the total misalignment angle γ, it is necessary to use either two stellar devices tracking different stars simultaneously, or one stellar device alternately tracking different stars.

Several ways to formulate and mechanize the stellar monitoring procedure are possible. For the purpose of illustration, suppose that two star trackers are employed, each tracker commanded to point along the nominal direction to the respective reference star. Since the platform would not generally be in alignment with the nominal inertial axes, the stars will not be centered in the field-of-view. Each tracker is then rotated in two planes to center the star - this rotation being measured by the two gimbal angles. The set of gimbal angles may then be used to compute the platform misalignment.

To illustrate how this procedure may be formulated, let (a_1^*, a_2^*, a_3^*) and (b_1^*, b_2^*, b_3^*) denote the known direction cosine sets of the two stars in the reference inertial frame

(X,Y,Z), and let (θ_1, ϕ_1) and (θ_2, ϕ_2) denote the measured gimbal angle sets of the two star trackers. Here, small gimbal angles are assumed as the tracker rotation is referenced to the nominal pointing direction. Choosing the x-axis of each tracker to be the line-of-sight axis, the nominal orientation of each tracker with respect to the platform is given by the direction cosine matrices

$$C_1 = \begin{bmatrix} a_1^* & a_2^* & a_3^* \\ a_{21} & a_{22} & a_{23} \\ a_{31} & a_{32} & a_{33} \end{bmatrix} ; \; C_2 = \begin{bmatrix} b_1^* & b_2^* & b_3^* \\ b_{21} & b_{22} & b_{23} \\ b_{31} & b_{32} & b_{33} \end{bmatrix} \tag{36}$$

All the direction cosines are to be considered known quantities whose values depend upon the particular mechanization of the star trackers. With the above definitions, a set of 2 determinant equations may be derived for each star tracker, e.g.,

$$\begin{vmatrix} \gamma_X & \gamma_Y & \gamma_Z \\ a_{21} & a_{22} & a_{23} \\ a_1^* & a_2^* & a_3^* \end{vmatrix} = \theta_1 \tag{37}$$

$$\begin{vmatrix} \gamma_X & \gamma_Y & \gamma_Z \\ a_{31} & a_{32} & a_{33} \\ a_1^* & a_2^* & a_3^* \end{vmatrix} = \phi_1 \tag{38}$$

These equations express the projection of $\underline{\Upsilon}$ in the plane normal to the star direction. The three components of $\underline{\Upsilon}$ may then be found from the complete set of 4 gimbal angle equations. In the ideal situation of no instrumentation errors, one of these equations is linearly dependent and, hence, could be eliminated from the computation. When errors are considered, the redundant information could be used to improve the accuracy of $\underline{\Upsilon}$ determination.

As an example of a somewhat trivial computation, if the two stars and the stellar monitor mechanization were chosen such that

$$C_1 = \begin{bmatrix} 0 & 1 & 0 \\ 1 & 0 & 0 \\ 0 & 0 & -1 \end{bmatrix} \quad ; \quad C_2 = \begin{bmatrix} 0 & 0 & 1 \\ 1 & 0 & 0 \\ 0 & 1 & 0 \end{bmatrix}$$

then the components of platform misalignment are simply

$$\Upsilon_X = \phi_1 = \phi_2$$

$$\Upsilon_Y = -\theta_2$$

$$\Upsilon_Z = \theta_1$$

Platform Attitude Correction

With a measure of the platform misalignment determined by the stellar monitor, it is possible to apply corrections to the platform in order to compensate for gyro drift. Assuming

a proportional plus integral correction procedure (Ref. 10), Equation (13) is modified to read

$$\dot{\underline{\gamma}} = \underline{\varepsilon}_g - K_p(\underline{\gamma} + \underline{\eta}) - K_I \int_o^t (\underline{\gamma} + \underline{\eta})\,dt \qquad (39)$$

where K_p and K_I are gain constants and $\underline{\eta}$ is the measurement error introduced by the stellar monitor. In reality, the measurement and correction of platform attitude may be described more accurately by a sampled-data process since the stellar information would likely be obtained at discrete intervals and the correction would likely be performed by a digital computer. For the puspose of simplicity, however, we will ignore the sampled-data aspects of the system. Furthermore, we will only consider a single-axis model of the correction process, thereby ignoring the cross-coupling which would likely exist in the stellar monitor error components. These assumptions are felt to be justified for the purpose of the following analysis, which is to describe the relative efffects of the gyro and stellar monitor errors on the corrected platform attitude.

The single-axis closed-loop correction process of (3a) is shown below in block diagram form

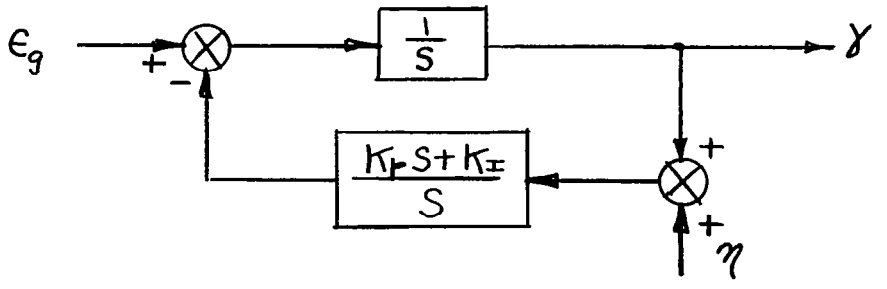

The output response of this system may be expressed in transform notation (initial conditions are taken as zero)

$$\gamma(S) = \frac{S}{S^2 + K_p S + K_I}\,\varepsilon_g(S) - \frac{K_p S + K_I}{S^2 + K_p S + K_I}\,\eta(S) \qquad (40)$$

If the input quantities, ε_g and η, are both constant, the steady-state response is

$$\gamma_{ss}\Big|_{\text{constant input}} = -\eta \qquad (41)$$

Hence, the proportional plus integral correction eliminates the unbounded effect of gyro drift on platform misalignment, substituting in its place the relatively small stellar monitor error. However, the effect of random inputs must also be studied.

For the purpose of the random input analysis, it will be assumed that both gyro drift and stellar monitor errors are adequately represented by "band-limited" white noise (exponential correlation function), i.e.,

$$P(\omega) = \frac{\frac{1}{\pi}\,\sigma^2\Omega}{\omega^2 + \Omega^2} \qquad (42$$

or

$$\phi(\tau) = \sigma^2 \varepsilon^{-\Omega|\tau|}$$

σ_g^2 and σ_η^2 will denote the variances of the random gyro drift and stellar monitor error, respectively, while Ω_g and Ω_η will

denote the reciprocals of the gyro and stellar monitor correlation time constants, respectively. Expressing the platform "torquing" gains in terms of a natural frequency ω_o and a damping ratio ζ

$$K_p = 2\zeta\omega_o$$

$$K_I = \omega_o^2 \tag{43}$$

the characteristic equation of the system may be written

$$S^2 + K_p S + K_I = (S + a\omega_o)(S + b\omega_o) \tag{44}$$

where

$$a = \zeta + \sqrt{\zeta^2 - 1}$$

$$b = \zeta - \sqrt{\zeta^2 - 1} \tag{45}$$

Since the gyro drift and stellar monitor error may be assumed uncorrelated with each other, the correlation function of Υ may be written as the sum of two independent terms

$$\phi_\Upsilon(\tau) = \phi_{\Upsilon g}(\tau) + \phi_{\Upsilon \eta}(\tau) \tag{46}$$

The contributions of gyro drift and stellar monitor error are found to be

$$\phi_{\gamma g}(\tau) = \sigma_g^2 \left\{ \frac{a\Omega_g}{\omega_o (b^2-a^2)(a^2\omega_o^2-\Omega_g^2)} \varepsilon^{-a\omega_o|\tau|} \right.$$

$$+ \frac{b\Omega_g}{\omega_o (a^2-b^2)(b^2\omega_o^2-\Omega_g^2)} \varepsilon^{-b\omega_o|\tau|} \qquad (47)$$

$$\left. - \frac{\Omega_g^2}{(a^2\omega_o^2-\Omega_g^2)(b^2\omega_o^2-\Omega_g^2)} \varepsilon^{-\Omega_g|\tau|} \right\}$$

$$\varphi_{\gamma\eta}(\tau) = \sigma_\eta^2 \left\{ \frac{\Omega_\eta \omega_o \left[1-(a+b)^2 \right]}{a(a^2-b^2)(a^2\omega_o^2-\Omega_\eta^2)} \varepsilon^{-a\omega_o|\tau|} \right.$$

$$+ \frac{\Omega_\eta \omega_o \left[1-a+b)^2 \right]}{b(b^2-a^2)(b^2\omega_o^2-\Omega_\eta^2)} \varepsilon^{-b\omega_o|\tau|} \qquad (48)$$

$$\left. + \frac{\omega_o^2 \left[\omega_o^2 - (a+b)^2 \Omega_\eta^2 \right]}{(a^2\omega_o^2-\Omega_\eta^2)(b^2\omega_o^2-\Omega_\eta^2)} \varepsilon^{-\Omega_\eta|\tau|} \right\}$$

These expressions apply to damping ratios less than or greater than unity, hence, a and b may be complex or real. For the purpose of this analysis, we will consider a damping ratio very near to unity, i.e.,

$$a \approx 1 + \Delta$$

$$b \approx 1 - \Delta$$

where $\Delta << 1$. Neglecting terms of order (Δ) and higher, equations (47) and (48) may be closely approximated by

$$\phi_{\gamma g}(\tau) = \sigma_g^2\left[\frac{\Omega_g(\omega_o^2+\Omega_g^2)}{\omega_o(\omega_o^2-\Omega_g^2)^2}\varepsilon^{-\omega_o|\tau|} - \frac{\Omega_g^2}{(\omega_o^2-\Omega_g^2)^2}\varepsilon^{-\Omega_g|\tau|}\right] \quad (49$$

$$\phi_{\gamma\eta}(\tau) = \sigma_\eta^2\left[\frac{3\Omega_\eta\omega_o(3\omega_o^2-\Omega_\eta^2)}{2(\omega_o^2-\Omega_\eta^2)^2}\varepsilon^{-\omega_o|\tau|} + \frac{\omega_o^2(\omega_o^2-4\Omega_\eta^2)}{(\omega_o^2-\Omega_\eta^2)^2}\varepsilon^{-\Omega_\eta|\tau|}\right] \quad (50)$$

Examination of (49) and (50) suggests that ω_o should be as large as possible in order to minimize the mean-squared platform misalignment. In the limit, as ω_o becomes infinite, we have

$$\lim_{\omega_o \to \infty} \phi_\gamma(\tau) = \sigma_\eta^2 \varepsilon^{-\Omega_\eta|\tau|} \quad (51)$$

which is equivalent to perfect tracking of the stellar monitor by the platform as was the case for constant error inputs. Again, the effect of gyro drift has been eliminated. Although infinite loop gains are impractical, the result depicted by (51) could be approached very closely by an appropriate choice of ω_o. To illustrate this, suppose that $\omega_o >> \Omega_g$ and $\omega_o >> \Omega_\eta$. Then, the mean-squared value of platform misalignment could be

approximated by

$$\sigma_\gamma^2 = \phi_{\gamma g}(o) + \phi_{\gamma \eta}(o)$$

$$= \frac{\sigma_g^2 \Omega_g}{\omega_o^3} + \sigma_\eta^2 \left(1 + \frac{9}{2} \frac{\Omega_\eta}{\omega_o}\right) \tag{52}$$

As a numerical example, we assume the values

Gyro drift:

$$\sigma_g = 10^{-8} \text{ rad/sec} \quad (0.002\ ^\circ/\text{hr})$$

$$\Omega_g = (3600)^{-1} \text{ rad/sec}$$

Stellar Monitor:

$$\sigma_\eta = 5 \times 10^{-5} \text{ rad} \quad (10 \text{ sec arc})$$

$$\Omega_\eta = (3600)^{-1} \text{ rad/sec}$$

Platform frequency:

$$\omega_o = (360)^{-1} \text{ rad/sec}$$

Substituting into (52), we have

$$\sigma_\gamma^2 = (0.013 + 36.2) \times 10^{-10}$$

$$\sigma_\gamma \approx 6 \times 10^{-5} \text{ rad}$$

The gyro drift is seen to contribute a negligible amount to the over-all error which is only slightly greater than the stellar monitor error. For this example, the correlation function of γ could be closely approximated by

$$\phi_\gamma(\tau) = \sigma_\eta^2 \left(1 + \frac{9}{2} \frac{\Omega_\eta}{\omega_o}\right) e^{-\Omega_\eta |\tau|}$$

$$= 36 \times 10^{-10} e^{-\frac{|\tau|}{3600}}$$

As a result of the above analysis, we will make the simplifying assumption that the corrected platform misalignment can be adequately represented (for the purpose of trajectory estimation) by the stellar monitor error. We further assume that the stellar monitor error consists of both a low-frequency and high-frequency component, each statistically independent, and each exponentially correlated. We have, then, for a single axis

$$-\gamma(t) = \eta(t) = \eta_\ell(t) + \eta_h(t) \tag{53}$$

$$\phi_{\eta,\ell}(\tau) = \sigma^2_{\eta,\ell} \varepsilon^{-\frac{|\tau|}{\tau_{\eta,\ell}}} \tag{54}$$

$$\phi_{\eta,h}(\tau) = \sigma^2_{\eta,h} \varepsilon^{-\frac{|\tau|}{\tau_{\eta,h}}} \tag{55}$$

3.5 Linearized Navigation Model

Having discussed the celestial-inertial navigation concept in terms of its separate parts, we may now consider the mathematical formulation of the complete systems concept as it pertains to estimating the trajectory state. The optimal estimation procedure to be described in the next section requires that the state variables of the system, and this includes all instrumentation errors that are time-correlated, be represented in the form of a linear dynamical model excited by a "white noise" input process. In this section, then, we present the

set of augmented state equations and celestial observation equations which describe this model.

Consider first the vehicle motion equations which have been given in the general nonlinear form by equation (4). Suppose that a solution of these equations, corresponding to a pre-specified thrust acceleration program and satisfying prescribed boundary conditions, has been obtained and is termed the reference solution. Under the assumption that all perturbing conditions are sufficiently small so that the actual trajectory does not deviate significantly from the reference trajectory, it is possible and convenient to describe the trajectroy state in terms of linear perturbation equations. Thus, the linearized differential equations of motion are written

$$\dot{\underline{r}}\ (t) = \underline{v}(t) \tag{55}$$

$$\dot{\underline{v}}\ (t) = G(t)\underline{r}(t) + \underline{z}(t) \tag{56}$$

where we define

$$\begin{bmatrix} \underline{r} \\ \underline{v} \\ \underline{z} \end{bmatrix} = \begin{bmatrix} \underline{R} - \underline{R}^* \\ \underline{V} - \underline{V}^* \\ \underline{a} - \underline{a}^* \end{bmatrix} \tag{57}$$

Here, $\underline{R}^*$, $\underline{V}^*$, and $\underline{a}^*$ are the known position, velocity, and acceleration time history as given by the reference solution. When the gravitational field present is primarily due to the Sun, we have from (6),

$$G = \left[\frac{\partial \underline{g}}{\partial \underline{R}}\right] = \begin{bmatrix} \frac{\mu_S}{R^5}(3X^2-R^2) & \frac{\mu_S}{R^5}\,3XY & \frac{\mu_S}{R^5}\,3XZ \\ \frac{\mu_S}{R^5}\,3XY & \frac{\mu_S}{R^5}\,(3Y^2-R^2) & \frac{\mu_S}{R^5}\,3YZ \\ \frac{\mu_S}{R^5}\,3XZ & \frac{\mu_S}{R^5}\,3YZ & \frac{\mu_S}{R^5}\,(3Z^2-R^2) \end{bmatrix} \tag{58}$$

where the partial derivative elements are to be evaluated at points along the reference trajectory.

Introducing the inertial measurement information, we have from (7) and (57)

$$\begin{aligned} \underline{a}(t)-\underline{a}^*(t) &= \left[\underline{a}_m(t) - \underline{a}^*(t)\right] - \Delta\underline{a}(t) \\ &= \underline{z}_m(t) - \underline{\varepsilon}_a(t) - \Lambda(t)\underline{\Upsilon}(t) \end{aligned} \tag{59}$$

Now, with reference to our previous discussion, the accelerometer error $\underline{\varepsilon}_a$ and the platform misalignment $\underline{\Upsilon}$ are each assumed to be made up of two independent additive components, one due to "low-frequency" random noise and the other due to relatively "high-frequency" random noise.

$$-\varepsilon_a(t) = \underline{\varepsilon}_\ell(t) + \underline{\varepsilon}_h(t) \tag{60}$$

$$-\underline{\Upsilon}(t) = \underline{\eta}_\ell(t) + \underline{\eta}_h(t) \tag{53}$$

Substituting from (59), and (60) and (53), equation (56) is modified to read

$$\dot{\underline{v}}(t) = G(t)\underline{r}(t) + \underline{z}_m(t) + \underline{\varepsilon}_\ell(t) + \underline{\varepsilon}_h(t) + \Lambda(t)\eta_\ell(t) + \Lambda(t)\eta_h(t) \tag{61}$$

In the case of error sources which have correlated noise characteristics, the optimal estimation procedure requires that these errors be estimated along with the position and velocity state vectors. Regarding the low-frequency error components in (61), the fact that we have assumed stationary, exponentially-correlated statistics allows the random error model to be described by constant coefficient, linear dynamical equations of the form

$$\dot{\underline{\varepsilon}}_\ell(t) = L_1\underline{\varepsilon}_\ell(t) + \underline{u}_1(t) \tag{62}$$

$$\dot{\underline{\eta}}_\ell(t) = L_2\underline{\eta}_\ell(t) + \underline{u}_2(t) \tag{63}$$

where L_1 and L_2 are (3 x 3) diagonal matrices,

$$L_1 = -\frac{1}{\tau_{a\ell}} \circ I \tag{64}$$

$$L_2 = -\frac{1}{\tau_{\eta\ell}} \circ I \tag{65}$$

and $\underline{u}_1$ and $\underline{u}_2$ are independent, zero-mean "white noise" inputs having covariance matrices

$$E\left[\underline{u}_1(t)\underline{u}_1^T(t)\right] = U_1 = \frac{2\sigma_{a\ell}^2}{\tau_{a\ell}} \cdot I \tag{66}$$

$$E\left[\underline{u}_2(t)\underline{u}_2^T(t)\right] = U_2 = \frac{2\sigma_{\eta\ell}^2}{\tau_{\eta\ell}} \cdot I \tag{67}$$

The quantities $(\sigma_{a\ell}^2, \tau_{a\ell})$ and $(\sigma_{\eta\ell}^2, \tau_{\eta\ell})$ are the variances and correlation times of the low-frequency components of the accelerometer and stellar monitor errors, respectively.

Although the high-frequency components of these errors are also considered to be exponentially-correlated, if the respective correlation times are significantly smaller than the sampling interval of the celestial position fixes, we may make the simplifying assumption that these components can be represented as "white noise" (see eq. (16)). That is,

$$\underline{\varepsilon}_h(t) = \underline{u}_3(t) \tag{68}$$

$$\underline{\eta}_h(t) = \underline{u}_4(t) \tag{69}$$

where $\underline{u}_3$ and $\underline{u}_4$ are independent, zero-mean "white noise" inputs having covariance matrices

$$E\left[\underline{u}_3(t)\underline{u}_3^T(t)\right] = U_3 = 2\sigma_{ah}^2\,\tau_{ah} \cdot I \tag{70}$$

$$E\left[\underline{u}_4(t)\underline{u}_4^T(t)\right] = U_4 = 2\sigma_{\eta h}^2\,\tau_{\eta h} \cdot I \tag{71}$$

The final state equation to be considered is due to the bias-type celestial observation error. This may be expressed simply as

$$\dot{\underline{n}}_b = 0 \tag{72}$$

The dimension of $\underline{n}_b$ is 2 in the case of a theodolite-type measurement and 1 in the case of a sextant-type measurement.

For the purpose of notational convenience, we define an augmented state vector

$$\underline{x} = \begin{bmatrix} \underline{r} \\ \underline{v} \\ \underline{\varepsilon}_\ell \\ \underline{\eta}_\ell \\ \underline{n}_b \end{bmatrix} \tag{73}$$

and the "white noise" input vector

$$\underline{u} = \begin{bmatrix} \underline{u}_1 \\ \underline{u}_2 \\ \underline{u}_3 \\ \underline{u}_4 \end{bmatrix} \tag{74}$$

The augmented set of differential equations may then be expressed as

$$\dot{\underline{x}}(t) = A(t)\underline{x}(t) + B(t)\underline{u}(t) + D\underline{z}_m(t) \tag{75}$$

where the coefficient matrices in partitioned form are

$$A = \begin{bmatrix} 0 & I & 0 & 0 & 0 \\ G & 0 & k_T I & \Lambda & 0 \\ 0 & 0 & L_1 & 0 & 0 \\ 0 & 0 & 0 & L_2 & 0 \\ 0 & 0 & 0 & 0 & 0 \end{bmatrix} \tag{76}$$

$$B = \begin{bmatrix} 0 & 0 & 0 & 0 \\ 0 & 0 & k_T I & \Lambda \\ I & 0 & 0 & 0 \\ 0 & I & 0 & 0 \\ 0 & 0 & 0 & 0 \end{bmatrix} \tag{77}$$

$$D = \begin{bmatrix} 0 \\ I \\ 0 \\ 0 \\ 0 \end{bmatrix} \tag{78}$$

The factor k_T in (76) and (77) is introduced to account for the assumption that acceleration measurements (and, hence, accelerometer errors) are not in effect during nominal coast periods. This factor is then defined as

$$k_T = \begin{cases} 1 & \text{if } \underline{a}^* \neq 0 \\ 0 & \text{if } \underline{a}^* = 0 \end{cases}$$

Employing state transition concepts, the solution of (76) can be written in the form

$$\begin{aligned} \underline{x}(t) &= \Phi(t,t_o)\underline{x}(t_o) + \int_{t_o}^{t} \Phi(t,\tau)B(\tau)\underline{u}(\tau)d\tau \\ &+ \int_{t_o}^{t} \Phi(t,\tau)D\underline{z}_m(\tau)d\tau \end{aligned} \tag{79}$$

where $\Phi(t,t_o)$ is the transition matrix of the augmented system whose solution is obtained from the matrix differential equation

$$\dot{\Phi}(t,t_o) = A(t)\Phi(t,t_o) \tag{80}$$

with initial conditions $\Phi(t_o,t_o) = I$. An important property of this matrix is

$$\begin{aligned} \Phi(t,\tau) &= \Phi(t,t_o)\Phi(t_o,\tau) \\ &= \Phi(t,t_o)\Phi^{-1}(\tau,t_o) \end{aligned} \tag{81}$$

If t_{k-1} and t_k denote any two successive time instants in the interval (t_o, t_f) then the generalized state transition equation may be written

$$\underline{x}(t_k) = \Phi(t_k, t_{k-1})\underline{x}(t_{k-1}) + \underline{q}(t_k, t_{k-1}) + \Delta\underline{x}_m(t_k, t_{k-1}) \tag{82}$$

where, for notational convenience, we define

$$\underline{q}(t_k, t_{k-1}) = \int_{t_{k-1}}^{t_k} \Phi(t_k, \tau) B(\tau) \underline{u}(\tau) d\tau \tag{83}$$

$$\Delta\underline{x}_m(t_k, t_{k-1}) = \int_{t_{k-1}}^{t_k} \Phi(t_k, \tau) D\underline{z}_m(\tau) d\tau$$

$$= \begin{bmatrix} \Delta\underline{r}_m(t_k, t_{k-1}) \\ \Delta\underline{v}_m(t_k, t_{k-1}) \\ 0 \\ 0 \\ 0 \end{bmatrix} \tag{84}$$

In (85), $\Delta\underline{r}_m$ and $\Delta\underline{v}_m$ are the measured changes in position and velocity due to the thrust acceleration acting in the interval (t_{k-1}, t_k).

To complete the formulation of the navigation model, it is necessary to relate the space angle observations to the state variables. With reference to the discussion of celestial

measurements and errors presented in Section 3.3, the first-order difference between the measured observation vector $\underline{\theta}_m$ and the reference value $\underline{\theta}^*$ may be derived as a linear function of $\underline{x}$ plus additive terms due to the celestial sensor and stellar monitor random errors. This may be expressed as

$$\begin{aligned} \underline{y}_m &= \underline{\theta}_m - \underline{\theta}^* \\ &= M\underline{x} + \underline{n} \end{aligned} \tag{85}$$

where the partitioned form of M is

$$M = \left[H \,\vdots\, 0 \,\vdots\, 0 \,\vdots\, -H_1 \,\vdots\, I \right] \tag{86}$$

Recall that we have considered the possibility of planetary observations using either a theodolite or a sextant. For these two cases we have:

Theodolite-type measurement

$$H = \left[\underline{h}_\alpha \quad \underline{h}_\beta \right]^T \tag{87}$$

$$H_1 = \left[\underline{h}_{\alpha\gamma} \quad \underline{h}_{\beta\gamma} \right]^T \tag{88}$$

$$\underline{n} = -H_1 \underline{u}_4 + \underline{n}_r \tag{89}$$

Here, H and H_1 are each (2 x 3) matrices whose elements are given by equations (25), (26), (34) and (35). $\underline{n}_r$ is a 2-vector consisting of the random errors (attributed to the theodolite

device) in measuring the planetary latitude and longitude angles α and β. The errors attributed to the platform misalignment (or stellar monitor error) are accounted for by the H_1 matrix.

Sextant-type measurement

$$H = h_\theta^T \tag{90}$$

$$H_1 = 0 \tag{91}$$

$$\underline{n} = n_r \tag{92}$$

Here, H is a (1 x 2) matrix or row vector whose elements may be found from equation (28), and n_r is the random error in measuring the star-planet included angle θ.

The celestial-inertial navigation model described above may be summarized in terms of its input-output relationships by the following block diagram

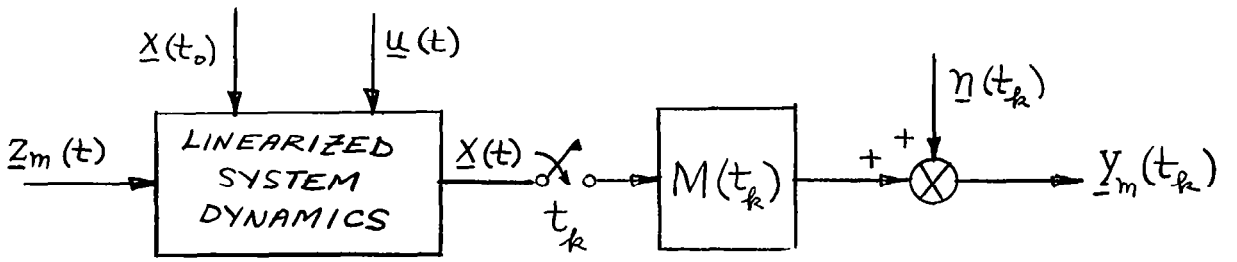

Information obtained by direct measurement is available to the system at the input through the continuous inertial acceleration measurements $\underline{z}_m(t)$, and at the output through the discrete-time celestial angle measurements $\underline{y}_m(t_k)$. The input $\underline{u}(t)$ is a "white noise" random process with zero mean and covariance matrix

$$U = E\left[\underline{u}(t)\underline{u}^T(t)\right] = \begin{bmatrix} U_1 & 0 & 0 & 0 \\ 0 & U_2 & 0 & 0 \\ 0 & 0 & U_3 & 0 \\ 0 & 0 & 0 & U_4 \end{bmatrix} \tag{93}$$

The output measurement error $\underline{n}(t_k)$ is a zero-mean random variable uncorrelated from one observation to the next and has a covariance matrix (a scalar in the case of sextant measurements)

$$N(t_k) = E\left[\underline{n}(t_k)\underline{n}^T(t_k)\right] \tag{94}$$

Finally, the initial state $\underline{x}(t_o)$ is a zero-mean random vector with a covariance matrix

$$P(t_o) = E\left[\underline{x}(t_o)\underline{x}^T(t_o)\right]$$

$$= \left[\begin{array}{cc|ccc} P_{rr} & P_{rv} & 0 & 0 & 0 \\ P_{rv}^T & P_{vv} & 0 & 0 & 0 \\ \hline 0 & 0 & P_{\varepsilon\varepsilon} & 0 & 0 \\ 0 & 0 & 0 & P_{\eta\eta} & 0 \\ 0 & 0 & 0 & 0 & P_{bb} \end{array}\right]_{t=t_o} \tag{95}$$

The upper (6 x 6) covariance matrix in (95) is associated with the initial position and velocity deviations from the reference trajectory. The other covariance matrices are associated with the time-correlated instrumentation errors and are given by

$$P_{\varepsilon\varepsilon}(t_o) = E\left[\underline{\varepsilon}_\ell(t_o)\underline{\varepsilon}_\ell^T(t_o)\right]$$

$$= \sigma_{a\ell}^2 \cdot I \tag{96}$$

$$P_{\eta\eta}(t_o) = E\left[\underline{\eta}_\ell(t_o)\underline{\eta}_\ell^T(t_o)\right]$$

$$= \sigma_{\eta\ell}^2 \cdot I \tag{97}$$

$$P_{bb}(t_o) = E\left[\underline{n}_b\,\underline{n}_b^T\right]$$

$$= \sigma_b^2 \cdot I \tag{98}$$

Finally, the covariance of $\underline{q}(t_k, t_{k-1})$, which has been defined by (83), can be computed from the integral equation

$$Q(t_k,t_{k-1}) = E\left[\underline{q}(t_k,t_{k-1})\ \underline{q}^T\ (t_k,\ t_{k-1})\right]$$

$$= \int_{t_{k-1}}^{t_k} \Phi(t_k,\tau)B(\tau)UB^T(\tau)\Phi^T(t_k,\tau)\,d\tau \qquad (99)$$

3.6 Optimal State Estimation

Having described the celestial-inertial navigation system in terms of its explicit dynamical model and probabilistic aspects, we now consider the problem of state estimation. Since the current state of the system cannot be determined precisely, we seek a method of processing the available observational data so that the "best" estimate of the state is obtained. The meaning of "best" in this context is related to the particular optimality criterion chosen. Quite generally, one would like to minimize some function of the error in the estimate. Specifically, one would like to choose an error function which is physically meaningful and yet leads to an easily implemented estimation procedure, e.g., linear processing of the observational data.

It has been shown by several investigators of the general estimation problem that the unrestricted optimal estimate of a linear system subject to Gaussian statistics is of a linear form. In the event that Gaussian statistics cannot be

assumed, the linear estimate is still optimal if the criterion chosen is to minimize the expected value of a quadratic error function. This is the vector equivalent of the familiar mean-squared error criterion. Given this general result, Kalman proceeded to treat the estimation problem from a dynamic filtering point of view (Ref. 1). The Kalman filter theory has been applied extensively to the space navigation problem, with particular emphasis placed on "free-fall" trajectories and output measurements related to the system state through linear algebraic equations (Refs. 2,3,4,5). The present problem differs from these applications mainly in that we are dealing with thrusted trajectories and measurements of the system input as well as its output. Nevertheless, the basic Kalman filter theory is applicable to the present problem and will, therefore, be utilized.

The notation used in the estimation equations is defined as follows:

t_k, t_{k-1}	successive time instants at which celestial observations are obtained
$\hat{\underline{x}}'(t_k)$	estimate of $\underline{x}(t_k)$ prior to including the current observation
$\hat{\underline{x}}(t_k)$	estimate of $\underline{x}(t_k)$ after including the current observation
$P(t_k)$	covariance matrix of the error in the estimate $\tilde{\underline{x}}(t_k) = \underline{x}(t_k) - \hat{\underline{x}}(t_k)$, $E\left[\tilde{\underline{x}}(t_k)\tilde{\underline{x}}^T(t_k)\right]$
$K(t_k)$	optimal filter matrix for weighting the current observation

With the above definitions, the estimation procedure may be described by the following recursion equations:

Extrapolated Estimate

$$\hat{\underline{x}}'(t_k) = \Phi(t_k,t_{k-1})\hat{\underline{x}}(t_{k-1}) + \Delta\underline{X}_m(t_k,t_{k-1}) \tag{100}$$

Extrapolated Error Covariance

$$P'(t_k) = \Phi(t_k,t_{k-1})P(t_{k-1})\Phi^T(t_k,t_{k-1}) + Q(t_k,t_{k-1}) \tag{101}$$

Optimal Filter

$$K(t_k) = P'(t_k)M^T(t_k)\left[M(t_k)P'(t_k)M^T(t_k) + N(t_k)\right]^{-1} \tag{102}$$

New Estimate

$$\hat{\underline{x}}(t_k) = \hat{\underline{x}}'(t_k) + K(t_k)\left[\underline{y}_m(t_k) - M(t_k)\hat{\underline{x}}'(t_k)\right] \tag{103}$$

New Error Covariance

$$P(t_k) = P'(t_k) - K(t_k)M(t_k)P'(t_k) \tag{104}$$

In the linear estimation equation (103), the quantity $M(t_k)\hat{\underline{x}}'(t_k)$ is the estimated value of the observation $\underline{y}_m(t_k)$, this estimate being made just prior to taking the observation. This quantity is then compared with the actual data and the residual is weighted by the filter K to produce an incremental correction to the previous estimate of the state. The new

error covariance matrix is computed, and the entire sequential estimation procedure is repeated at the next observation time. It is noted that, in the interval (t_{k-1}, t_k), information concerning the position and velocity state is obtained through the continuous inertial acceleration measurements. This information appears as $\Delta\underline{x}_m(t_k,t_{k-1})$ in the discrete-time estimation procedure described above. This additive term in (100) is the essential difference between "free-fall" trajectory estimation and thrusted trajectory estimation employing acceleration measurements.

If an estimate of the state is desired at points between the celestial observation times, it may be obtained from the equation (with $t_{k-1} \leq t \leq t_k$)

$$\hat{\underline{x}}(t) = \Phi(t,t_{k-1})\hat{\underline{x}}(t_{k-1}) + \int_{t_{k-1}}^{t} \Phi(t,\tau)D\underline{z}_m(\tau)d\tau \qquad (105)$$

or, alternatively, from the differential equation

$$\frac{d\hat{\underline{x}}}{dt} = A(t)\hat{\underline{x}}(t) + D\underline{z}_m(t) \qquad (106)$$

with the initial condition, $\hat{\underline{x}}(t_{k-1})$. The error covariance matrix corresponding to this estimate may be computed from the equation

$$P(t) = \Phi(t,t_{k-1})P(t_{k-1})\Phi^T(t,t_{k-1}) + Q(t,t_{k-1}) \qquad (107)$$

or alternatively, from the differential equation

$$\dot{P}(t) = A(t)P(t) + P(t)A^T(t) + B(t)UB^T(t) \tag{108}$$

with the initial condition, $P(t_{k-1})$. It can be readily shown that the covariance matrix of "white noise" effects, Q, can be computed from the differential equation

$$\dot{Q}(t,t_{k-1}) = A(t)Q(t,t_{k-1}) + Q(t,t_{k-1})A^T(t) + B(t)UB^T(t) \tag{109}$$

with the initial condition, $Q(t_{k-1}, t_{k-1}) = 0$. This is a more convenient method of computing Q than was previously given by the integral form, equation (99).

The estimation equations given above may be simplified considerably by taking into account the partitioning of the state variables as defined in the previous section of this report. Appendix B summarizes the partitioned form of the estimation equations.

Although the estimation procedure has been formulated under the assumption of linear perturbations about a prespecified reference trajectory, this need not be a restriction in the actual implementation of the procedure. In fact, if linearization is to be employed, it is clear that the correct approach would be to linearize about the estimated trajectory since this trajectory is, on the average, closer to the actual trajectory than is the reference. It is true that the difference between the two linearization procedures would not be

significant if the actual trajectory deviations from the reference remain very small. In many cases this would be so, however, the possibility of unexpected large perturbations does exist. The navigation system should, therefore, be designed to handle this possibility.

It is readily deduced from the form of the estimation equations that the computational procedure could be implemented in terms of the original state variables rather than their deviations. Thus, for example, in the case of position we may write the estimation equation as

$$\hat{\underline{R}}(t_k) = \hat{\underline{R}}'(t_k) + K_r(t_k)\left[\underline{\theta}_m(t_k) - \hat{\underline{\theta}}'(t_k)\right]$$

where it is seen that the incremental correction is still of the linear form. In this case, the filter K_r weights the difference between the measured and estimated values of the observable space angles rather than their deviations. In computing the estimated angle, one would use the nonlinear geometric equations relating $\underline{R}$ and $\underline{\theta}$, and evaluate this equation at $\hat{\underline{R}}'(t_k)$. Similarly, in the time interval between space angle observations, position and velocity would be obtained by integrating the nonlinear equations of motion. Of course, the computation of P, M and K still requires the linearization approach, however, the evaluation of these matrices would be based on the current best estimate of the trajectory.

4. DESCRIPTION OF PERFORMANCE ANALYSIS PROGRAM

It is noted from the previous discussion that the optimal estimation procedure generates its own performance analysis. That is to say, the error covariance matrix P required in the computation of the filter matrix K is a measure of the average, or ensemble, performance of the system. Specifically, the diagonal elements of P represent the mean-square uncertainty in estimating the state variables of the system. The solution for P, given by the recursion equations (101), (102) and (104), is seen to depend upon the initial state uncertainty, the transition matrix of the reference trajectory, the observation types and schedules, and the instrumentation noise characteristics. Since these parameters appear in the solution in a fairly complex manner, very little could be said about performance without a certain amount of numerical experimentation. Accordingly, a digital computer program was developed to facilitate a numerical performance evaluation of the celestial-inertial navigation concept. In this section, we describe the main features and scope of the performance simulation.

4.1 Reference Trajectories

Application of the navigation theory is made to the midcourse, or heliocentric, phase of low-thrust interplanetary missions. The mission trajectory, then, begins with the Earth's orbital conditions and terminates at the heliocentric position of the target planet. Both rendezvous and fly-by missions are

considered. Orbital velocities of the vehicle and planet are matched in the case of rendezvous missions. Also considered are both variable thrust and constant thrust modes of propulsion. For each kind of mission and propulsive mode, the reference trajectories employed in this study are of an optimal type. That is, for a given target planet, terminal conditions and flight time, the thrust program is chosen so as to minimize the required propellant expenditure.

The simulation may be described as a three-dimensional performance analysis utilizing two-dimensional reference trajectories. That is, the reference trajectories are computed in the ecliptic plane (X,Y) under the assumption of coplanar planetary orbits, however, the state variables of the problem include the out-of-plane Z-components. The only reason for this simplification in vehicle and planetary motion was the availability of the digital computer program needed to generate the reference trajectories. This FORTRAN program, made available to IITRI by the Lewis Research Center, is restricted to coplanar trajectories. It is important to note that, since the planets of the solar system lie fairly close to the ecliptic plane, the restriction of coplanar heliocentric trajectories has only a minor or negligible effect on the results of the navigation system performance.

The Lewis trajectory optimization program is based on the indirect method of the variational calculus. Numerical

integration is performed by a fourth-order Runge-Kutta routine with provision for step size control based on truncation error checks. Converged tragectories are obtained by a multi-dimensional Newton-Raphson iteration scheme. No operations manual for this computer program exists, however, the mathematical formulation of the optimization problem has been published (Ref. 9).

4.2 Celestial Observation Policy

Space angle measurements for the purpose of position fixes are restricted to observations of the launch and target planets. A previous study of midcourse navigation for Venus and Mars missions has shown that additional observations of the Sun or other planets does not significantly improve navigation accuracy (Ref. 4). Although this conclusion may not be true for all missions, it is thought to be general enough for the purpose of the present performance analysis. Both theodolite and sextant-type measurements are included as separate options in the computer program, however, only the theodolite (line-of-sight) measurements will be considered when discussing numerical results.

Simultaneous observations of the launch and target planets are assumed for analysis purposes, and hence, yield a complete position fix (in practice, the observations would likely be made several minutes apart). The interval between observation times is held constant throughout the flight, but its value may be chosen arbitrarily. The one exception to this

schedule occurs in constant thrust flights with a coast period. In this case, observations are also made at the beginning and end of the coast period.

Finally, the random observation errors are assumed to have constant variances and be mutually uncorrelated, i.e., $N(t_k)$ in equation (102) is a constant, diagonal matrix.

4.3 The Computer Program

The method of solution decided upon was to integrate the reference trajectory and linear perturbation equations simultaneously (the alternative would be to compute the reference separately and store this information on tape). In developing the performance analysis program, then, the Lewis trajectory program served as the starting point. This program was first modified in a number of ways including the re-allocation and enlargement of variable arrays and common storage blocks, and the elimination of the Newton-Raphson iteration routine designed to produce "converged" trajectories. In eliminating the iteration routine, it is assumed that the starting conditions necessary to regenerate a "converged" trajectory of interest are available from some other source (e.g., the original Lewis program).

Figure 4 is a block diagram description of the computer program, showing the function of principal subroutines and the flow of computations. The subroutine EQUATE sets up the differential equations of the problem. These include (1) the

nonlinear equations of motion and the Lagrange multiplier equations which define the optimum thrust program, (2) the linear state transition equations Φ, and (3) the "white noise" covariance equations Q. The partitioned form of the differential equations for Φ and Q are given in Appendix B. The subroutine EQUATE is called from RUNGK which performs the numerical integration. In computing Φ and Q, the numerical integration proceeds in a step-wise manner rather than continuously. That is, the initial conditions Φ=I and Q=0 are reset after each celestial observation time t_k. This procedure avoids the indirect and lengthy computation for $\Phi\ (t_k, t_{k-1})$ and $Q\ (t_k, t_{k-1})$ which would be required if the integration ran continuously. The subroutine NAVIG, called at each observation time, computes the observation matrix M, the filter matrix K and the estimation error covariance matrix P. Navigation performance results are then printed, control is returned to RUNGK, and the cycle is repeated over the next observation interval.

Besides the current error covariance, another useful measure of navigation performance is the terminal error covariance predicted, or extrapolated, on the basis of current information. This may be expressed as

$$P(t_f|t_k) = E\left\{ \left[\underline{x}(t_f)-\hat{\underline{x}}(t_f|t_k)\right] \left[\underline{x}(t_f)-\hat{\underline{x}}(t_f|t_k)\right]^T \right\}$$

$$= \Phi\ (t_f,t_k)P(t_k)\ \Phi^T(t_f,t_k)+Q(t_f,t_k) \qquad (110)$$

where $\hat{\underline{x}}\ (t_f|t_k)$ is defined as

$$\hat{\underline{x}}\ (t_f|t_k) = \Phi\ (t_f,t_k)\ \hat{\underline{x}}\ (t_k) + \Delta\underline{x}_m(t_f,t_k) \qquad (111)$$

The meaning of this matrix should be clarified. It is not directly associated with the covariance of the error in predicting the terminal state. Since $\Delta\underline{x}_m(t_f,t_k)$ is a quantity to be measured in the future by the inertial instrumentation, equation (111) is not a prediction equation but, rather, it represents the estimate of the state that would exist at t_f assuming that no further celestial position fixes are taken. $P(t_f|t_k)$, then, represents the current (conditional) prediction of the uncertainty in the terminal state. The diagonal elements of this matrix decrease in magnitude with each successive celestial fix, and finally approach the corresponding values of $P(t_f)$.

The subroutine TARGET shown in Figure 4 provides for the computation of $P(t_f|t_k)$ on an <u>optional</u> basis. The algorithm for computing this matrix makes use of the following recursion relationships

$$\Phi\ (t_f,t_k) = \Phi(t_f,t_{k-1})\ \Phi^{-1}(t_k,t_{k-1}) \qquad (112)$$

$$Q\ (t_f,t_k) = Q(t_f,t_{k-1}) - \Phi(t_f,t_k)\ Q(t_k,t_{k-1})\Phi^{T}(t_f,t_k) \qquad (113)$$

where it is necessary to have available the matrices $\Phi(t_f,t_o)$ and $Q(t_f,t_o)$ which relate the initial and terminal state conditions. Hence, when using TARGET, it is first necessary to obtain these matrices by running through the computations indicated

above the dotted line in Figure 4. The integration in this case is continuous rather than step-wise. When the terminal time is reached, $\Phi(t_f,t_o)$ and $Q(t_f,t_o)$ are stored by the subroutine TERCON. The program then proceeds to compute the navigation performance results as previously described. It should be noted that only the position and velocity components of $P(t_f|t_k)$ are actually computed.

For convenience in presenting numerical results, the statistical data are given only in terms of the magnitudes of vector-valued quantities such as position, velocity, etc. Hence, we define the following root-mean-square measures of the uncertainty in estimating the state variables:

Position Uncertainty

$$\tilde{r}_{rms} = \sqrt{E\,\tilde{x}_1^2 + E\,\tilde{x}_2^2 + E\,\tilde{x}_3^2}$$
$$= \sqrt{\text{Trace } P_{rr}}$$

Velocity Uncertainty

$$\tilde{v}_{rms} = \sqrt{E\,\tilde{x}_4^2 + E\,\tilde{x}_5^2 + E\,\tilde{x}_6^2}$$
$$= \sqrt{\text{Trace } P_{vv}}$$

Accelerometer Error Uncertainty (Low frequency component)

$$\tilde{a}_{rms} = \sqrt{E\,\tilde{x}_7^2 + E\,\tilde{x}_8^2 + E\,\tilde{x}_9^2}$$
$$= \sqrt{\text{Trace } P_{\varepsilon\varepsilon}}$$

Stellar Monitor Error Uncertainty (Low frequency component)

$$\tilde{\eta}_{rms} = \sqrt{E\,\tilde{x}_{10}^2 + E\,\tilde{x}_{11}^2 + E\,\tilde{x}_{12}^2}$$
$$= \sqrt{\text{Trace } P_{\eta\eta}}$$

5. RESULTS OF PERFORMANCE ANALYSIS

5.1 Reference Trajectory Data

Navigation performance results have been obtained for five low-thrust interplanetary missions whose characteristics differ in terms of the target planet, terminal conditions, thrust mode, and flight time. These missions are

(1) Mars rendezvous - 205.4 days

(2) Mars rendezvous - 181.6 days

(3) Venus rendezvous - 120 days

(4) Mars fly-by - 120 days

(5) Jupiter fly-by - 360 days

It is to be recalled that only the heliocentric (Earth-planet transfer) phase of these missions are considered here. Table I lists several descriptive conditions of these reference trajectories. The two Mars rendezvous flights employ an optimal constant thrust program with and without a coast period. Propulsion parameters assumed here are a specific impulse of 8000 seconds and an initial thrust acceleration of 0.981×10^{-3} m/sec^2 or 10^{-4}g. The remaining three trajectories employ an optimal variable thrust program. In the case of the Venus rendezvous, acceleration reaches a minimum value about mid-flight and thereafter increases to a terminal value approximately equal to the initial acceleration. In the case of the fly-by trajectories, acceleration decreases monotonically with time reaching a zero value at t_f. The hyperbolic approach velocities for the Mars

and Jupiter fly-bys are 12.6 km/sec and 28.3 km/sec, respectively. Also shown in Table I are the values of $\int a^2 \, dt$ which are somewhat analogous to ΔV requirements for ballistic flight in that they determine propellant expenditure and payload capability for a given vehicle system (see Section 2.1 of this report or Ref. 8).

Reference trajectory diagrams are given in Figures 5 through 9. These diagrams show the Earth, vehicle, and target planet positions at various times in the flight. Also shown is the direction of applied thrust.

The 205.4 day Mars rendezvous trajectory will be used as a primary example to illustrate the performance of the navigation scheme for different error parameter assumptions. This reference trajectory was chosen for this purpose because a constant thrust rendezvous mission including a coast period is considered a more practical example of electric propulsion application. Results for the remaining reference trajectories listed above will be summarily described, and will serve to broaden the conclusions to be drawn from this performance analysis.

5.2 Nominal Parameter Assumptions

Nominal values of the error model parameters are listed in Table II. The error magnitudes are given in terms of their standard deviation or RMS values. Initial velocity uncertainty is taken as 5 m/sec in each of the X, Y and Z components which

are assumed to be mutually uncorrelated. The initial position uncertainty is taken as zero (the effect of reasonable position errors is small in comparison with the effect of the velocity error assumed). The low frequency component of the accelerometer error is assumed to be a constant bias for any one flight (infinite correlation time) having an ensemble average of 10^{-6} m/sec^2. This error magnitude is about 0.1 percent of the acceleration level to be measured. This same magnitude is assumed for the high frequency error component which has a correlation time of 30 minutes. All optical instrumentation errors are assumed 10 seconds of arc. A 30 minute correlation time is taken for the stellar monitor error, whereas the planet sensor, or theodolite, error is assumed uncorrelated between observations taken at 2 day intervals.

The nominal parameter values were chosen somewhat arbitrarily for the purpose of example; however, they are considered reasonably representative of actual system errors that may be expected. In any case, the effect of changes in these parameter values will be discussed.

5.3 Navigation Performance for Mars Rendezvous Mission

In this section, we discuss the performance results obtained for navigating along the 205.4 day Mars rendezvous trajectory which is shown in Figure 5. Unless otherwise specified, the system parameters have the nominal values given in Table II.

For reference purposes, let us first consider the performance of the stellar monitored inertial system alone. Figures 10 (a) and (b) show the effects of individual system errors on the accuracy of position and velocity estimation in the absence of planetary observations. These results are obtained from the estimation covariance equations with $N(t_k)$ set equal to a very large value, which is equivalent to not taking planetary sightings. It is seen that the initial velocity uncertainty and the accelerometer bias have about the same effect on the terminal state uncertainty, which is on the order of 200,000 km and 30 m/sec. The error buildup due to the accelerometer bias is, of course, much slower. During the first 40 days of flight, the initial velocity uncertainty is the predominant cause of navigation inaccuracy. The high frequency accelerometer error, although having the same magnitude as the bias error, is only about $1/40^{th}$ as effective as the latter in its contribution to navigation inaccuracy. The stellar monitor error has a completely negligible effect on the inertially measured position and velocity. This error cannot be ignored, however, as far as its effect on planet line-of-sight measurements is concerned since these measurements are assumed to be referenced to the coordinate frame established by the stellar monitor.

Performance results of the optimal celestial-inertial navigation procedure are presented in Figures 11 (a) - (d).

Figure 11 (a) compares the position uncertainty time histories for inertial-only, celestial-only, and celestial-inertial measurements. The inertial measurement curve is the combined result of the individual error effects given in Figure 10 (a). The celestial measurement curve depicts the position determination accuracy available from a complete and independent position fix at points along the trajectory. The celestial position information is not particularly good, yielding position uncertainties ranging from 7000-27,000 km. However, beyond 20 days of flight, it is far better than the inertially determined position. The shape of the celestial position fix curve is influenced by the distance and angular intersection of the vehicle-Earth and vehicle-Mars vectors. Although Earth and Mars, respectively, are closest (10^6km) to the vehicle at the first and last observation points, the best accuracy is attained at mid-flight.

The performance improvement offered by optimal processing of both celestial and inertial information is clearly indicated by the lower curve of Figure 11 (a). Here, position uncertainty is held below 4500 km throughout the flight. The terminal uncertainty is only 500 km - almost three orders-of-magnitude below that obtained with only inertial measurements. The largest components of position uncertainty lie in the plane of motion. The out-of-plane component never exceeds 500 km, and the average value over the flight is much less than this.

Figure 11 (b) shows the time history of the velocity estimate uncertainty for both inertial and celestial-inertial measurements. As in the case of position, the performance improvement due to the addition of celestial information is quite significant. The five planetary observations taken during the first 10 days of flight reduce the velocity uncertainty from 8.66 m/sec to 1.3 m/sec. The upturn in the curve at this point is due to the effect of accelerometer errors which are now becoming significant (see Figure 10b). This trend is then damped by the additional celestial information. Velocity uncertainty is kept below 1 m/sec after 70 days, and reduces to a value of only 0.25 m/sec at the end of the flight.

It is recalled that accelerometer bias is being estimated along with position and velocity. Figure 11 (c) shows the time history of the uncertainty in estimating this quantity. Knowledge of the accelerometer bias is significantly improved as a result of celestial information. After 100 days, the bias uncertainty has been reduced by a factor of 16, and then further reduced by a factor of 2 during the next 100 days of flight. Even though the accelerometer bias is not in effect during the coast period (52-149 days), celestial information obtained during this time does allow continuing improvement in its estimation. This is akin to estimating the value of a step function input to a system after the input has been removed - a procedure which is made possible by measurements of the system response.

The expected asymptotic behavior of this procedure as time elapses is in evidence in Figure 11 (c).

Figure 11 (d) shows a time history of the predicted terminal state uncertainty, both position and velocity. One may read this figure as the reduction of terminal uncertainty resulting from successive planetary observations. It is noted that the first observation taken at 2 days reduces the position uncertainty by 100,000 km and the velocity uncertainty by 12 m/sec. This same reduction then occurs again after 40 days of flight. At 120 days, the predicted terminal position and velocity uncertainty has been reduced to values 5500 km and 1 m/sec, respectively. The remaining 40 observations bring the terminal uncertainty down to 510 km and 0.25 m/sec, with the greatest improvement occuring during the last 20 days of flight when the vehicle closes on Mars.

Effect of Parameter Changes

We will now consider the effect on navigation performance when different values are assumed for the system model parameters. All parameters not specifically varied are kept at their nominal values as summarized in Table II. Generally, the format for data presentation is to plot the time history of position uncertainty and tabulate the time histories of velocity, accelerometer bias, and predicted terminal position uncertainties.

Figure 12 together with Tables III (a)-(c) compare the performance results for initial velocity uncertainties of 0,5 and 10 m/sec. In the case of perfect initial velocity information, performance is significantly improved over the first 80 days of flight, but very little thereafter. At the final time, the uncertainty in position is reduced only 100 km from the nominal value. In the case of 10 m/sec initial uncertainty, no discernable performance degradation exists beyond 10 days of flight. These results imply that on-board measurements are sufficiently accurate so as to give little weight to a priori velocity information, at least for initial uncertainties above several meters per second.

Table IV shows the effect on performance of different correlation times associated with the low frequency accelerometer error. Listed are the RMS uncertainties in the estimates of position, velocity and accelerometer error (low frequency) at various points along the trajectory. Results are shown for correlation times of 5,50,100 and 200 days in addition to the nominal value ∞ (bias). Correlation time is seen to have a rather complicated effect on system performance. During the early portion of flight, position and velocity uncertainty is least for low values of correlation time, although the differences are not very significant. This situation then reverses as time progresses. At the terminal time, position and velocity uncertainty range from 2050 - 514 km and 1.36 - 0.252 m/sec,

respectively, as τ_{al} ranges from 5 days to ∞. The explanation of this result lies in the opposing effects of changing τ_{al}. In particular, the more highly correlated the accelerometer error the larger the effect on position and velocity uncertainty. On the other hand, the more highly correlated the error the greater the accuracy in estimating this error. When the low frequency error is a pure bias, $\tilde{a}_{rms}$ is seen to decrease very rapidly with successive celestial observations. However, for finite correlation times even as large as the total flight time, the estimate hardly improves at all. This was a somewhat surprising and discouraging result. Figure 13 shows a more detailed comparison of the position uncertainty for correlation times of 200 days and ∞. The relatively poorer performance associated with the finite-time correlation error is a significant result in that it is probably unrealistic to expect the low-frequency accelerometer error to remain constant throughout the entire mission. Rather, this error may be attributed to a slowly changing calibration, such as due to aging.

Figure 14 together with tables V (a)-(c) show the effect of varying the magnitude of both the random and bias components of accelerometer error. Errors of 1/10 th and 10 times the nominal value are considered. Without the benefit of celestial observations, the corresponding terminal position uncertainties are 266,000 km and 1,950,000 km. When celestial observations are included, these uncertainties are reduced to 377 km and 1890 km - about three orders of magnitude. The corresponding terminal

velocity uncertaintites are 0.151 m/sec and 1.23 m/sec. These results are to be compared with 514 km and 0.252 m/sec for the nominal accelerometer error. As seen from the figure, the magnitude of the accelerometer error affects the shape of the position uncertainty time history. The explanation for this lies in the relative weighting of inertial and celestial information. Thus, for large σ_a, the celestial information is weighted more heavily as time progresses. This is especially true during the coast period (52-149 days) when accelerometer errors do not directly influence state uncertainty; hence, the pronounced dip in the response.

Considering the fact that the assumed accelerometer error has ranged over two decades, the difference in performance is not nearly as significant as one might have expected. This is an important result as it relates to the accuracy requirements of low-level accelerometers. Although this example is certaintly not conclusive, it would seem to indicate first, that an extremely good accelerometer may not appreciably improve navigation accuracy, and second, that a rather poor (1 percent) accelerometer may be used, if necessary, without too serious of a performance loss.

It was of interest to examine the effect of celestial sensor errors on state estimation accuracy. The results for sensor errors of 5,10 and 20 seconds of arc are compared in Figure 15 and tables VI (a)-(c). During the first 20-30 days of flight, performance is not appreciably affected by sensor error since inertial information is weighted more heavily in this region.

An expected breakaway then occurs, and in the region 40-180 days the performance ratios remain roughly proportional to the sensor error ratios. As the terminal time is approached this proportionate effect of sensor error is somewhat reduced. With respect to the nominal case, final position uncertainty is improved by 30 percent for the 5 second of arc sensor and degraded about 66 percent for the 20 second of arc sensor.

Figure 15 and tables VII (a) and (b) show the effect of changing the frequency of celestial observations. For this example the nominal observation interval of 2 days was first reduced to 1 day and then increased to 5 days. Again, during the first 30 days of flight navigation accuracy is not appreciably affected by the observation interval. In the region 40-180 days, the 1 day observation interval produced about a 25 percent reduction in both position and velocity uncertainty while the 5 day observation interval increases theuncertainty by roughly 50 percent. At the final time, theposition uncertainties for the 1,2 and 5 day observation intervals are, respectively, 420, 510 and 870 kilometers. The corresponding velocity uncertainties range from 0.22 to 0.35 meters per second. With respect to the terminal uncertainties, there is no significant difference between the 1 and 2 day observation schedules. However, if one considers navigation performance over the entire trajectory, the daily observation schedule is definitely perferable.

Figure 17 is a plot of position uncertainty over the first 80 days of flight for different combinations of celestial sensor random and bias error. The addition of a 5 second of arc bias to the nominal 10 second of arc random error causes the maximum position uncertainty to increase by 1000 km, or about 20 percent. When the random and bias errors are each 5 seconds of arc, the maximum uncertainty is reduced 1000 km below the nominal case. Figure 18 shows the time history of this uncertainty in estimating the bias components of β, α and η. Initially, each of the bias uncertainties are 5 seconds of arc. The largest improvement is obtained for the stellar monitor bias (η) where, at the end of 80 days, the uncertainty has been reduced to 3.5 seconds of arc. The least improvement occurs in estimating the planet longitude bias (β) where, at the end of 80 days, the uncertainty has been reduced to only 4.4 seconds of arc. In general, and as expected, no great gains are made in estimating the celestial sensor bias components.

5.4 Navigation Performance for Other Missions

A brief summary of navigation performance for the four other missions listed in Table I is now given. The nominal parameter values listed in Table II are used for this example with one exception. In the case of the Jupiter flyby mission, the celestial observation interval is 5 days. Results are shown in Figures 19 through 22 where we have plotted the predicted terminal position uncertainty, $\tilde{r}_{rms}(t_f|t)$, as a function of time. The figures then show the reduction of terminal position uncertainty with successive celestial observations.

This was felt to be a suitable summary performance index to plot in lieu of presenting the great amount of performance data obtained. Results are further summarized in the table below which gives the terminal position and velocity uncertainties.

Mission	$\tilde{r}_{rms}(t_f)$, k_m	$\tilde{v}_{rms}(t_f)$, m/sec
Mars rendezvous (181.6)	334	0.212
Venus rendezvous (120)	301	0.247
Mars flyby (120)	1410	0.397
Jupiter flyby (360)	7120	0.630

Performance results for the two rendezvous missions are about the same, and also agree quite well with the results previously given for the 205.4 day Mars rendezvous mission. The terminal position uncertainties for the two flyby missions are, however, considerably greater. One reason for this is that, in the case of the flybys, the vehicle spends relatively little time in the near vicinity of the target planet, say within 10 million kilometers. It is in this region where the terminal position uncertainties are greatly reduced. This is particularly true in the case of the Jupiter flyby where the next to last observation is made at a distance of 13 million kilometers from Jupiter. Obviously, the terminal position uncertainties could be reduced in each of the flyby cases by taking more frequent observations as the target planet is approached. The terminal uncertainties are not, however, the full measure of navigation performance. For the Mars flyby,

the estimate of vehicle motion obtained over the entire trajectory is about equally as good as that obtained for the rendezvous missions. This is not the case, however, for the Jupiter flyby. The principal reason for this is that the vehicle is at great distances from both Earth and Jupiter during most of the flight. Hence, the celestial position fixes are of relatively poor quality. As a means of improving navigation accuracy, one could consider the possibility of observing Mars at appropriate points along the Jupiter transit. Of course, the phasing of the planets would be an important factor here. Another, and even better, solution would be to observe certain selected asteroids as the vehicle passes through the asteroid belt between Mars and Jupiter. Due to the large number of such asteroids, the measurement baselines and angular relationships could be judiciously chosen so as to obtain extremely accurate position fixes.

6. CONCLUDING REMARKS

Results have shown that the optimal celestial-inertial navigation concept performs quite well and offers several orders-of-magnitude improvement over pure inertial navigation. The stellar monitor observation and correction process effectively eliminates gyro drift as a significant error parameter. In its place is substituted the stellar monitor error; however, this error has relatively little effect on acceleration measurement error. The low frequency accelerometer error, then, remains as the major source of information uncertainty. However, the frequent celestial angle observations serve to reduce this uncertainty. When the accelerometer error is initially a constant but unknown bias, the improvement is marked. In this case, vehicle position and velocity uncertainty throughout the heliocentric flight may be held to within quite acceptable limits for the purpose of midcourse guidance. The terminal uncertainties (at the target planet's sphere of influence) are typically within 1000 km in position and 1 m/sec in velocity. One important result that has been found is the relative insensitivity of navigation performance over a wide range of accelerometer bias magnitudes. This would imply the possible use of rather poor instruments (1 percent), if necessary, without serious performance degradation.

Specific numerical results described in this report should best be considered indicative of the performance that

may be expected of celestial-inertial navigation systems applied to low-thrust vehicles. Final performance results could only be obtained after such systems are actually designed and tested so that improved instrumentation error models are available for analysis. Apart from the important problem of practical design of the navigation system, future analytical studies in this area should be concerned with the following problems:

1. Application of the navigation concept to the planetocentric phases of interplanetary missions, i.e., the escape and capture spiral phases. This would be necessary in order to tie together the navigational requirements and performance for a complete mission.

2. Investigate the effect of false assumptions in a priori statistical data. That is, how do the true and estimated navigation errors compare when false a priori covariance data are used in the state estimation procedure.

APPENDIX A

LIST OF SYMBOLS

Matrices:

A	linearized state coefficient matrix
B	"white noise" influence matrix
D	thrust acceleration influence matrix
G	gravitational acceleration partials with respect to position
H	submatrix in M containing geometry vectors $\underline{h}$
H_1	submatrix in M to account for platform misalignment (stellar monitor errors)
I	identity (unit) matrix of appropriate dimensions
K	filter or weighting matrix
L	diagonal matrix of correlation time reciprocals
M	celestial observation matrix
N	covariance matrix of random celestial sensor errors
O	null matrix of appropriate dimensions
P	covariance matrix of state estimation errors
Q	covariance matrix of integrated "white noise" effects
U	covariance matrix of "white noise" inputs
Λ	coefficient matrix relating platform misalignment to acceleration measurement error
Φ	state transition matrix

Vectors:

All vectors are to be considered column vectors unless otherwise specified.

$\underline{a}$	thrust acceleration
$\underline{g}$	gravitational acceleration
$\underline{h}$	geometry vector relating space angle and position variations
$\underline{i}_s$	unit vector in direction of star
$\underline{n}$	random (time-uncorrelated) celestial sensor errors
$\underline{n}_b$	bias error of theodolite or sextant-type measurements
$\underline{q}$	integrated effects of $\underline{u}$ on state variables
$\underline{r}$	vehicle position deviation from reference trajectory
$\underline{R}$	vehicle position
$\underline{R}_{vp}$	vehicle-planet vector
$\underline{u}$	"white noise" input
$\underline{v}$	vehicle velocity deviation from reference trajectory
$\underline{V}$	vehicle velocity
$\underline{x}$	augmented state
$\hat{\underline{x}}$	estimate of $\underline{x}$
$\tilde{\underline{x}}$	error in estimate, $\underline{x} - \hat{\underline{x}}$
$\underline{y}_m$	measured space angle from reference value
$\underline{z}_m$	measured thrust acceleration from reference value
$\underline{\gamma}$	platform (inertial measurement frame) misalignment
$\Delta\underline{x}_m$	change in $\underline{x}$ over time interval as measured by accelerometers
$\underline{\varepsilon}_a$	accelerometer errors

$\underline{\varepsilon}_\ell$ low frequency component of $\underline{\varepsilon}_a$

$\underline{\varepsilon}_h$ high frequency component of $\underline{\varepsilon}_a$

$\underline{\eta}_\ell$ low frequency stellar monitor errors

$\underline{\eta}_h$ high frequency stellar monitor errors

$\underline{\theta}_m$ measured space angle

Scalars:

a thrust acceleration

$\tilde{a}_{rms}$ RMS error in estimating accelerometer error

F thrust force

g_o Earth surface gravity, 9.806 m/sec^2

I_{sp} specific impulse

k_T factor to account for IMU shutdown during coast; 1 if $a^* \neq o$, o if $a^* = o$.

M vehicle mass

P_j kinetic power in exhaust jet

$P(\omega)$ power spectral density

$\tilde{r}_{rms}$ RMS error in estimating position

S Laplace operator

t time

t_k time instant at k^{th} celestial observation

$\tilde{v}_{rms}$ RMS error in estimating velocity

V_j jet (exhaust) velocity

(X,Y,Z) position components in fixed cartesian frame

α planet latitude as seen from vehicle

β planet longitude as seen from vehicle

θ included angle between planet and star

μ_s solar gravitational constant, 1.327×10^{20} m^3/sec^2

$\sigma^2_{a\ell}$ variance of low frequency accelerometer error

σ^2_{ah} variance of high frequency accelerometer error

σ^2_b variance of theodolite or sextant bias

σ^2_g variance of gyro drift

σ^2_r variance of theodolite or sextant random error

$\sigma^2_{\eta\ell}$ variance of low frequency stellar monitor error

$\sigma^2_{\eta h}$ variance of high frequency stellar monitor error

$\tau_{a\ell}$ correlation time of low frequency accelerometer error

τ_{ah} correlation time of high frequency accelerometer error

$\tau_{\eta\ell}$ correlation time of low frequency stellar monitor error

$\tau_{\eta h}$ correlation time of high frequency stellar monitor error

$\phi(\tau)$ auto correlation function

ω frequency variable

Operators:

$E(\ )$ expected value of ( )

$(\ )^T$ transpose of matrix ( )

$(\ )^{-1}$ inverse of matrix ( )

$(\dot{\ })$ time derivative of ( )

Subscripts:

f final or terminal value

o initial value

(X,Y,Z) components of vector quantity

Superscripts:

* reference value

APPENDIX B

PARTITIONED FORM OF ESTIMATION EQUATIONS

1. State Vector

$$\underline{x} = \begin{bmatrix} \underline{r} \\ \underline{v} \\ \underline{\varepsilon}_\ell \\ \underline{\eta}_\ell \\ \underline{n}_b \end{bmatrix} \tag{B1}$$

2. Transition Matrix

$$\Phi = \begin{bmatrix} \Phi_{rr} & \Phi_{rv} & \Phi_{r\varepsilon} & \Phi_{r\eta} & 0 \\ \Phi_{vr} & \Phi_{vv} & \Phi_{v\varepsilon} & \Phi_{v\eta} & 0 \\ 0 & 0 & \Phi_{\varepsilon\varepsilon} & 0 & 0 \\ 0 & 0 & 0 & \Phi\eta\eta & 0 \\ 0 & 0 & 0 & 0 & I \end{bmatrix} \tag{B2}$$

$$\dot{\Phi}_{rr} = \Phi_{vr} \tag{B3}$$

$$\dot{\Phi}_{rv} = \Phi_{vv} \tag{B4}$$

$$\dot{\Phi}_{vr} = G\Phi_{rr} \tag{B5}$$

$$\dot{\Phi}_{vv} = G\Phi_{rv} \tag{B6}$$

$$\dot{\Phi}_{r\varepsilon} = \Phi_{v\varepsilon} \tag{B7}$$

$$\dot{\Phi}_{v\varepsilon} = G\Phi_{r\varepsilon} + \beta_r \Phi_{\varepsilon\varepsilon} \tag{B8}$$

$$\dot{\Phi}_{r\eta} = \Phi_{v\eta} \tag{B9}$$

$$\dot{\Phi}_{v\eta} = G\Phi_{r\eta} + \Lambda\Phi_{\eta\eta} \tag{B10}$$

$$\Phi_{\varepsilon\varepsilon}(t,t_o) = e^{-\frac{1}{\tau_{a\ell}}(t - t_o)} \cdot I \tag{B11}$$

$$\Phi_{\eta\eta}(t,t_o) = e^{-\frac{1}{\tau_{\eta\ell}}(t - t_o)} \cdot I \tag{B12}$$

In equations (B3) through (B10), all initial conditions are zero with the exception of $\Phi_{rr}(t_o, t_o) = \Phi_{vv}(t_o, t_o) = I$.

3. Inverse Transition Matrix

$$\Phi^{-1} = \begin{bmatrix} \Phi_{vv}^T & -\Phi_{rv}^T & \Lambda_1 & \Lambda_2 & 0 \\ -\Phi_{vr}^T & \Phi_{rr}^T & \Lambda_3 & \Lambda_4 & 0 \\ 0 & 0 & \Phi_{\varepsilon\varepsilon}^{-1} & 0 & 0 \\ 0 & 0 & 0 & \Phi_{\eta\eta}^{-1} & 0 \\ 0 & 0 & 0 & 0 & I \end{bmatrix} \tag{B13}$$

where

$$\Lambda_1 = -(\Phi_{vv}^T \Phi_{r\varepsilon} - \Phi_{rv}^T \Phi_{v\varepsilon})\Phi_{\varepsilon\varepsilon}^{-1} \tag{B14}$$

$$\Lambda_2 = -(\Phi_{vv}^T \Phi_{r\eta} - \Phi_{rv}^T \Phi_{v\eta})\Phi_{\eta\eta}^{-1} \tag{B15}$$

$$\Lambda_3 = -(-\Phi_{vr}^T \Phi_{r\varepsilon} + \Phi_{rr}^T \Phi_{v\varepsilon})\Phi_{\varepsilon\varepsilon}^{-1} \tag{B16}$$

$$\Lambda_4 = -(-\Phi_{vr}^T \Phi_{r\eta} + \Phi_{rr}^T \Phi_{v\eta})\Phi_{\eta\eta}^{-1} \tag{B17}$$

This simplification in obtaining the inverse transition matrix is due to a special property of the transistion matrix associated with the position and velocity state variables (Ref. 11).

4. Error Covariance Matrix

$$P = \begin{bmatrix} P_{rr} & P_{rv} & P_{r\varepsilon} & P_{r\eta} & P_{rn} \\ & P_{vv} & P_{v\varepsilon} & P_{v\eta} & P_{vn} \\ & & P_{\varepsilon\varepsilon} & P_{\varepsilon\eta} & P_{\varepsilon n} \\ \text{SYMMETRIC} & & & P_{\eta\eta} & P_{\eta n} \\ & & & & P_{nn} \end{bmatrix} \tag{B18}$$

5. Optimal Filter

$$K = \begin{bmatrix} K_r \\ K_v \\ K_\varepsilon \\ K_\eta \\ K_n \end{bmatrix}$$

$$= \begin{bmatrix} P_{rr}H^T - P_{r\eta}H_1^T + P_{rn} \\ P_{rv}^T H^T - P_{v\eta}H_1^T + P_{vn} \\ P_{r\varepsilon}^T H^T - P_{\varepsilon\eta}H_1^T + P_{\varepsilon n} \\ P_{r\eta}^T H^T - P_{\eta\eta}H_1^T + P_{\eta n} \\ P_{rn}^T H^T - P_{\eta n}^T H_1^T + P_{nn} \end{bmatrix} \cdot W^{-1} \tag{B19}$$

where

$$W = H(P_{rr}H^T - P_{r\eta}H_1^T + P_{rn}) - H_1(P_{r\eta}^T H^T - P_{\eta\eta}H_1^T + P_{\eta n}) \quad \text{(B20)}$$

$$+ P_{rn}^T H^T - P_{\eta n}^T H_1^T + P_{nn} + N$$

6. Q Matrix

$$Q = \begin{bmatrix} Q_{rr} & Q_{rv} & Q_{r\varepsilon} & Q_{r\eta} & 0 \\ & Q_{vv} & Q_{v\varepsilon} & Q_{v\eta} & 0 \\ & & Q_{\varepsilon\varepsilon} & 0 & 0 \\ & \text{SYMMETRIC} & & Q_{\eta\eta} & 0 \\ & & & & 0 \end{bmatrix} \quad \text{(B21)}$$

$$\dot{Q}_{rr} = Q_{rv} + Q_{rv}^T \quad \text{(B22)}$$

$$\dot{Q}_{rv} = Q_{vv} + Q_{rr}G^T + k_T Q_{r\varepsilon} + Q_{r\eta}\Lambda^T \quad \text{(B23)}$$

$$\dot{Q}_{vv} = GQ_{rv} + (GQ_{rv})^T + (Q_{v\varepsilon} + Q_{v\varepsilon}^T)k_T$$

$$+ (Q_{v\eta}\Lambda^T) + (Q_{v\eta}\Lambda^T)^T \quad \text{(B24)}$$

$$+ 2\sigma_{ah}^2 \tau_{ah} \cdot I + 2\sigma_{\eta h}^2 \tau_{\eta h} \Lambda\Lambda^T$$

$$\dot{Q}_{r\varepsilon} = Q_{v\varepsilon} - \frac{1}{\tau_{a\ell}} Q_{r\varepsilon} \quad \text{(B25)}$$

$$\dot{Q}_{v\varepsilon} = GQ_{r\varepsilon} - \frac{1}{\tau_{a\ell}} Q_{v\varepsilon} + k_T Q_{\varepsilon\varepsilon} \quad \text{(B26)}$$

$$\dot{Q}_{r\eta} = Q_{v\eta} - \frac{1}{\tau_{\eta\ell}} Q_{r\eta} \quad \text{(B27)}$$

$$\dot{Q}_{v\eta} = GQ_{r\eta} - \frac{1}{\tau_{\eta\ell}} Q_{v\eta} + \Lambda Q_{\eta\eta} \quad \text{(B28)}$$

$$Q_{\varepsilon\varepsilon}(t,t_o) = \sigma^2_{a\ell}\left[1 - e^{\frac{-2(t-t_o)}{\tau_{a\ell}}}\right]\cdot I \qquad \text{(B29)}$$

$$Q_{\eta\eta}(t,t_o) = \sigma^2_{\eta\ell}\left[1 - e^{\frac{-2(t-t_o)}{\tau_{\eta\ell}}}\right]\cdot I \qquad \text{(B30)}$$

In equations (B22) through (B28), the initial condition is zero.

REFERENCES

1. Kalman, R., "A New Approach to Linear Filtering and Prediction Problems." Journal of Basic Engineering, Trans. ASME, Vol. 82, No. 1, March 1960.

2. Smith, G., Schmidt, S. and McGee, L., "Application of Statistical Filter Theory to the Optimal Estimation of Position and Velocity On Board a Circumlunar Vehicle." NASA TR-135, 1962.

3. Smith, G., "Secondary Errors and Off-Design Conditions in Optimal Estimation of Space Vehicle Trajectories." NASA TN D-2129, 1964.

4. White, J., Callas, G., and Cicolani, L., "Application of Statistical Filter Theory to the Interplanetary Navigation and Guidance Problem." NASA TN D-2697, 1965.

5. Battin, R., "A Statistical Optimizing Navigation Procedure for Space Flight." MIT Instrumentation Laboratory Report R-341, May 1962.

6. Friedlander, A., "A Midcourse Guidance Procedure for Electrically Propelled Interplanetary Spacecraft." M.S. Thesis, Case Institute of Technology, 1963.

7. Stuhlinger, E., Ion Propulsion for Space Flight, McGraw-Hill, 1964.

8. Melbourne, W., "Interplanetary Trajectories and Payload Capabilities of Advanced Propulsion Vehicles," JPL Technical Report No. 32-68, March 1961.

9. MacKay, J., Rossa, L., and Zimmerman, A., "Optimum Low-Acceleration Trajectories for Earth-Mars Transfer," Proceedings of the IAS Symposium on Vehicle Systems Optimization, Garden City (N.Y.), Nov. 28-29, 1961.

10. Blumhagen, V., "Stellar Inertial Navigation Applied to Cruise Vehicles." IEEE Trans. on Aerospace and Navigational Electronics, Vol. ANE-10, No. 3, September 1963.

11. Friedlander, A., "Inversion Property of the Fundamental Matrix in Trajectory Perturbation Problems," AIAA Journal Vol. 1, No. 4, April 1963.

TABLE I - REFERENCE TRAJECTORY CONDITIONS

Mission	Thrust Mode	a_o, m/sec^2	a_f, m/sec^2	V_∞ km/sec	$\int_o^{t_f} a^2 dt$, m^2/sec^3
Mars Rendezvous 205.4 days	Constant Thrust with Coast Period I_{sp} = 8000 sec	0.981×10^{-3}	1.11×10^{-3}	0	10.2
Mars Rendezvous 181.6 days	Constant Continuous Thrust I_{sp} = 8000 sec	0.981×10^{-3}	1.22×10^{-3}	0	18.8
Venus Rendezvous 120 days	Variable Thrust	2.04×10^{-3}	2.06×10^{-3}	0	12.0
Mars Flyby 120 days	Variable Thrust	1.78×10^{-3}	0	12.6	9.27
Jupiter Flyby 360 days	Variable Thrust	1.44×10^{-3}	0	28.3	22.8

TABLE II - NOMINAL PARAMETER VALUES

1. Initial Position and Velocity Uncertainty

Position: $P_{rr} = 0$

Velocity: $P_{vv} = (5 \text{ m/sec})^2 \cdot I$

Correlation: $P_{rv} = 0$

2. Accelerometer Errors

a) Low frequency: $\sigma_{a\ell} = 10^{-6} \text{ m/sec}^2$
$\tau_{a\ell} = \infty$ (Bias)

b) High frequency: $\sigma_{ah} = 10^{-6} \text{ m/sec}^2$
$\tau_{ah} = 30$ minutes

3. Stellar Monitor Errors

a) Low frequency: $\sigma_{n\ell} = 0$

b) High frequency: $\sigma_{nh} = 10$ seconds of arc
$\tau_{nh} = 30$ minutes

4. Planet Sensor (Theodolite) Errors

a) Random: $\sigma_r = 10$ seconds of arc

b) Bias: $\sigma_b = 0$

5. Celestial Observation Interval

2 days (Both launch and target planets are observed)

TABLE III - EFFECT OF INITIAL VELOCITY UNCERTAINTY ON STATE ESTIMATION ACCURACY, MARS RENDEZVOUS (205.4)

(a) Velocity Uncertainty, $\tilde{v}_{rms}$

Time, days	Initial Velocity Uncertainty σ_v		
	0	5 m/sec	10 m/sec
	Velocity Uncertainty, m/sec		
0	0	8.66	17.3
20	.661	1.74	1.75
40	.660	2.50	2.50
60	.745	1.58	1.58
80	.610	.792	.792
100	.413	.462	.462
120	.289	.322	.322
140	.238	.277	.277
160	.272	.330	.330
180	.326	.439	.439
205.4	.209	.252	.252

Other parameters have nominal values - table II

TABLE III - EFFECT OF INITIAL VELOCITY UNCERTAINTY ON STATE ESTIMATION ACCURACY, MARS RENDEZVOUS (205.4)

(b) Accelerometer Bias Uncertainty, $\tilde{a}_{rms}$

Time, days	Initial Velocity Uncertainty σ_v		
	0	5 m/sec	10 m/sec
	Accelerometer Bias Uncertainty, m/sec^2		
0	1.73×10^{-6}	1.73×10^{-6}	1.73×10^{-6}
20	.381	1.15	1.16
40	.184	.701	.703
60	.141	.302	.302
80	.099	.144	.144
100	.071	.101	.101
120	.060	.089	.089
140	.056	.084	.084
160	.054	.082	.082
180	.051	.076	.076
205.4	.042	.053	.053

Other parameters have nominal values - table II

TABLE III - EFFECT OF INITIAL VELOCITY UNCERTAINTY ON STATE ESTIMATION ACCURACY, MARS RENDEZVOUS (205.4)

(c) Predicted Terminal Position Uncertainty, $\tilde{r}_{rms}(t_f|t)$

	Initial Velocity Uncertainty, σ_v		
	0	5 m/sec	10 m/sec
Time, days	Terminal Position Uncertainty, 10^3km		
0	194	328	565
4	155	224	254
8	100	201	204
10	97.2	196	198
20	52.5	178	180
30	35.0	160	161
40	28.6	126	126
50	25.2	84.2	84.2
-	-	-	-
-	-	-	-
205.4	0.401	0.514	0.514

Other parameters have nominal values - table II

TABLE IV - EFFECT OF ACCELEROMETER ERROR LOW-FREQUENCY CORRELATION TIME ON STATE ESTIMATION ACCURACY, MARS RENDEZVOUS (205.4)

Time, days	Correlation Time τ_{a_ℓ}, days	State Uncertainty		
		$\tilde{r}_{rms}$, km	$\tilde{v}_{rms}$, m/sec	$\tilde{a}_{rms}$, m/sec^2
20	5	1240	1.27	1.69×10^{-6}
	50	1640	1.69	1.35
	100	1670	1.71	1.27
	200	1690	1.72	1.21
	∞	1700	1.74	1.15
51.8	5	3590	1.92	1.72
	50	4390	2.43	1.30
	100	4430	2.37	1.08
	200	4430	2.29	.875
	∞	4410	2.14	.436
100	5	2100	588	1.73
	50	2110	.592	1.64
	100	2090	.559	1.45
	200	2060	.529	1.17
	∞	1970	.462	.101
149	5	1870	.359	1.73
	50	1830	349	1.72
	100	1790	.338	1.63
	200	1750	.326	1.41
	∞	1550	.273	.083
180	5	3170	1.62	1.70
	50	3830	2.38	1.32
	100	3810	2.36	1.16
	200	3620	2.16	.982
	∞	1970	.438	.076
205.4	5	2050	1.36	1.66
	50	1970	1.44	1.14
	100	1750	1.25	.919
	200	1540	1.05	.719
	∞	514	.252	.053

Other parameters have nominal values - table II

TABLE V - EFFECT OF ACCELEROMETER ERROR MAGNITUDE (RANDOM AND BIAS) ON STATE ESTIMATION ACCURACY, MARS RENDEZVOUS (205.4)

(a) Velocity Uncertainty, $\tilde{v}_{rms}$

Time, days	Velocity Uncertainty, m/sec		
	Accelerometer Errors $\sigma_{a\ell}$, σ_{ah}		
	10^{-7} m/sec^2	10^{-6} m/sec^2	10^{-5} m/sec^2
0	8.66	8.66	8.66
20	.286	1.74	5.15
40	.433	2.50	3.68
60	.574	1.58	1.91
80	.557	.792	.949
100	.416	.462	.573
120	.302	.322	.411
140	.257	.277	.359
160	.283	.330	1.14
180	.346	.439	1.51
205.4	.151	.252	1.23

Other parameters have nominal values - table II

TABLE V - EFFECT OF ACCELEROMETER ERROR MAGNITUDE (RANDOM AND BIAS) ON STATE ESTIMATION ACCURACY, MARS RENDEZVOUS (205.4)

(b) Accelerometer Bias Uncertainty, $\tilde{a}_{rms}$

Accelerometer Errors σ_{a_ℓ}, σ_{ah}		
10^{-7} m/sec^2	10^{-6} m/sec^2	10^{-5} m/sec^2

Time, days	Accelerometer Bias Uncertainty, m/sec^2		
0	$.173 \times 10^{-6}$	1.73×10^{-6}	17.3×10^{-6}
20	.165	1.15	3.20
40	.141	.701	1.19
60	.121	.302	.657
80	.097	.144	.566
100	.074	.101	.548
120	.063	.089	.542
140	.058	.084	.538
160	.054	.082	.524
180	.051	.076	.457
205.4	.021	.053	.381

Other parameters have nominal values - table II

TABLE V - EFFECT OF ACCELEROMETER ERROR MAGNITUDE (RANDOM AND BIAS) ON STATE ESTIMATION ACCURACY, MARS RENDEZVOUS (205.4)

(c) Predicted Terminal Position Uncertainty, $\tilde{r}_{rms}(t_f|t)$

	Accelerometer Errors σ_{a_ℓ}, σ_{ah}		
	10^{-7} m/sec^2	10^{-6} m/sec^2	10^{-5} m/sec^2
Time, days	Terminal Position Uncertainty, 10^3km		
0	266	328	1,950
4	111	224	1,270
8	37.3	201	1,050
10	27.0	196	857
20	17.5	178	546
30	16.6	160	323
40	16.1	126	182
50	15.6	84.2	101
-	-	-	-
-	-	-	-
205.4	0.377	0.514	1.89

Other parameters have nominal values - table II

TABLE VI - EFFECT OF CELESTIAL SENSOR RANDOM ERRORS ON STATE ESTIMATION ACCURACY, MARS RENDEZVOUS (205.4)

(a) Velocity Uncertainty, $\tilde{v}_{rms}$

Sensor Errors $\sigma_{\eta h}$, σ_r		
5 sec arc	10 sec arc	20 sec arc

Time, days	Velocity Uncertainty, m/sec		
0	8.66	8.66	8.66
20	1.50	1.74	1.91
40	1.55	2.50	3.26
60	.820	1.58	2.84
80	.402	.792	1.55
100	.236	.462	.916
120	.166	.322	.636
140	.144	.277	.545
160	.199	.330	.619
180	.277	.439	.786
205.4	.192	.252	.376

Other parameters have nominal values - table II

TABLE VI - EFFECT OF CELESTIAL SENSOR RANDOM ERRORS ON STATE ESTIMATION ACCURACY, MARS RENDEZVOUS (205.4)

(b) Accelerometer Bias Uncertainty, $\tilde{a}_{rms}$

Time, days	Accelerometer Bias Uncertainty, m/sec^2		
	Sensor Errors $\sigma_{\eta h}$, σ_r		
	5 sec arc	10 sec arc	20 sec arc
0	1.73×10^{-6}	1.73×10^{-6}	1.73×10^{-6}
20	.938	1.15	1.33
40	.434	.701	.939
60	.163	.302	.540
80	.087	.144	.266
100	.070	.101	.177
120	.066	.089	.149
140	.064	.084	.138
160	.063	.082	.132
180	.057	.076	.123
205.4	.045	.053	.074

Other parameters have nominal values - table II

TABLE VI - EFFECT OF CELESTIAL SENSOR RANDOM ERRORS ON STATE ESTIMATION ACCURACY, MARS RENDEZVOUS (205.4)

(c) Predicted Terminal Position Uncertainty, $\tilde{r}_{rms}(t_f|t)$

Time, days	Terminal Position Uncertainty, 10^3km		
	Sensor Errors $\sigma_{\eta h}$, σ_r		
	5 sec arc	10 sec arc	20 sec arc
0	328	328	328
4	215	224	231
8	196	201	208
10	188	196	201
20	158	178	187
30	120	160	179
40	78.1	126	163
50	46.0	84.2	132
-	-	-	-
-	-	-	-
205.4	0.357	0.514	0.853

Other parameters have nominal values - table II

TABLE VII - EFFECT OF CELESTIAL OBSERVATION INTERVAL ON STATE ESTIMATION ACCURACY, MARS RENDEZVOUS (205.4)

(a) Velocity Uncertainty, $\tilde{v}_{rms}$

Time, days	Observation Interval		
	1 day	2 days	5 days
	Velocity Uncertainty, m/sec		
0	8.66	8.66	8.66
20	1.65	1.74	1.82
40	2.05	2.50	2.97
60	1.17	1.58	2.29
80	.576	.792	1.17
100	.335	.462	.693
120	.233	.322	.489
140	.200	.277	.427
160	.252	.330	.497
180	.345	.439	.645
205.4	.219	.252	.347

Other parameters have nominal values - table II

TABLE VII - EFFECT OF CELESTIAL OBSERVATION INTERVAL ON STATE ESTIMATION ACCURACY, MARS RENDEZVOUS (205.4)

(b) Accelerometer Bias Uncertainty, $\tilde{a}_{rms}$

Observation Interval		
1 day	2 days	5 days

Time, days	Accelerometer Bias Uncertainty, m/sec^2		
0	1.73×10^{-6}	1.73×10^{-6}	1.73×10^{-6}
20	1.06	1.15	1.24
40	.575	.701	.845
60	.226	.302	.436
80	.111	.144	.207
100	.082	.101	.142
120	.075	.089	.123
140	.072	.084	.114
160	.070	.082	.109
180	.065	.076	.102
205.4	.049	.053	.067

Other parameters have nominal values - table II

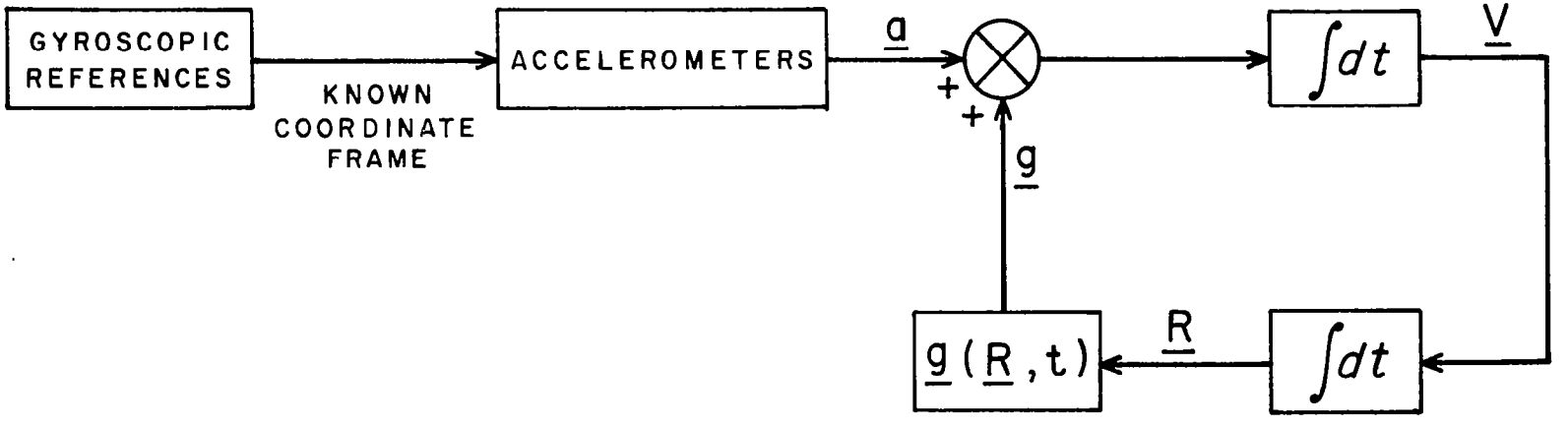

FIGURE 1 PURE INERTIAL SYSTEM, STANDARD FORM AND DYNAMICALLY EXACT

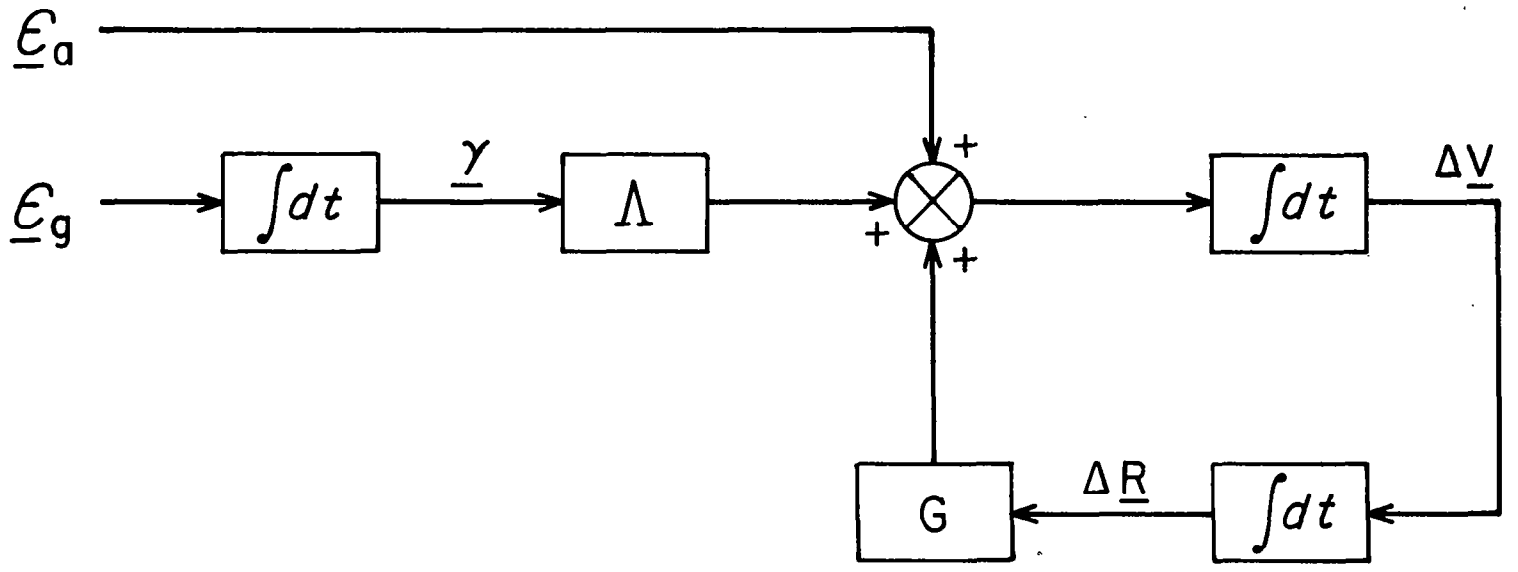

FIGURE 2 ERROR BLOCK DIAGRAM OF PURE INERTIAL SYSTEM

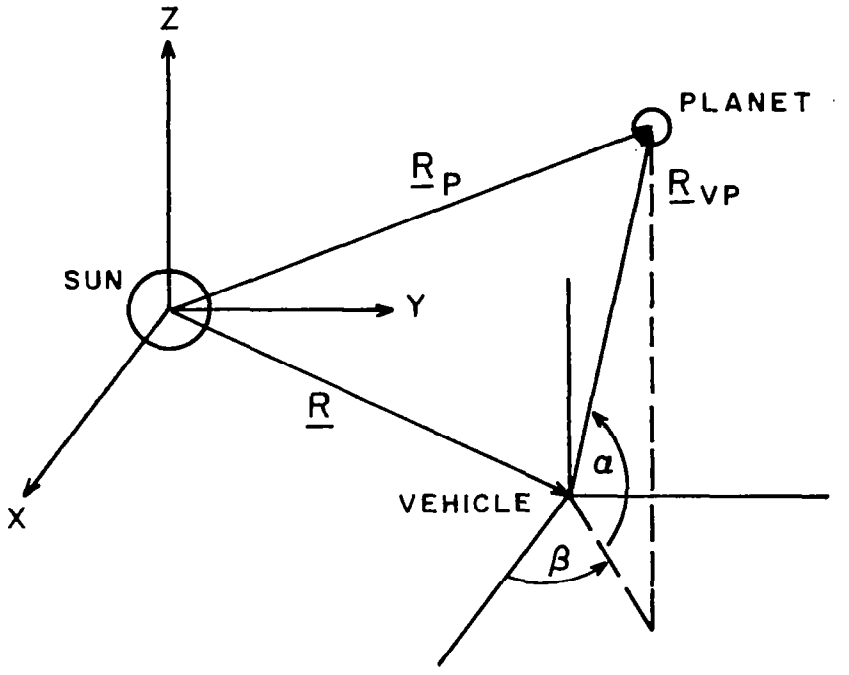

(a) THEODOLITE TYPE MEASUREMENT

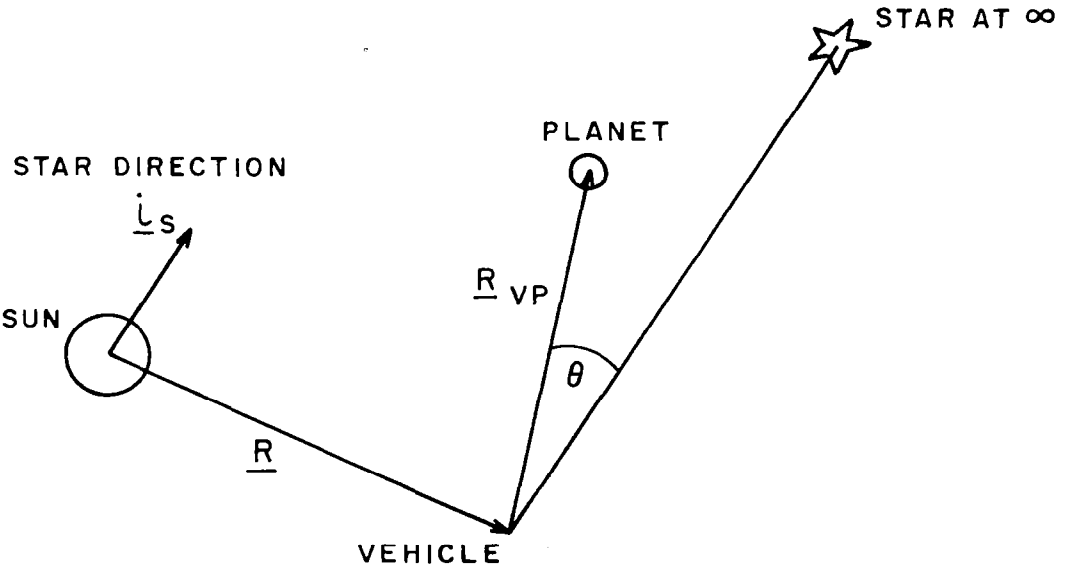

(b) SEXTANT-TYPE MEASUREMENT

FIGURE 3 CELESTIAL ANGLE MEASUREMENTS

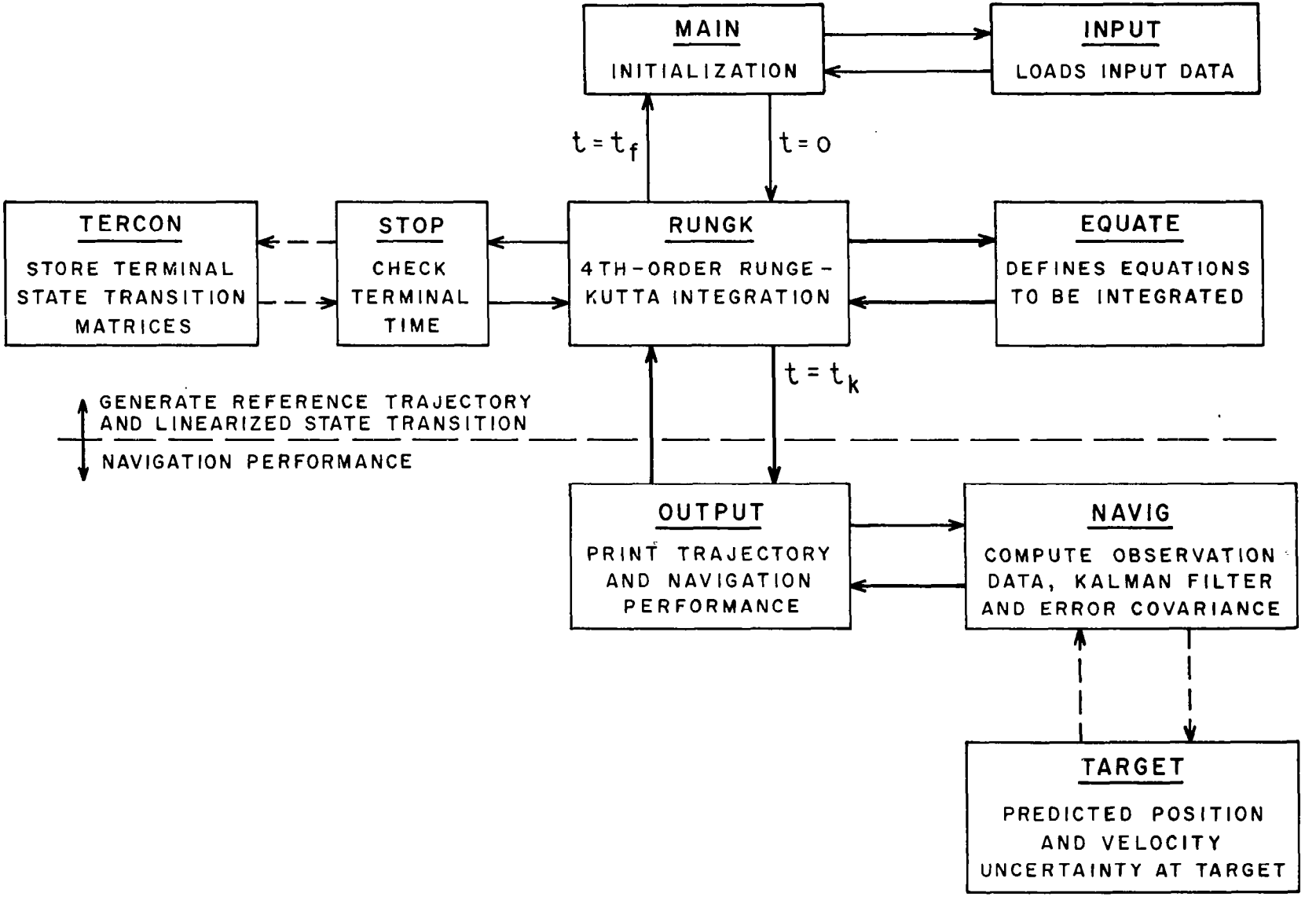

FIGURE 4 COMPUTER PROGRAM ORGANIZATION

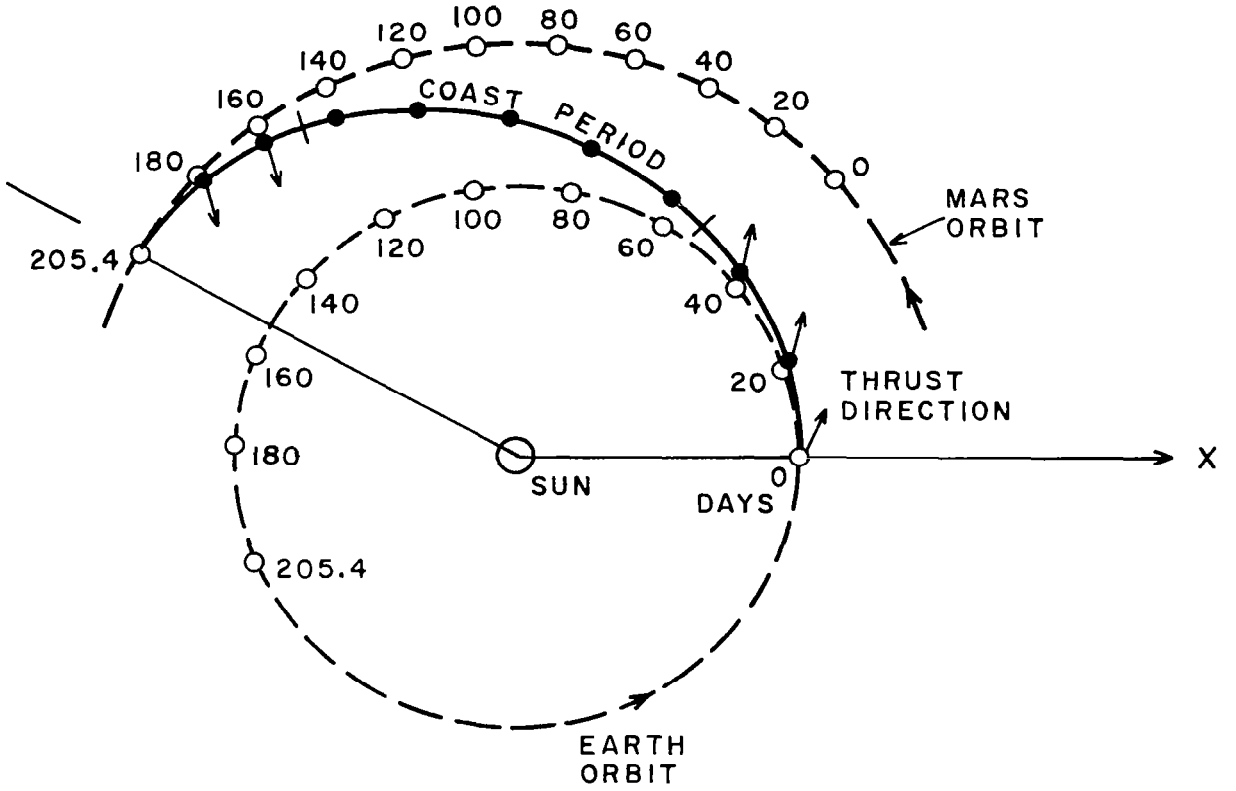

FIGURE 5 MARS RENDEZVOUS 205.4 DAYS, CONSTANT THRUST MODE WITH COAST PERIOD

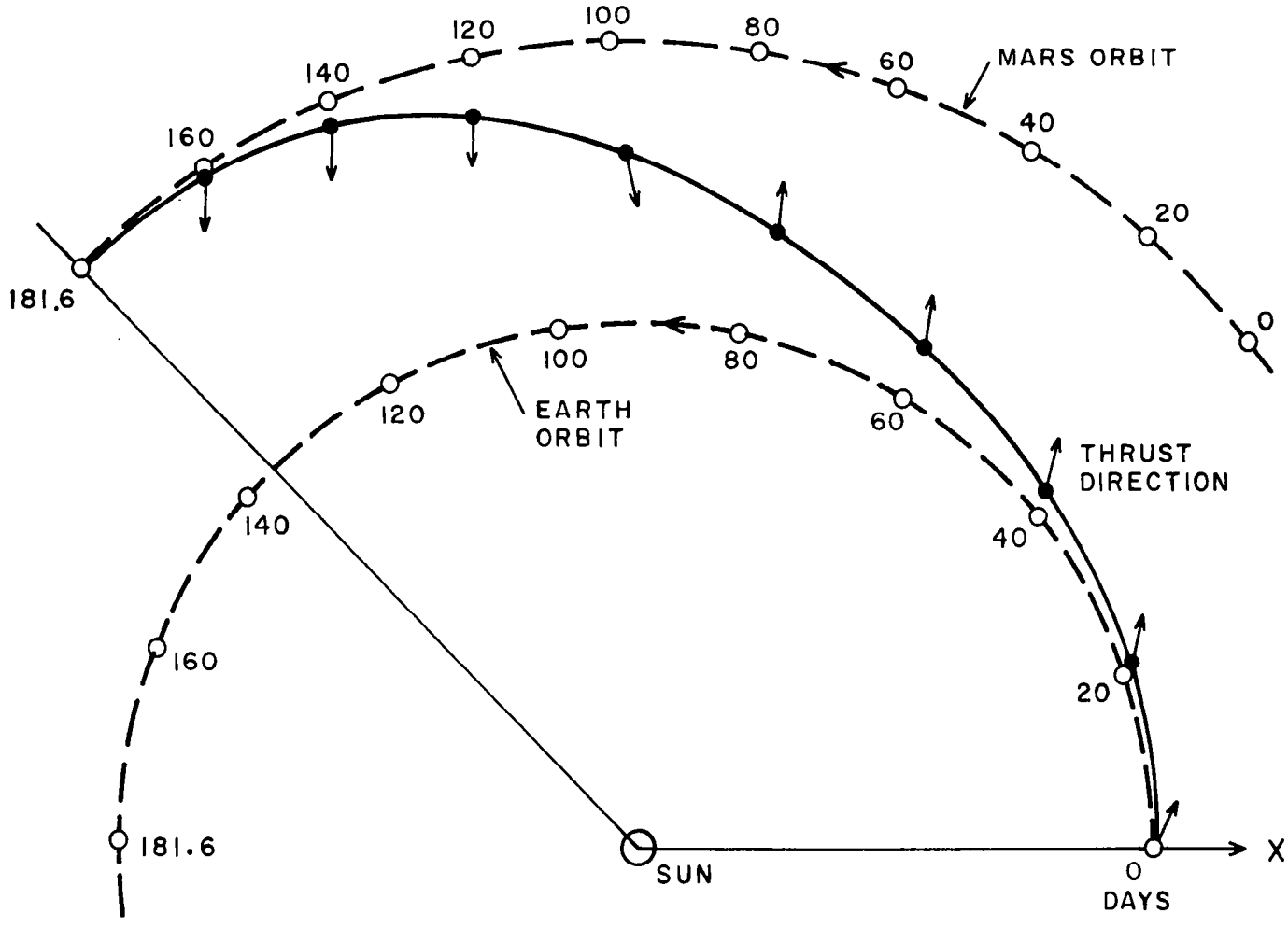

FIGURE 6 MARS RENDEZVOUS 181.6 DAYS, CONSTANT THRUST MODE WITHOUT COAST PERIOD

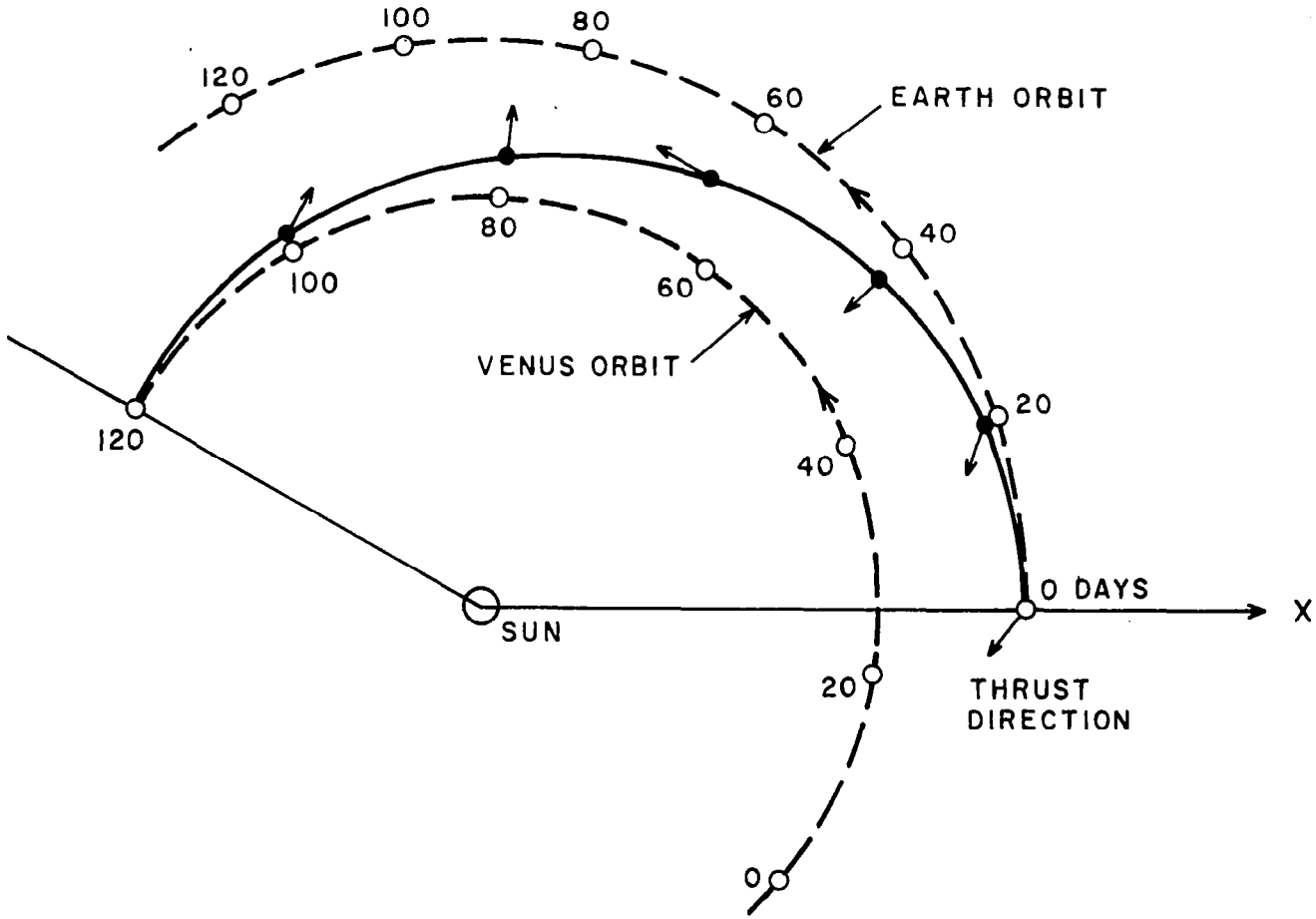

FIGURE 7 VENUS RENDEZVOUS 120 DAYS, VARIABLE THRUST MODE

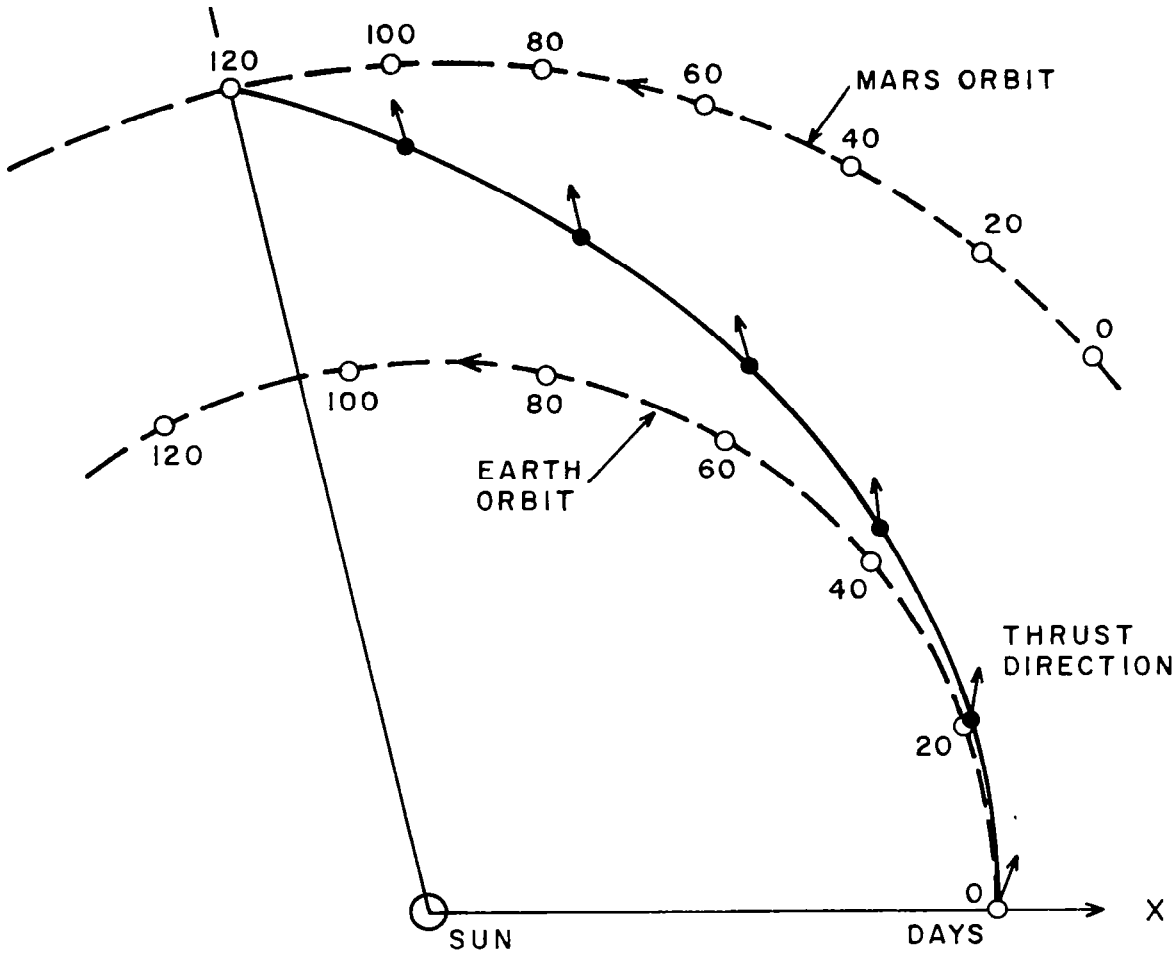

FIGURE 8 MARS FLYBY 120 DAYS, VARIABLE THRUST MODE

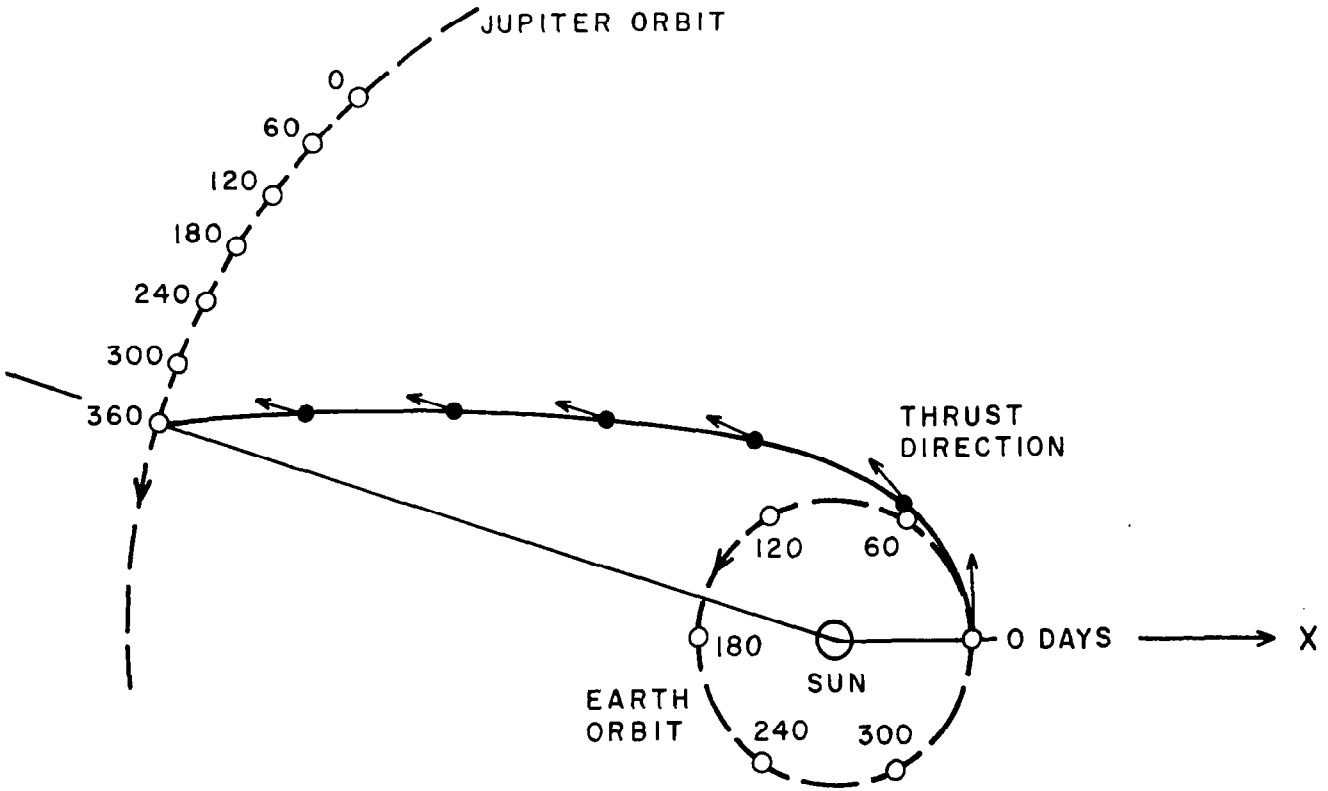

FIGURE 9 JUPITER FLYBY 360 DAYS, VARIABLE THRUST MODE

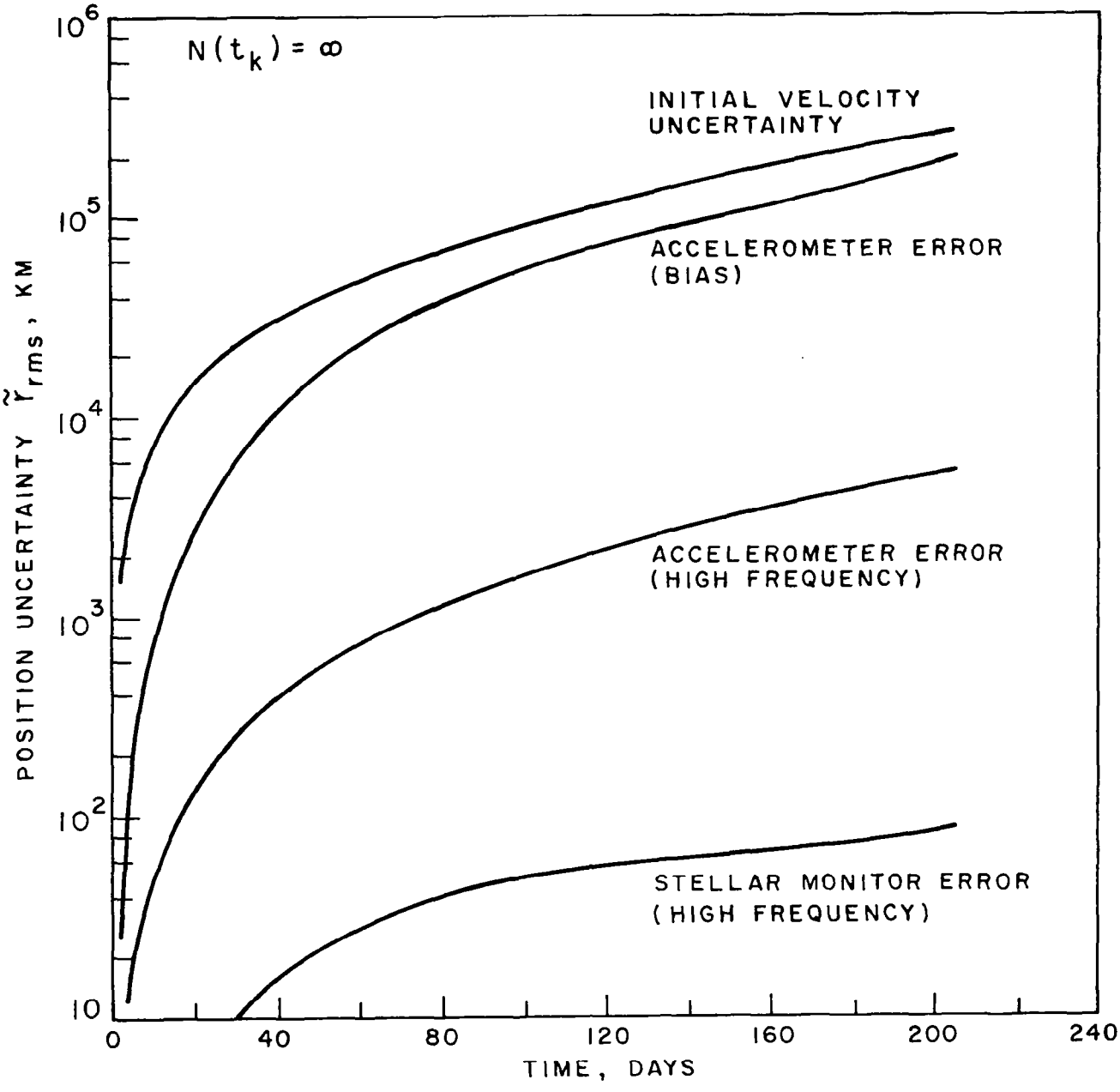

(a) POSITION UNCERTAINTY

FIGURE 10 EFFECT OF INERTIAL SYSTEM ERRORS IN THE ABSENCE OF PLANETARY OBSERVATIONS, MARS RENDEZVOUS (205.4)

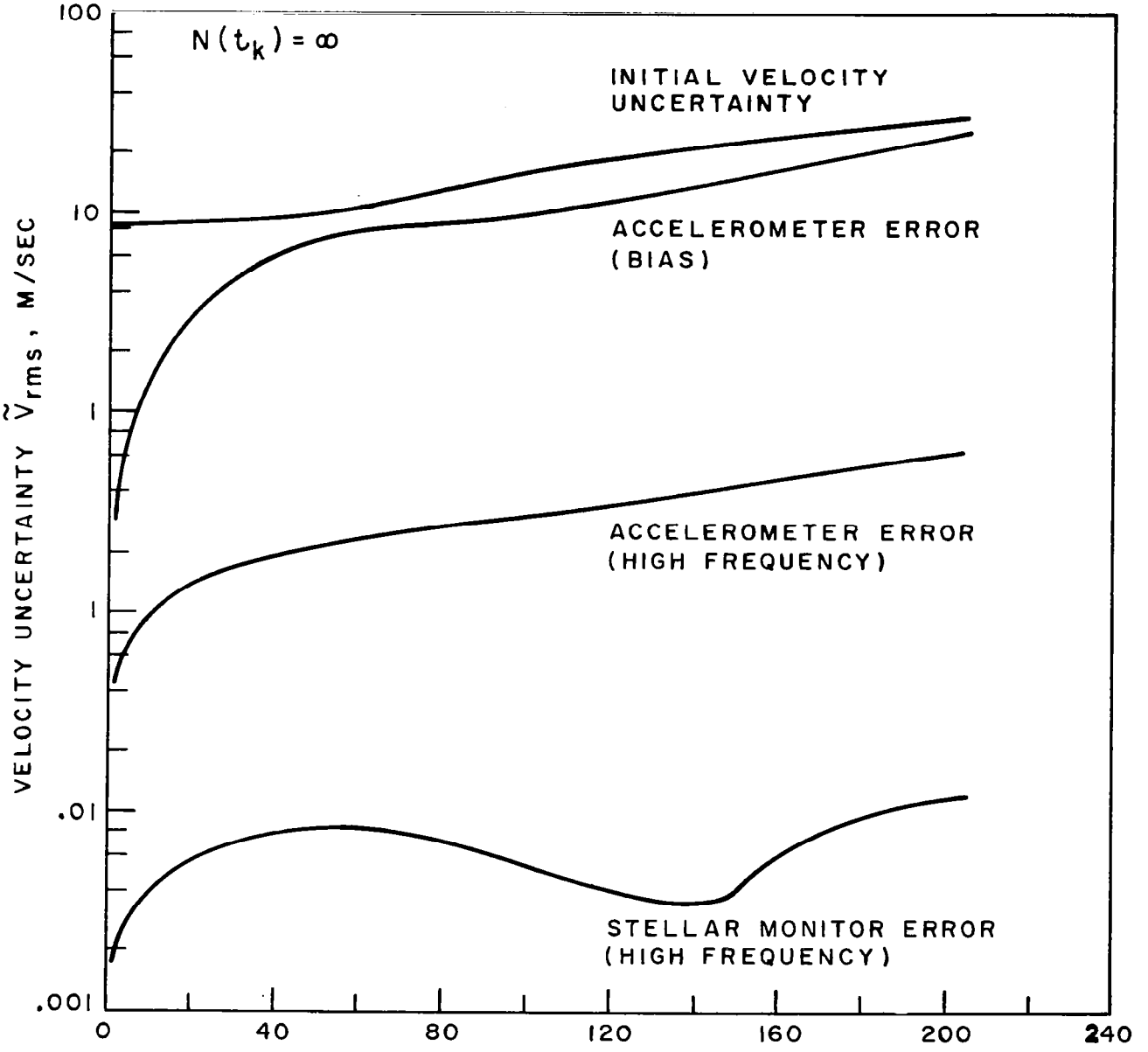

(b) VELOCITY UNCERTAINTY

FIGURE 10 CONTINUED

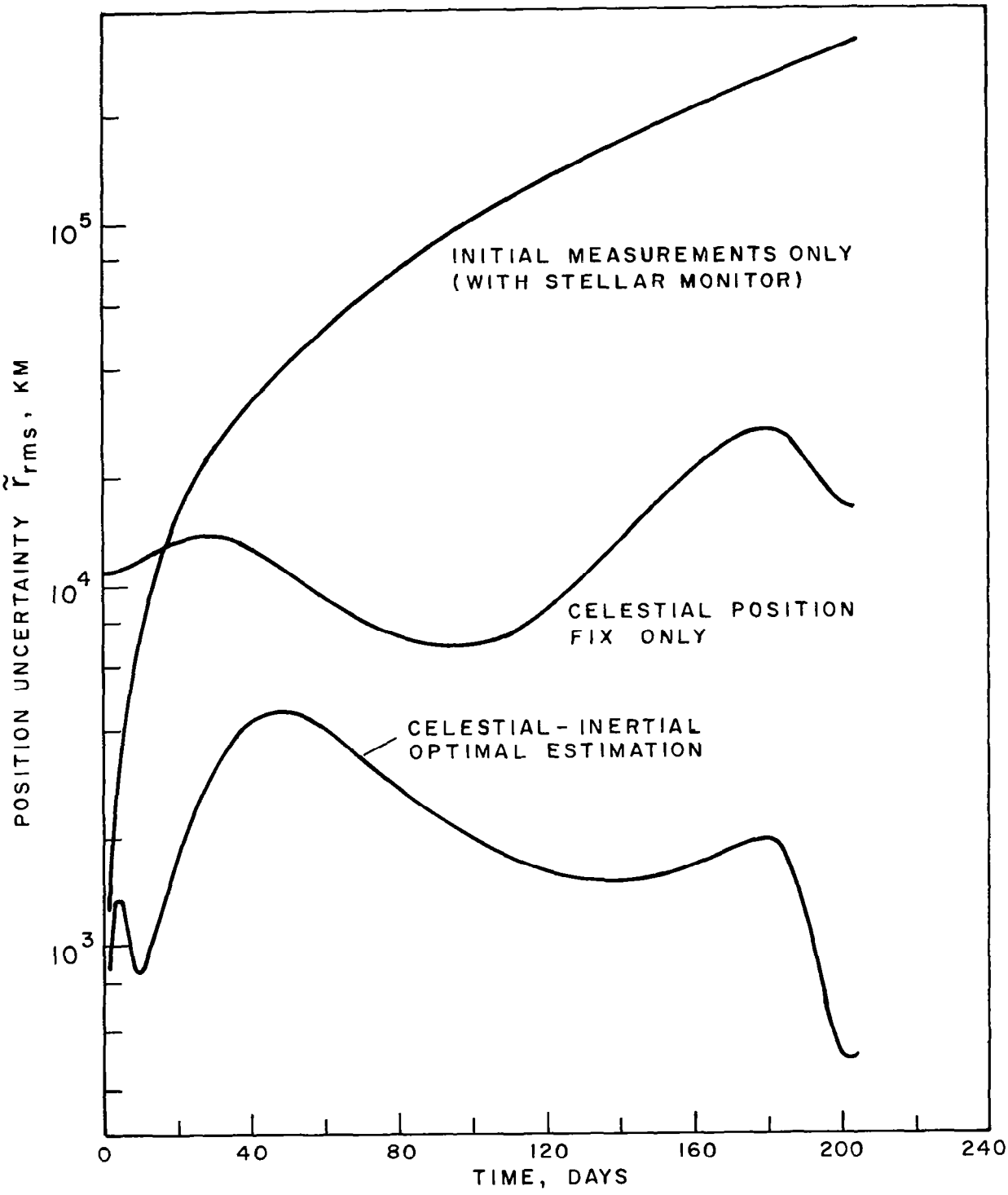

(a) POSITION ESTIMATION ACCURACY COMPARISON

FIGURE 11 PERFORMANCE OF OPTIMAL ESTIMATION PROCEDURE FOR MARS RENDEZVOUS (205.4).
ASSUMED PARAMETER VALUES - TABLE II

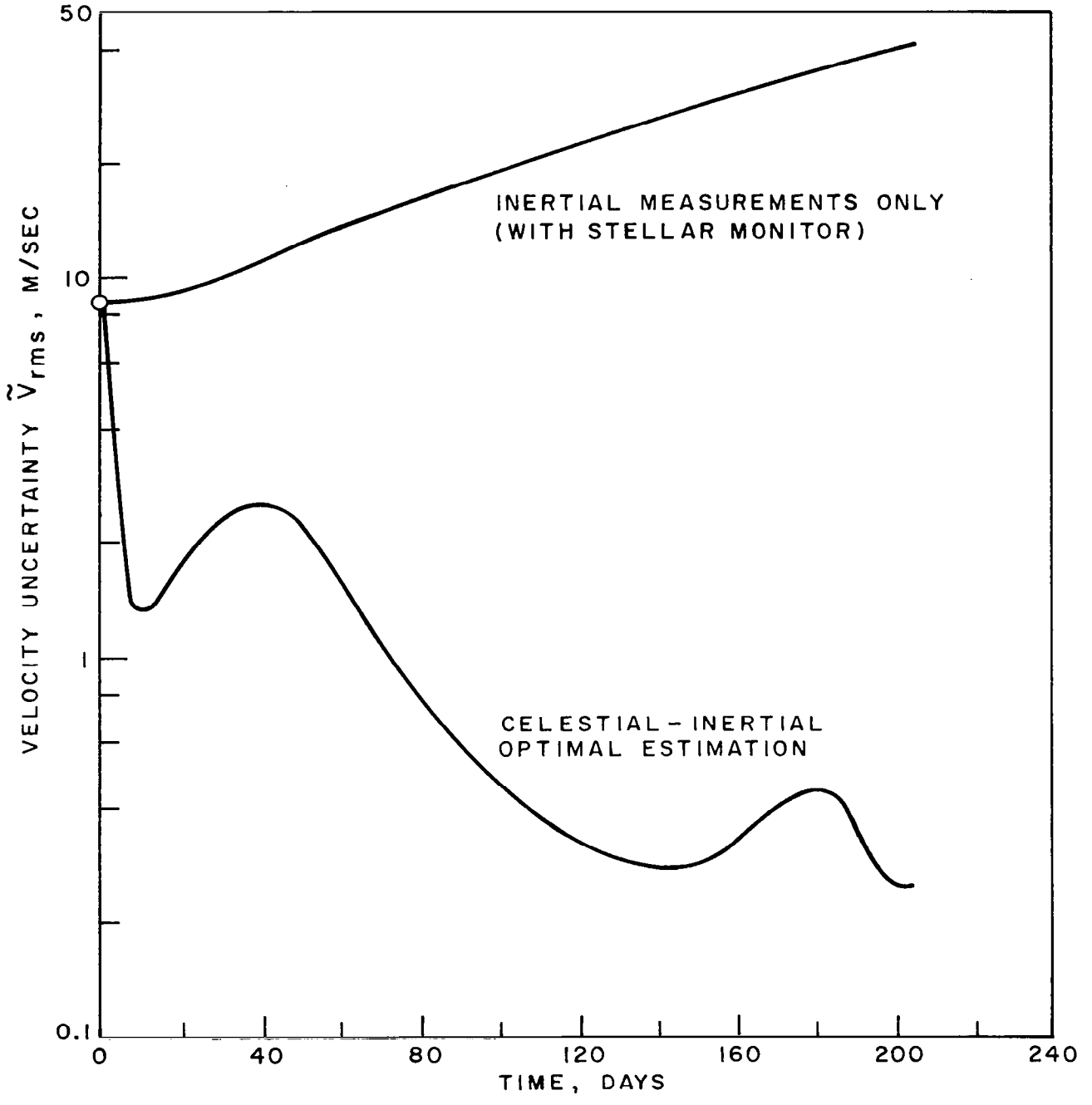

(b) VELOCITY ESTIMATION ACCURACY COMPARISON

FIGURE 11 CONTINUED

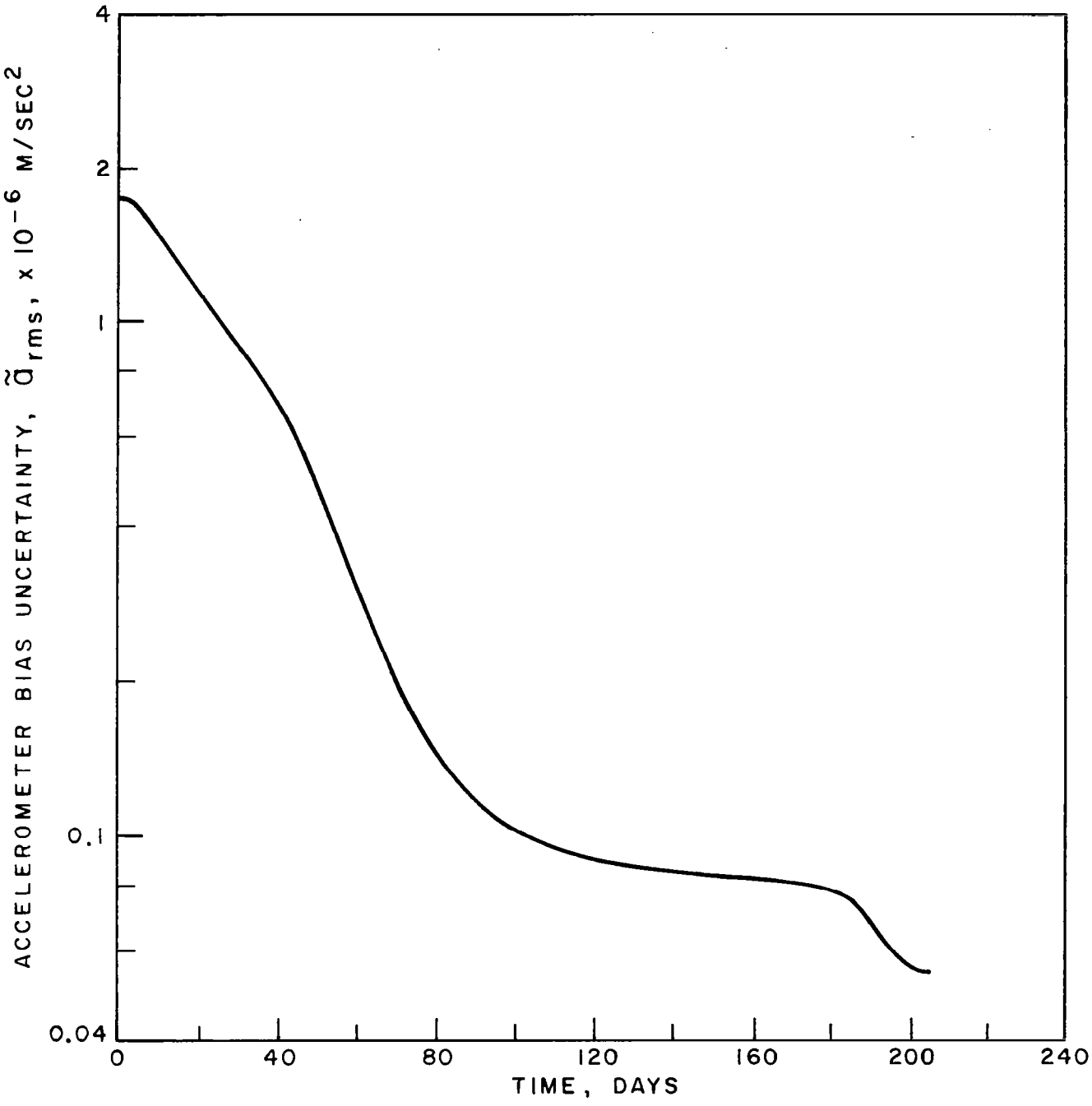

(c) ACCELEROMETER BIAS UNCERTAINTY

FIGURE 11 CONTINUED

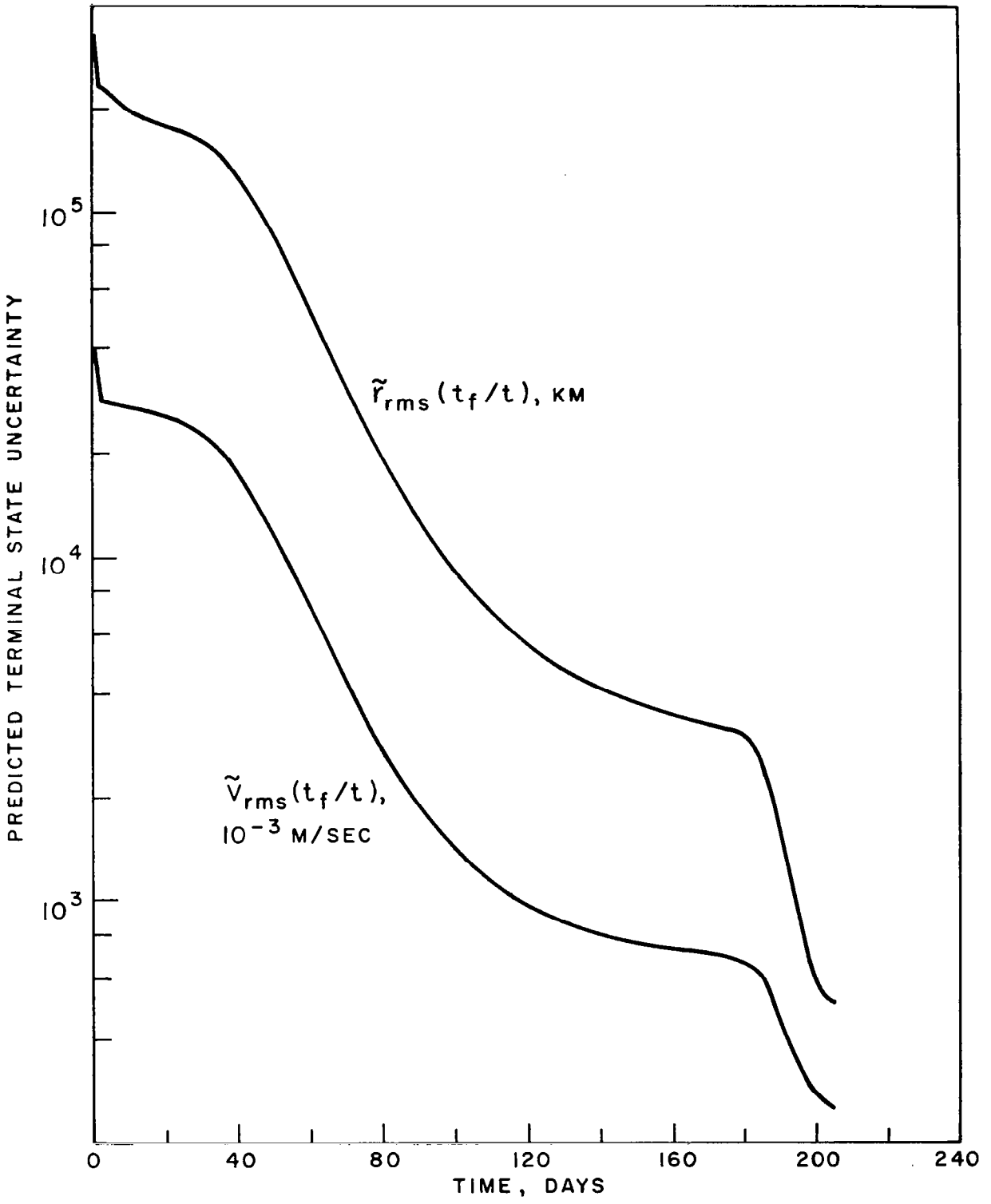

(d) PREDICTED TERMINAL POSITION AND VELOCITY UNCERTAINTY

FIGURE 11 CONTINUED

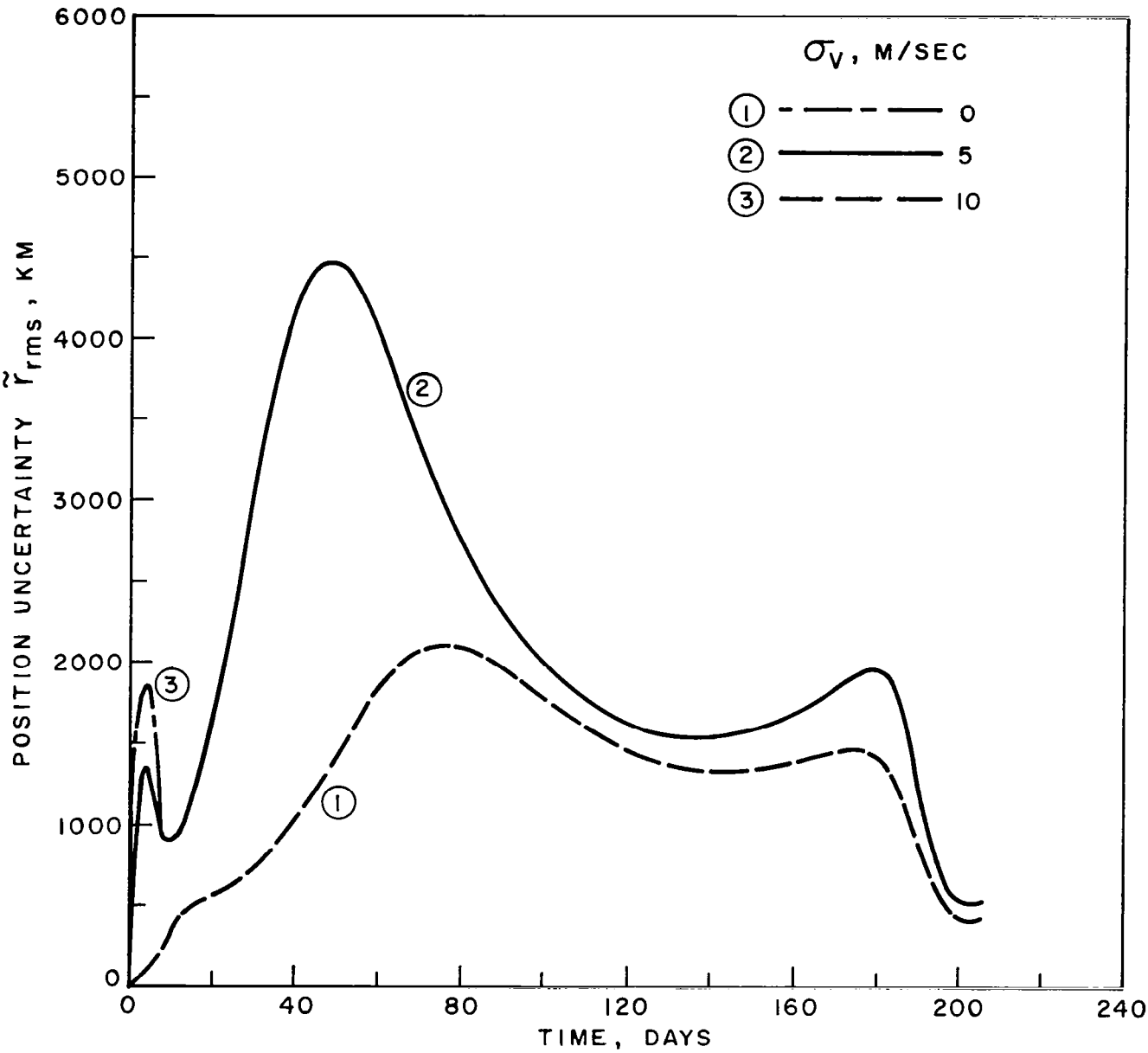

FIGURE 12 EFFECT OF INITIAL VELOCITY UNCERTAINTY ON THE ACCURACY OF POSITION ESTIMATION, MARS RENDEZVOUS (205.4)

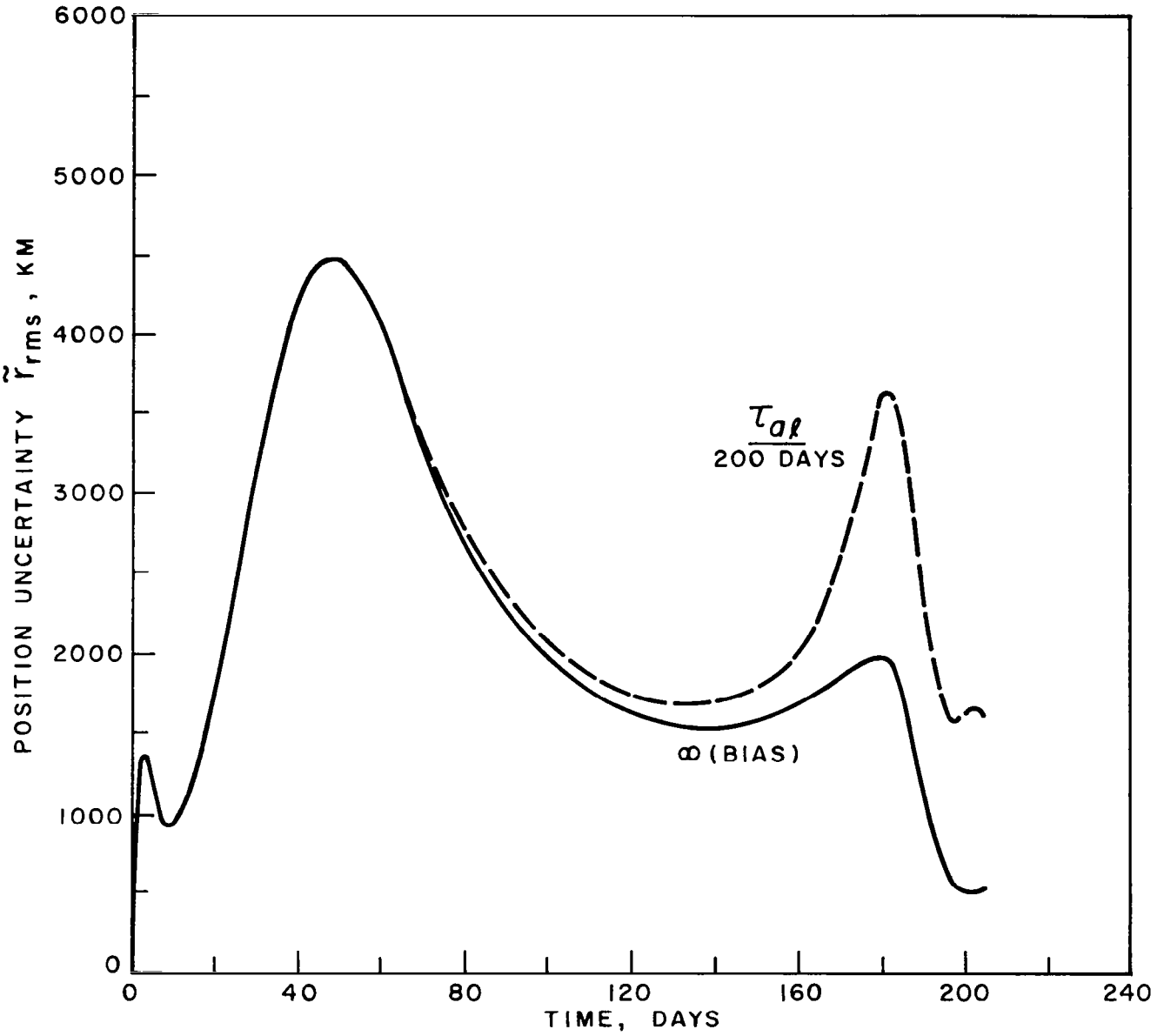

FIGURE 13 COMPARISON OF POSITION ESTIMATION ACCURACY FOR A PURE BIAS AND SLOWLY VARYING ACCELEROMETER ERROR, MARS RENDEZVOUS (205.4)

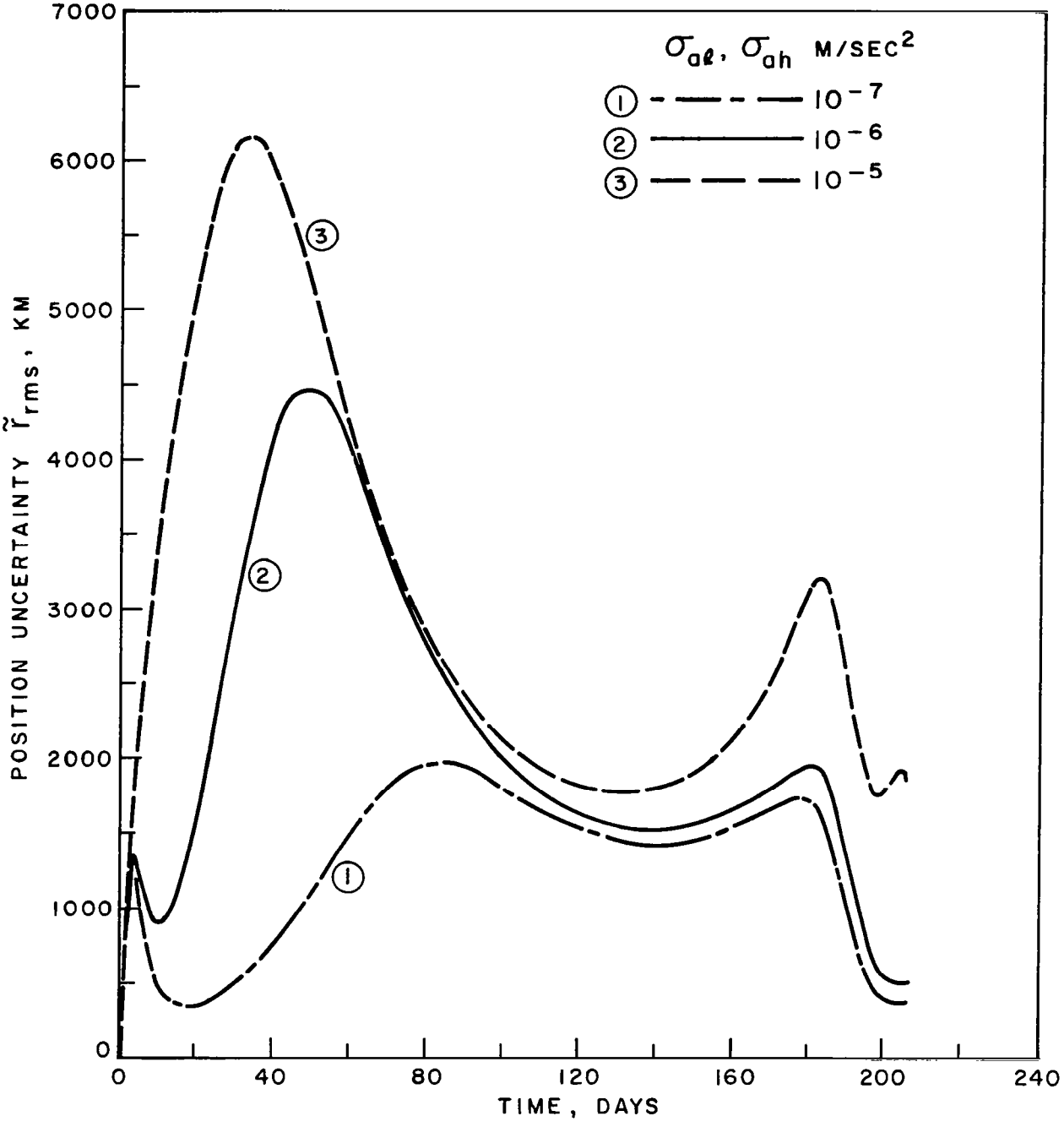

FIGURE 14 EFFECT OF ACCELEROMETER ERROR MAGNITUDE ON THE ACCURACY OF POSITION ESTIMATION, MARS RENDEZVOUS (205.4)

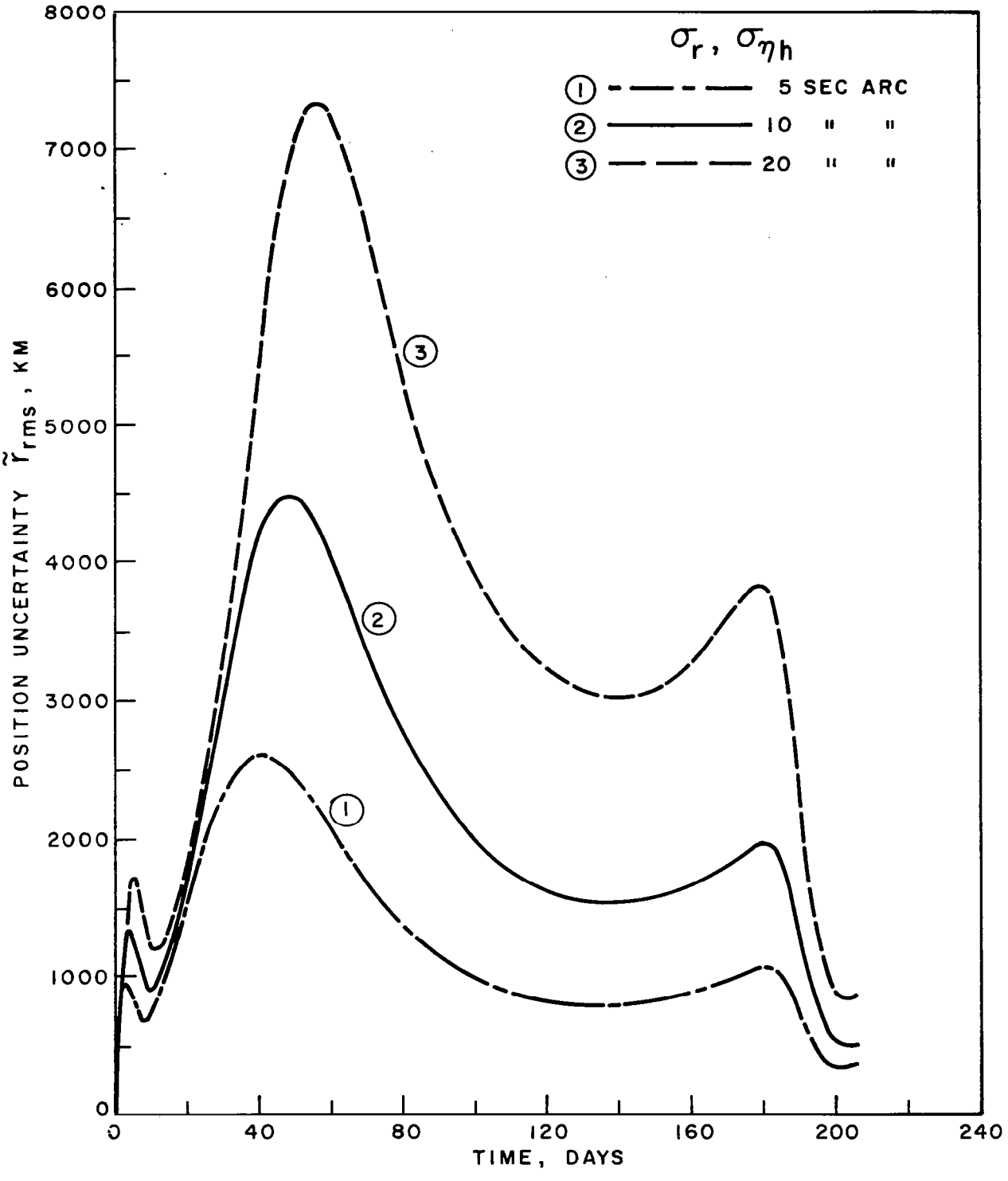

FIGURE 15 EFFECT OF CELESTIAL SENSOR RANDOM ERRORS ON THE ACCURACY OF POSITION ESTIMATION, MARS RENDEZVOUS (205.4)

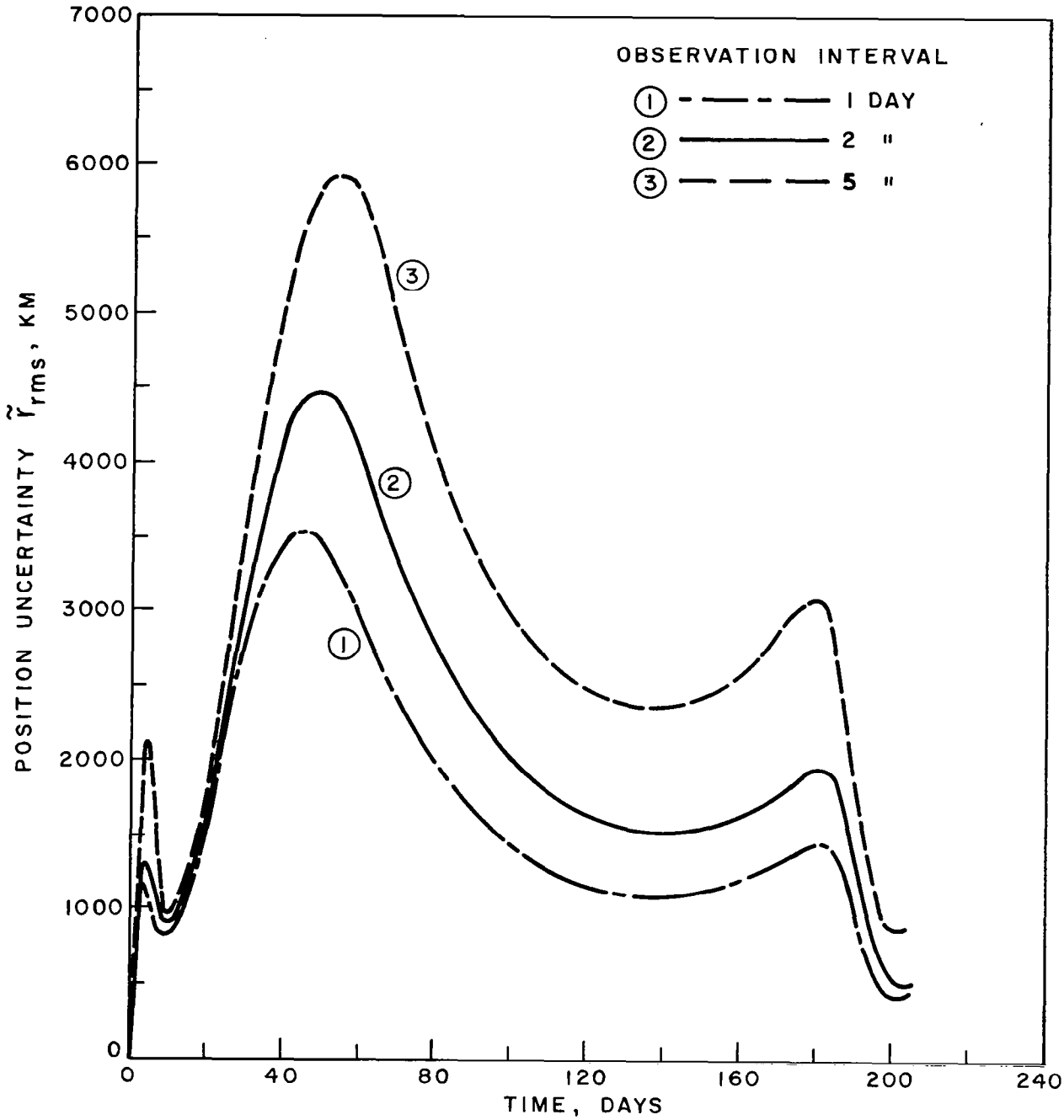

FIGURE 16 EFFECT OF CELESTIAL OBSERVATION INTERVAL ON THE ACCURACY OF POSITION ESTIMATION, MARS RENDEZVOUS (205.4)

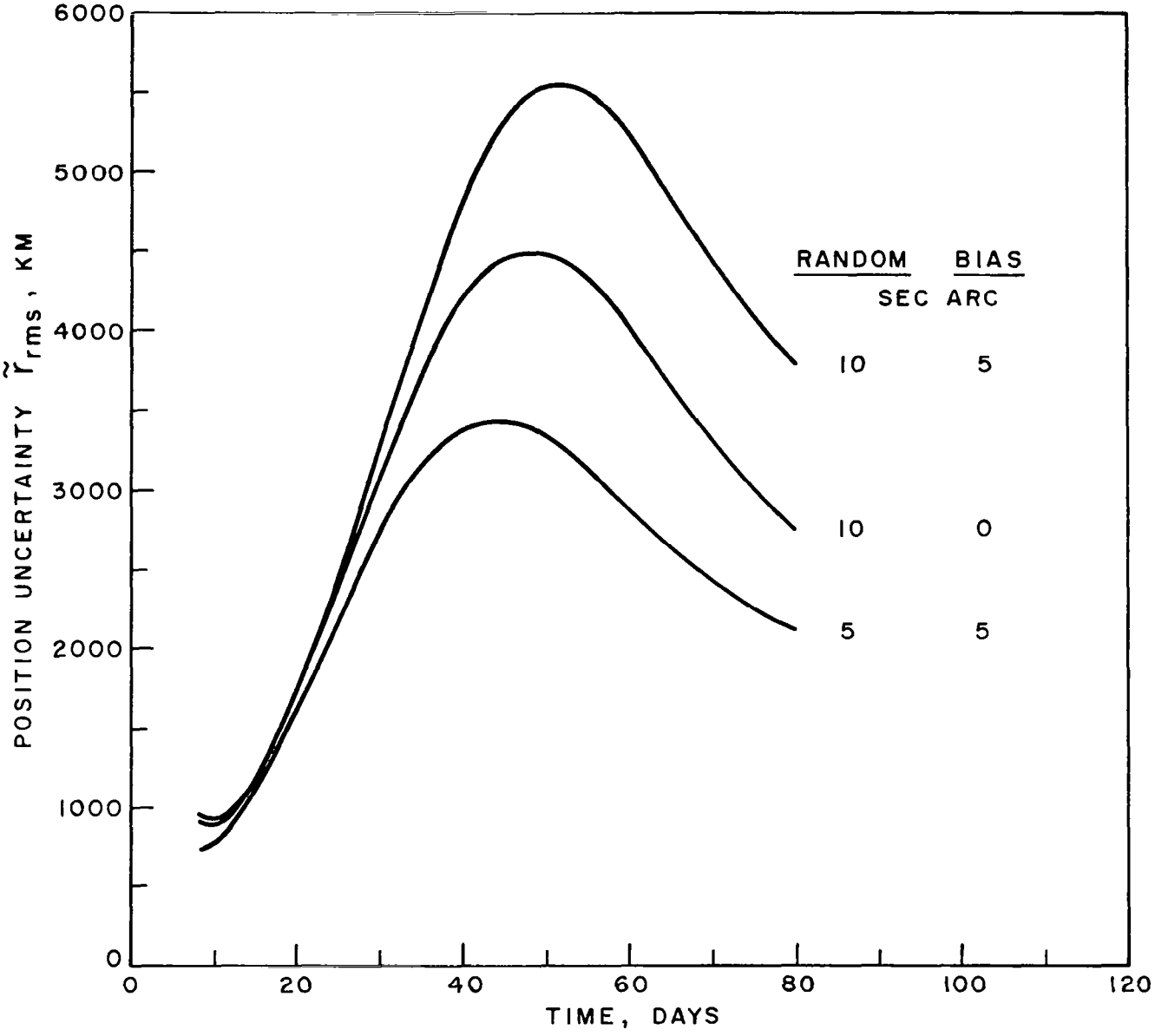

FIGURE 17 POSITION ESTIMATION ACCURACY FOR DIFFERENT COMBINATIONS OF CELESTIAL SENSOR RANDOM AND BIAS ERRORS, MARS RENDEZVOUS (205.4)

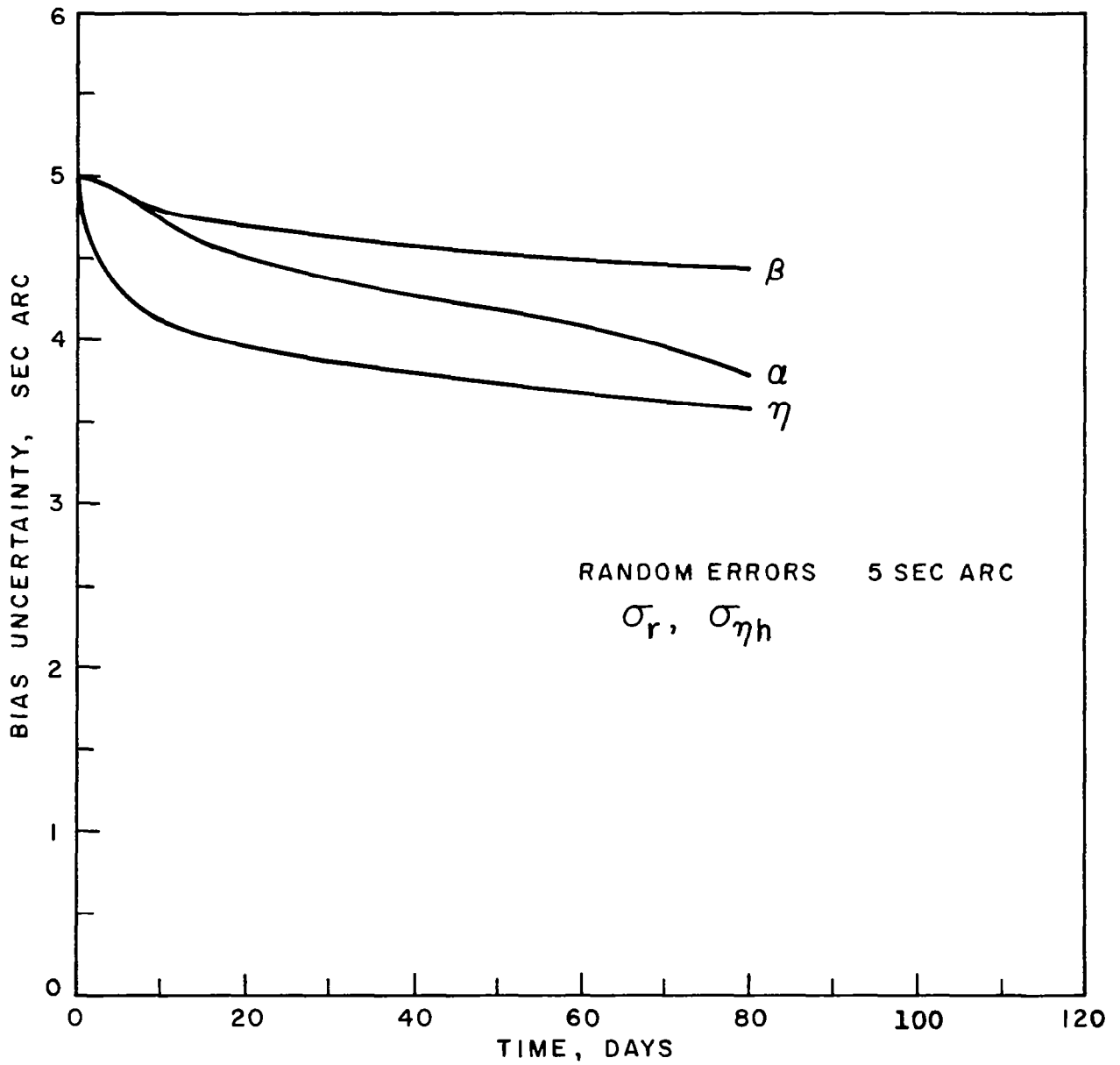

FIGURE 18 ESTIMATION PERFORMANCE FOR CELESTIAL SENSOR BIAS ERRORS, MARS RENDEZVOUS (205.4)

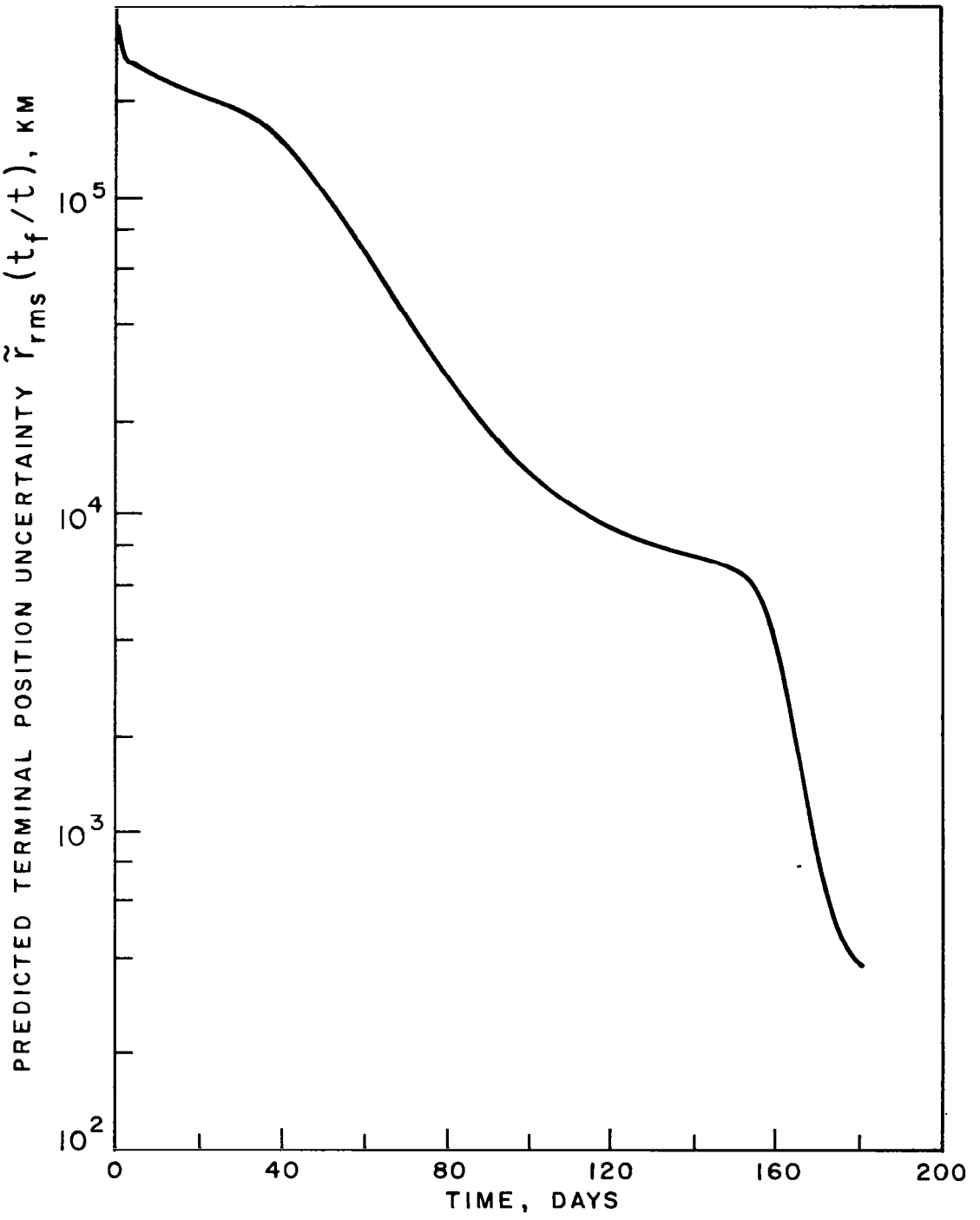

FIGURE 19 REDUCTION OF TERMINAL POSITION UNCERTAINTY WITH SUCCESSIVE CELESTIAL OBSERVATIONS, MARS RENDEZVOUS (181.6)

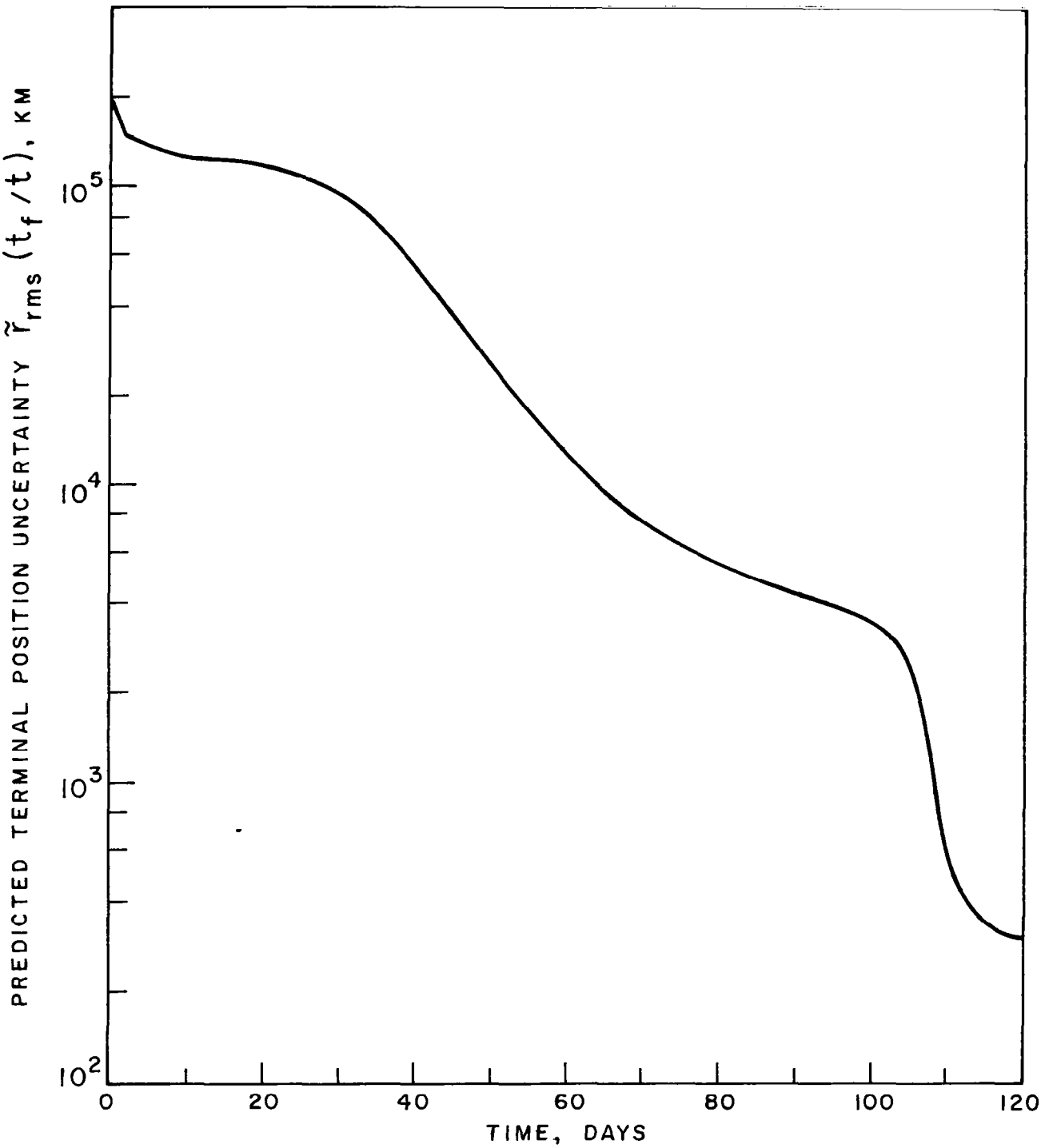

FIGURE 20 REDUCTION OF TERMINAL POSITION UNCERTAINTY WITH SUCCESSIVE CELESTIAL OBSERVATIONS, VENUS RENDEZVOUS (120)

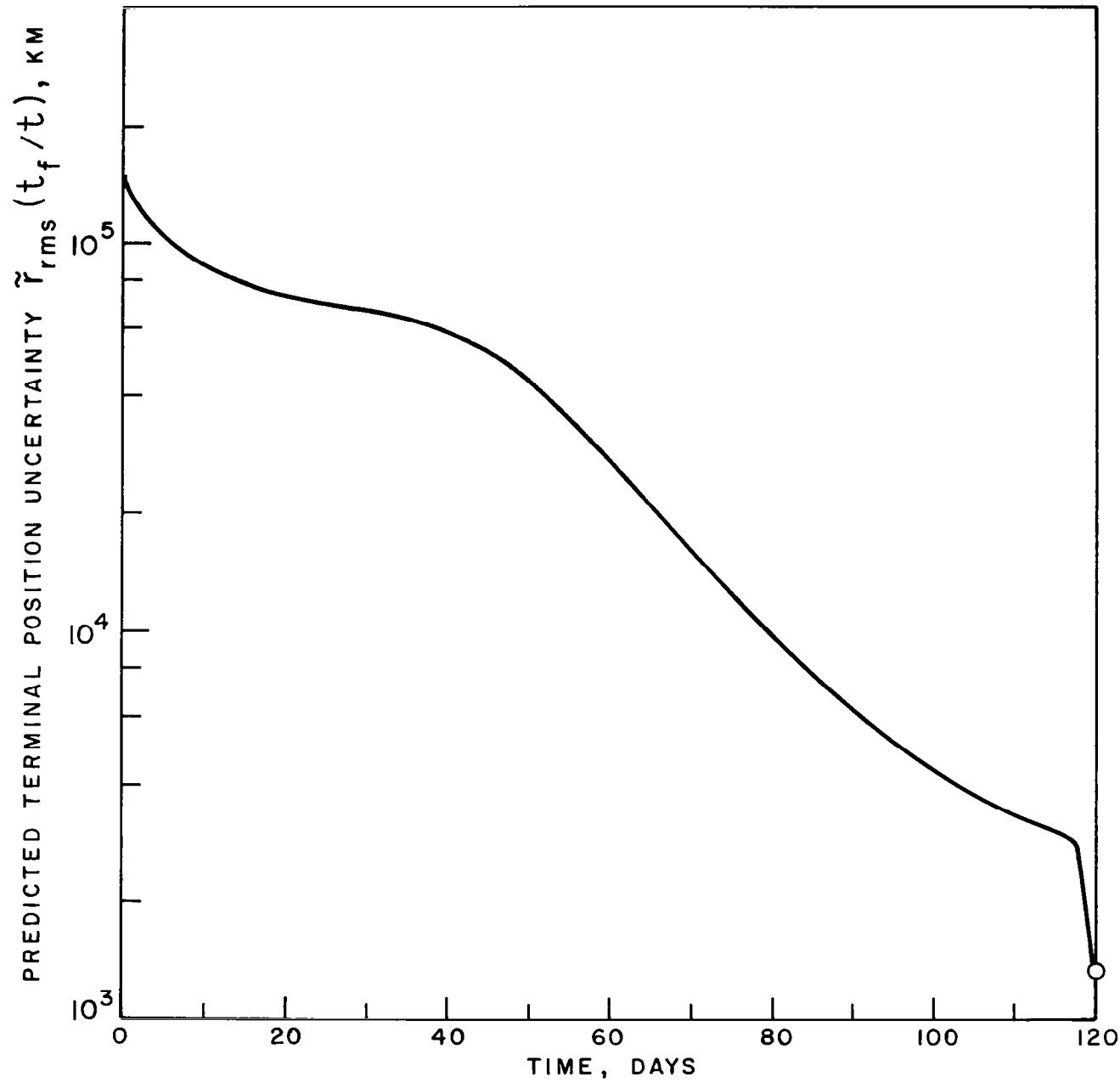

FIGURE 21 REDUCTION OF TERMINAL POSITION UNCERTAINTY WITH SUCCESSIVE CELESTIAL OBSERVATIONS, MARS FLYBY (120)

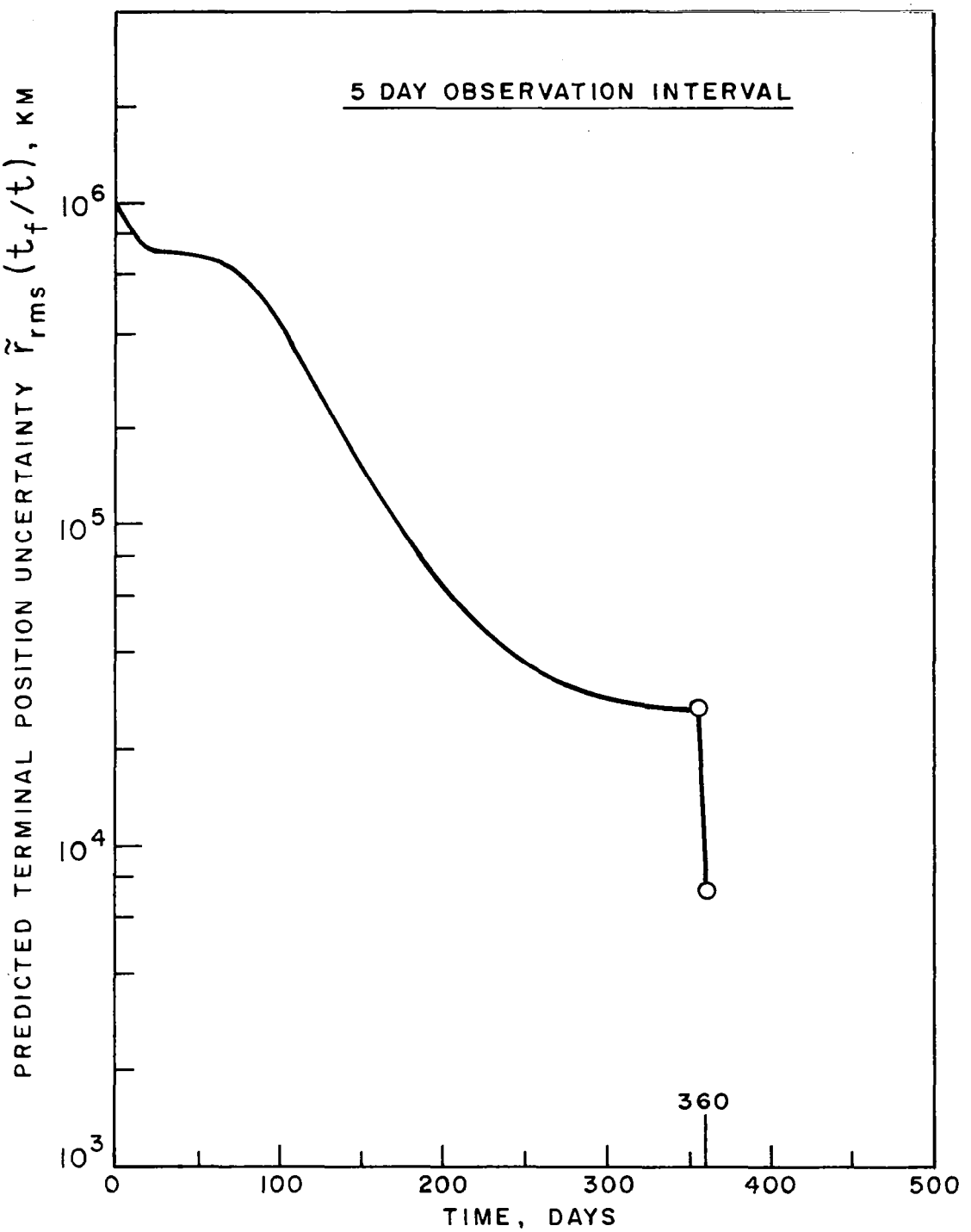

FIGURE 22 REDUCTION OF TERMINAL POSITION UNCERTAINTY WITH SUCCESSIVE CELESTIAL OBSERVATIONS, JUPITER FLYBY (360)

NASA-Langley, 1966 CR-457